P h i l i p p K r e n n

Experimental and theoretical analysis of the optimization potential of C-276 flux cored welding wire

Diploma thesis

Field of study: Production Science and Management

GRAZ UNIVERSITY OF TECHNOLOGY

Institute for Materials Science and Welding

Univ.-Prof.Dipl.-Ing.Dr.techn.Priv.-Doz. Christof Sommitsch

Advisor:

Dipl.-Ing.Dr.techn Rudolf Vallant IWE

Graz, 2010

STATUTORY DECLARATION

I declare that I have authored this thesis independently, that I have not used other than the declared sources / resources, and I have explicitly marked all material which has been quoted either literally or by content from the used sources.

Graz, 30.09.2010

ACKNOLEDGEMENTS

At this point I would like to thank my supervisor Dipl.-Ing. Dr.techn. Rudolf Vallant IWE for the supervision and support of this thesis.

Mr. Hötzel from the TU Bergakademie Freiberg should also be mentioned here, because he carried out the slag viscosity measurements.

I am also very thankful that the company Böhler Welding Technology made this work possible. All the people at Böhler, especially Mario Weiß, supported my work very well.

I would like to express my gratitude to the Institute for Material Science and Welding which is managed by Univ.-Prof.Dipl.-Ing.Dr.techn.Priv.-Doz. Christof Sommitsch. Special thanks go to the laboratory crew, to M.Sc Mathew Galler, who helped as a native speaker with complicated formulations and to Dipl.-Ing. Mizanur Rahman, who supported me with the Sysweld simulations that were performed.

Finally and most importantly, I would like to thank my family, especially my parents, for their support. Without them my thesis and my studies would not have been possible.

ABSTRACT

This work examined the welding behaviour of the nickel-based flux cored wire type C-276 for position welding using the MAG welding process.

The goal was to optimize the wire and filling composition so that the welding behaviour and mechanical properties were improved. The drop transition of different C-276 flux cored wires was examined in the welding laboratory of IWS TU Graz with a high resolution data logger and a high speed camera. Another target of the work was to improve the problem of degassing, which causes undesirable dimples on the surface of the weld. In order to accomplish this goal, the slag solidification of the different wires was measured with a viscometer to evaluate the optimization potential of the flux. Finally, an equilibrium, a Scheil, and a kinetics simulation with the program Matcalc of alloy C-276 with different alloying compositions was carried out in order to find out more about the influence of the main alloying elements on phase precipitations.

It was determined that the degassing problem can be optimized, but probably not solved completely for a welding wire for position welding, because the slag has to solidify quickly in order to support the weld pool. Regarding the intermetallic phase precipitation the Matcalc simulations showed that if a certain amount of alloying elements is reached, the precipitation of intermetallic phases increases quickly, which causes hot cracking.

INHALT

Diese Arbeit befasst sich mit der Untersuchung des Schweißverhaltens von Nickelbasis Fülldrähten der Legierung C-276 für die Positionsschweißung.
Das Ziel war die Optimierung der Draht- beziehungsweise der Füllungszusammensetzung um die Verschweißbarkeit und die mechanischen Eigenschaften zu verbessern. Der Tropfenübergang von verschiedenen Testdrähten wurde im IWS Schweißlabor mit Hilfe von hochauflösenden Strom- Spannungsmessungen und einer High Speed Kamera analysiert. Weiters war die Verbesserung eines Entgasungsproblems, welches Oberflächenabdrücke auf der fertigen Schweißnaht verursacht, Teil dieser Arbeit. Dafür wurden die Erstarrungsverläufe der verschiedenen Schweißschlacken mit einem Viskosimeter gemessen, um ein mögliches Verbesserungspotential für die Drahtfüllung zu ermitteln. Zuletzt wurden eine Gleichgewichts-, eine Scheil- und eine Ausscheidungskinetikberechnung mit Matcalc durchgeführt, um die Einflüsse der Hauptlegierungselemente auf die Ausscheidung von intermetallischen Phasen zu untersuchen.
Das Resultat der Schlackeviskositätsmessung ist, dass das Entgasungsproblem bei Drähten für Positionsschweißungen vermindert, wahrscheinlich aber nicht ganz behoben werden kann, weil die Schlacke sehr schnell erstarren muss, um das Schmelzbad zu stützen. Die Matcalc Simulationen zeigen, wie sich die Ausscheidungsmenge der intermetallischen Phasen mit der Zusammensetzung ändert und ab welchem Legierungsgehalt sich Heißrisse bilden.

ABBREVIATIONS

AOD	Argon oxygen decarburization
BSE	Backscattert electron mode
CMT	Cold metal transfer
EBW	Electron beam welding
EDX	Energy dispersive X-Ray
ESW	Electroslag welding
FCAW	Flux cored arc welding
FGD	Flue gas desulfurization
GMAW	Gas-metal arc welding
GTAW	Gas tungsten arc welding
HAZ	Heat affected zone
HSC	High speed camera
IWS	Institute for Material Science and Welding
LBW	Laser beam welding
MAG	Metal active gas
NACE	National Association of Corrosion Engineers
OAW	Oxyacetylene welding
PA	Downhand position
PAW	Plasma arc welding
PC	Horizontal vertical position
PF	Overhead position
PW	Position weld
SAW	Submerged arc welding
SEM	Scanning electron microscope
SMAW	Shielded metal arc welding
TCP	Topologically closed packed
TTT	Time Temperature Transformation
TU	University of Technology
UNS	Unified Numbering System
UTS	Ultimate tensile strength

Content

1 INTRODUCTION

The motivation for this thesis stems from several reasons. The most important one is that Böhler Welding wants to develop and establish a new product on the nickel based alloy market. Alloy C-276 is the “workhorse”-alloy (1) for flue gas desulfurization plants on the American market. A very important precondition for selling a welding wire especially in North America is the easy to use principle. That means that the wire should also be process able for less trained welders. That is the reason for the decision of Böhler Welding to develop a nickel-based flux core wire type for position welding. The versatility of a position weldable wire should be paired with simple usage.
Nickel based alloys are special also in matters of the basic problems they make in the development phase.
Dimple formations under the slag coverage and slag inclusions in the weld have been observed. Another problem is the very viscous molten weld metal, which causes coarse drop transition and as a consequence of that declined weldability.

Four basic tasks have been elaborated within this thesis:

- Literature study C-276: Mechanical properties, corrosion behaviour, microstructure, possible precipitates et cetera
- Analysis of the welding behaviour of different C-276 prototype wires with a high speed camera.
- Finding the reason and if possible a solution for the occurring dimples and slag inclusions.
- A Matcalc calculation of the different alloy compositions regarding to possible precipitates to find out trends for a optimized composition.

As a soft introduction into the nickel topic some interesting facts about nickel:

1.1 THE TERM NICKEL:

The name nickel comes from old German. A “Nickel” is a mountain goblin. The superstitious German miners believed that the reddish mineral, which they couldn’t melt, is from the “Nickel” enchanted copper ore. That’s why they called it “Kupfernickel”, which means copper nickel or copper goblin in English. In fact it was nickel ore (2).

1.2 SOME INTERESTING STATISTICS:

1.2.1 NICKEL FIRST USE:

About 60% of the Nickel is used for the production of stainless steels. Only 12% are used for non-ferrous alloys.

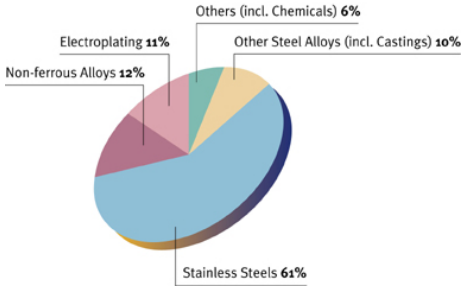

Figure 1-1: Nickel first use (3)

1.2.2 THE END USE OF NICKEL:

The biggest part of Nickel is used for engineering (24%) and the second biggest part for metal goods (16%).

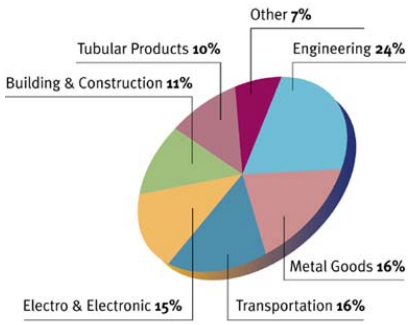

Figure 1-2: Nickel end use (3)

2 THE ALLOY C-276

This chapter includes information about the mechanical and metallurgical properties of C-276. Further there will be described the applications of C-276 and the history of the C-family alloys.

2.1 COMMON PROPERTIES OF ALLOY C-276

First patented in 1965 (4) the nickel based C-276 is known for its outstanding corrosion resistance in oxidizing as well as in reducing environments. It is resistant to crevice corrosion (50°C), pitting (>85°C) and stress-corrosion cracking (5). The alloy is also identified as INCONEL C-276 (INCO), Hastelloy C-276 (Special Metals), Nicrofer 5716 (Thyssen Krupp) or with its identification numbers UNS N10276 or W.Nr, 2.4819.

2.1.1 PHYSICAL AND MECHANICAL PROPERTIES

The values given below for yield strength and tensile strength are minimum values for room temperature of a C-276 plate.

- Density: δ = 8,9 [g/cm^3]
- Youngs modulus: E = 205 [GPa]
- Yield strength (0,2% Offset): $R_{p0,2}$ = 280 [MPa]
- Tensile strength: UTS = 700 [MPa]
- Elongation at fracture: 60%

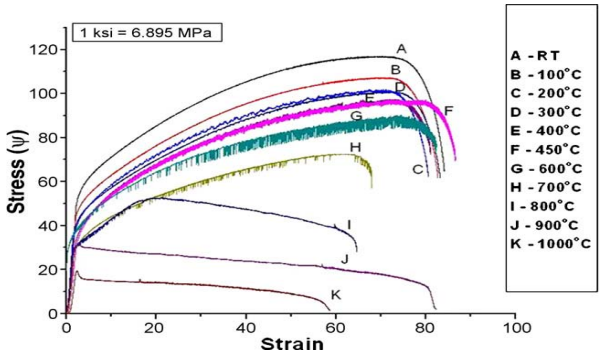

Figure 2-1: Stress - strain diagrams vs temperature (6)

Figure 2-1 shows the temperature range in which C-276 is usable. C-276 is used up to 500°C in less corrosive environments. The limit in corrosive environments is 120°C (7).

2.1.2 CHEMICAL COMPOSITION

The main alloying elements aside from nickel are molybdenum, chrome, iron, and tungsten (see Table 2-1).

Name	Limits	C	Co	Cr	Fe	Mn	Mo	Ni	P	S	Si	W
C-275	min			14.5	4.0		15.0	balance				3.0
	max	0.01	2.5	16.5	7.0	1.0	17.0		0.04	0.03	0.08	4.5

Table 2-1: Chemical composition of C-276 according to ISO 9722 (November 1992)

2.1.3 PREN: PITTING RESISTANCE EQUIVALENT NUMBER

The PREN is a theoretical value for the quantification of the pitting resistance of different alloys. The higher the PREN is the better. This makes different materials comparable with respect to pitting resistance. The values below each formula are calculated values with the minimum composition according to the ERNiCrMo4 (Standard abbreviation for C-276 weld metal) specification.

The most common formula is:

$$\mathrm{PREN} = \mathrm{Cr} + 3{,}3 \times \mathrm{Mo} + 30\mathrm{N}$$

Equation 2-1 (8)

PREN = 64 for ERNiCrMo4 minimum composition

The formula used in the NACE standards for oilfield applications (MR0175/ISO15156) is:

$$\mathrm{PREN} = \mathrm{Cr} + 3{,}3 * (\mathrm{Mo} + 0{,}5 \times \mathrm{W}) + 16\mathrm{N}$$

Equation 2-2 (9)

PREN = 69 for ERNiCrMo4 minimum composition

Both of these formulas are used in datasheets of C-276. Each manufacturer uses one of these two.

2.2 PHASES

Following phases are stable in this alloy:

2.2.1 GAMMA-PHASE

This face centred cubic phase is the matrix phase. The Nickel, which is the main element, forms a solid solution with the other alloying elements.

2.2.2 P-PHASE

This phase is a TCP (Topologically Closed Packed) intermetallic phase which is very hard and brittle and therefore should be avoided, because it has a deteriorating effect on the mechanical properties. It has also a deteriorating effect on the corrosion resistance, because it influences the homogeneous distribution of Mo. The chemical formula for this phase is $Cr_9Mo_{21}Ni_{20}$, which means that this phase is a very molybdenum rich phase (10).

2.2.3 MU-PHASE

The μ-phase is like the P-phase a TCP phase with the same disadvantageous effects. It is suggested to be a long term transformation product of the P-phase (11). The formula for this phase is $(Co, Fe, Ni)_7 (Mo, W, Cr)_6$ (10).

Figure 2-2 shows the influence of TCP phases on the long period creep resistance. Reaching a certain time, the effect of the TCP phases becomes disadvantageous.

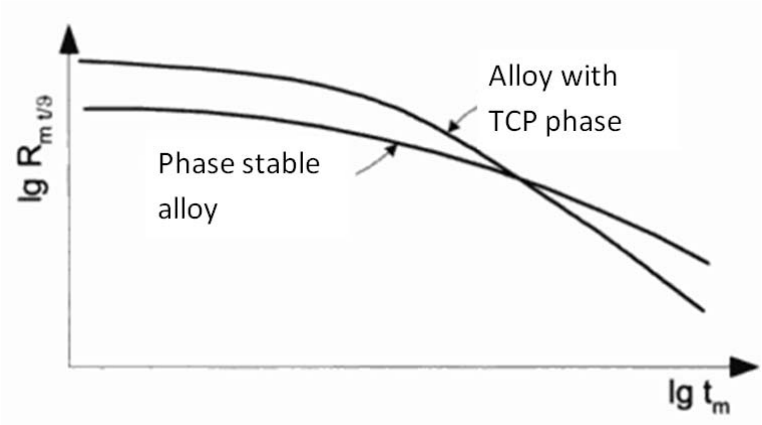

Figure 2-2 Influence of TCP phases on long period creep resistance (schematic) (12)

2.2.4 *CARBIDES*

Many different types of carbide can precipitate in nickel based alloys. The possible types are: MC, $M_{23}C_6$, M_7C_3, and M_6C. The only stable carbide in C-276 is the face centred M_6C type.
During heat treatment this carbide can precipitate along the grain boundaries, which has a unfavourable effect on the mechanical properties and corrosion resistance (intergranular corrosion). This carbide type precipitates preferably in alloys with high Mo and/or W contents like alloy C-276. The necessary W and Mo content for M6C precipitation is (Mo + 1/2W) > 6 weight percent (12). The chemical formula for this carbide is $(Ni, Co, Fe)_3 (Mo, W, Ta)_3 C$ (10).

2.3 HISTORICAL DEVELOPMENT OF THE C-FAMILY ALLOYS

(1)

Table 2-2 shows the development and the differences in chemical composition of the different C-alloys. All alloys show similar corrosion behaviour.

Alloy (UNS No.)	Decade introduced	Ni	Cr	Mo	W	Fe	Si	C	Cu
C (N10002)	1930's	55	16	16	4	6	0.7	0.05	-
C-276 (N10276)	1965	57	16	16	4	5	0.04	0.005	-
C-4 (N06455)	1970's	66	16	16	-	2	0.04	0.005	-
C-22 (N06022)	1982	57	21	13	3	3	0.04	0.005	-
59 (N06059)	1990	59	23	16	-	< 1	0.04	0.005	-
686 (N06686)	1993	56	21	16	4	2	0.04	0.005	-
C-2000 (N06200)	1995	57	23	16	-	2	0.04	0.005	1.6

Table 2-2: Chemical compositions of the "C" family (1)

2.3.1 *ALLOY C (1930'S - 1965)*

This alloy was one of the most versatile corrosion resistant alloys from the 1930's to the 1960's. It combined the advantages of a nickel-chrome alloy and a nickel-molybdenum alloy. The hazard of intergranular corrosion in the HAZ after welding limited the usefulness of this alloy. It had to be solution heat treated after welding to regain its corrosion resistance.

2.3.2 ALLOY C-276 (1965 - PRESENT)

Due to the invention of a new melting technology, known as AOD (Argon-Oxygen Decarburization) process the Carbon and the Silicon content could be reduced by more than ten-fold compared to Alloy C. That reduced the risk of intergranular corrosion in the as-welded state. Alloy C-276 could be used in the as-welded state for most applications, which was the biggest advantage compared to Alloy C.
For some process conditions C-276 is not thermally stable to precipitation of carbides and intermetallic phases, which are hard and brittle and make the matrix more susceptible to corrosion.
C-276 is established very well in the chemical process industry. It is still the most used alloy of the C-family.

2.3.3 ALLOY C-4 (1970'S – PRESENT)

The difference of this alloy compared to C-276 is the omission of tungsten and the reduction of Iron. Fe and W are one reason for the formation of the intermetallic "mu" and "p" phases. Thus C-4 is less susceptible in the sensitizing range (550°C – 1090°C) to the formation of these intermetallic phases, which are detrimental to ductility and corrosion resistance. In corrosive environments C-276 and C-4 have similar properties. C-276 is a little more resistant in reducing environments, but C-4 is better for oxidizing media. C-4 found greater acceptance in Europe in contrast to C-276, which is used more often in the USA.

2.3.4 ALLOY C-22 (1982 - PRESENT)

With the development steps for alloy C-4 a "mu" and "p" phase control was achieved. The problem was, that the reduction of Tungsten and Iron was not only beneficial for the corrosion resistance it also reduced the corrosion resistance in certain environments. The intermetallic phases mentioned above are detrimental to corrosion resistance, but Tungsten is a beneficial element in certain corrosive environments such as chloride solutions.

With Alloy C-22 the developers tried to find a compromise between intermetallic phase control and corrosion resistance improvement in chloride environments. C-276 and C-4 showed rather high corrosion rates in oxidizing, non-halide solutions which could be improved by raising the Chromium for level for C-22 from 16% to 21%. The Molybdenum content was lowered to 13 weight percent. The result was an alloy with superior corrosion resistance in highly oxidizing environments but due to the reduced Mo content compared to C-22 and C-276 it has inferior corrosion resistance in highly reducing environments.

2.3.5 ALLOY 59 (1990 – PRESENT)

Alloy 59 is the purest alloy within the "C" family. It combines thermal stability, which is dependent on intermetallic phase and carbide precipitation control, with very good corrosion resistance in reducing and oxidizing environments, due to the highest Mo and Cr content. The thermal stability is reached by omitting tungsten and reducing Iron to a level lower than one weight percent.

2.3.6 ALLOY 686 (1993 – PRESENT)

This alloy is very similar to Alloy C-276. The chromium level has been increased from 16% to 21%. This leads to an inferior thermal stability compared to Alloy 59 because more Mo, Cr, W and Fe is solved in less nickel compared to alloy 59. To prevent precipitation it has to be solution annealed at 1200°C and cooled very rapidly.

2.3.7 ALLOY C-2000 (1995 – PRESENT)

The composition of C-2000 is almost the same as Alloy 59, except that 1.6% of copper have been added. Tests showed that the addition of copper deteriorates the thermal stability compared to Alloy 59.

2.3.8 TIME-TEMPERATURE-SENSITIZING DIAGRAM

Figure 2-3 gives an overview about the thermal stability of different alloys.

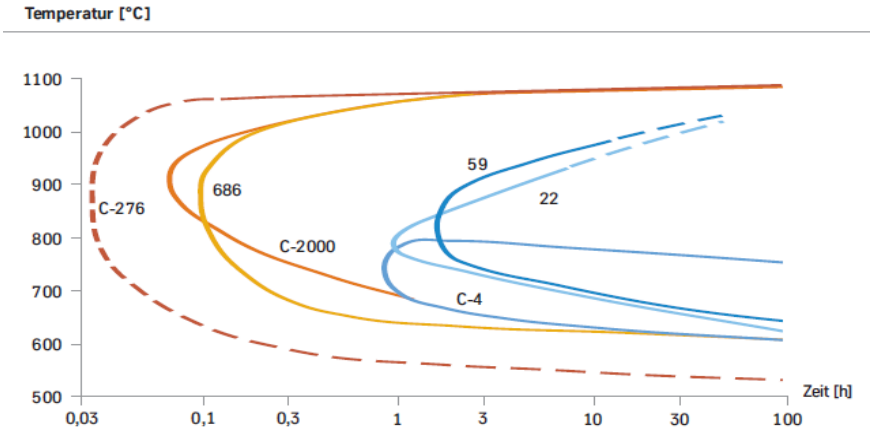

Figure 2-3: T-T-T diagram (8)

2.3.9 CONCLUSION

It may be that the newer alloys, such as Alloy 59 or C-2000, have better properties concerning weldability, corrosion resistance or thermal stability, but Alloy C-276 is established on the market. Several big companies (Thyssen, Arcelor Mittal, Special Metals and Haynes International) are producing this alloy, which leads to good availability. In the near future C-276 won't be replaced completely by other alloys.

2.4 ALLOYING ELEMENTS OF C-276

This is a description of the most important alloying elements and their properties.

2.4.1 NICKEL

Nickel is the matrix element in C-276. It can dissolve a rather big amount of elements to form a solid solution. Its atomic structure is face centred cubic at every temperature beneath the liquidus temperature. The most outstanding property besides the good solubility of other elements of nickel is that it doesn't lose its toughness at very low temperatures (2).

2.4.2 CHROME

The main reason for alloying Cr is that it improves the corrosion resistance in oxidizing environments by forming a Cr_2O_3 layer (2). It improves the pitting resistance as well (see 2.1.3 PREN). Another advantage of alloying Cr is the improvement of solid solution strength. A disadvantage of alloying Cr is that it supports the formation of TCP phases (12).

2.4.3 MOLYBDENUM

Mo improves the corrosion resistance in reducing media (2). It is a good solid solution strengthener (12) and it increases the pitting resistance (see 2.1.3 PREN). It enhances carbide formation and TCP phase formation (12).

2.4.4 TUNGSTEN

W is beneficial in certain corrosive environments such as chloride solutions (1). It is a very good solid solution strengthener. On the other hand it enhances the formation of intermetallic phases and M6C carbides.

2.4.5 IRON

Iron is very cheap and therefore a substitute for Nickel in a certain amount. It also promotes the formation of TCP phases, which should be avoided (12).

2.4.6 CARBON

C is a strong carbide former. Too much C leads to continuous grain boundary precipitation in the weld HAZ which is detrimental to corrosion behaviour and mechanical properties (1).

2.4.7 SILICON

Si is detrimental to the properties of alloy C-276, because it promotes TCP phase formation and it increases the risk of hot cracking during welding (12).

2.4.8 SOLID SOLUTION STRENGTHENERS

Since solid solution strengthening is the most important strengthening mechanism for alloy C-276 it is the only mechanism described here.

Substitution elements in the nickel lattice expand or tighten the lattice which leads to compression or tensile stresses. These stresses strengthen the material. The bigger/smaller the element compared to the matrix element, the higher the stresses and the better the strengthening. One limitation of this mechanism is the solubility of alloying elements. Elements which cause strong deformations have a lower solubility.

Equation 2-3 describes this mechanism (13):

$$\Delta\sigma_m = a \times G \times \sqrt{c}$$

Equation 2-3: Solid solution strengthening (13)

a…. constant (e.g. atom radius of the substitution element)
G…. shear modulus
c…. concentration of the alloying element

Figure 2-4 shows that tantalum and niobium are the strongest solution strengtheners, but also molybdenum, tungsten and titanium are good solution strengtheners. For C-276 molybdenum and tungsten are the most important solid solution strengtheners.

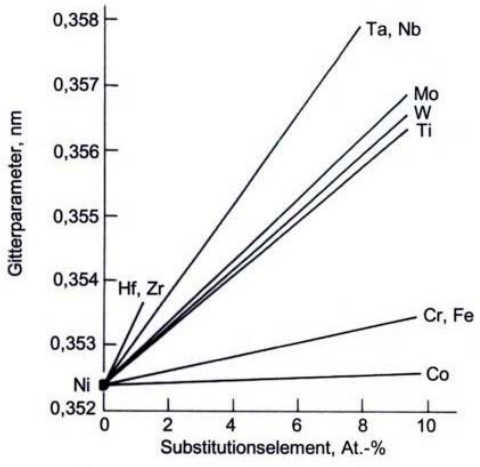

Figure 2-4: The change of the nickel lattice with certain alloying elements (12)

2.5 APPLICATIONS

C-276 has a wide range of applications due to the already mentioned good corrosion resistance in oxidizing and reducing media. Following industries are using alloy C-276:

- Petroleum
- Petrochemical
- Chemical process
- Pollution control
- Pulp and paper
- Marine
- Pharmaceutical
- Mining

One of the most popular applications for C-276 is Flue Gas Desulfurization (FGD). It is not the aim of this thesis to describe every application in detail, but since FGD is one of the main applications for C-276 it will be described a little bit more in detail, to see which parameters are critical for corrosion and where are endangered areas.

2.5.1 FGD – FLUE GAS DESULFURIZATION

FGD is mostly used in oil, coal or waste fired power plants. The reason for FGD is to avoid environmental damage caused by sour rain.

2.5.1.1 FGD SYSTEMS

There are three major FGD systems

- Wet scrubbing using: lime, limestone or seawater
- Dry sorbent injection
- Gas phase oxidation followed by ammonia

The most common FGD is wet scrubbing with limestone with an optional attached production of gypsum. For normal power stations this process removes about 95% of the SO_2

2.5.1.2 PRINCIPLE OF THE WET LIMESTONE FGD

Figure 2-5 shows the schematic principle of a wet limestone FGD plant:

- The raw gas enters the inlet duct: heat is recovered to increase the temperature of the clean gas to improve its buoyancy before it enters the stack.
- The raw gas enters the absorber vessel where it is scrubbed by the limestone slurry. Following reactions take place:
-
- $CaCO_3 + SO_2 \rightarrow CaSO_3 + CO_2$
- $CaSO_3 + H2O + 1/2O_2 \rightarrow CaSO_4 + H_2O$
- $H_2SO_4 + CaCO_3 \rightarrow CaSO_4 + H_2O + CO_2$
-
- After the absorber vessel the ash is removed by an electrostatic precipitator

- Before the clean gas leaves the stack it is heated to improve its buoyancy.

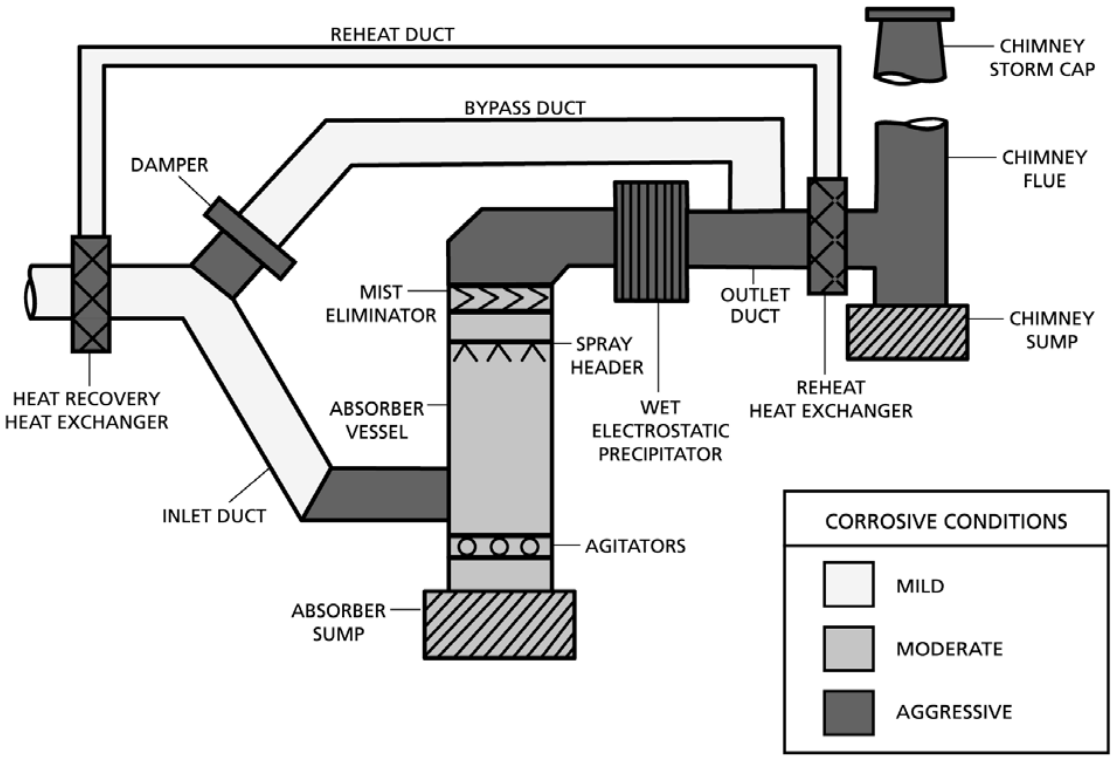

Figure 2-5: Principle of wet limestone FGD plus corrosive conditions (14)

This short description is idealized. As a matter of fact there are some other chemical constituents apart from the ones listed above. SO_3 can be formed which later on forms H_2SO_4, which is also known as sulphuric acid.
If Halides enter the system, which is possible via limestone and coal some additional corrosive media can form:

Hydrochloric acid: $NaCl + H_2SO_4 \rightarrow NaHSO_4 + HCl$
Hydrofluoric acid: $CaF_2 + H_2SO_4 \rightarrow CaSO_4 + 2HF$

2.5.1.3 PARAMETERS FOR CORROSIVE CONDITIONS (14)

Dew point: Condensation of acids cause most of the corrosion

Acidity: When the flue gases at the inlet of the FGD system are quenched acids are formed. The pH value can be 1 or less. The scrubbed gas leaving the vessel still contains a small amount of acids which can condense on the cold outlet tubing.

Temperature: Increasing temperature increases corrosion rate.

Halides: Halides entering the system via coal or limestone are increasing the corrosion.

Wet/Dry Conditions: Areas which are first moistened with acid and then dried experience the worst corrosion attack, because the acid temperature is elevated.

Crevice conditions: Tightly adhering deposits can build up on the walls and create crevice conditions. The best solution to avoid this inside the absorber vessel is to wash its walls.

Critical areas in the FGD system:
In Figure 2-5 all critical areas in regard to corrosion are marked. In the heat recovery heat exchanger and the inlet duct (quencher) the environment is very harmful for the materials.

The outlet duct, the stack and the reheat heat exchanger are also critical areas, but not as critical as the areas mentioned above.

2.5.1.4 USAGE OF ALLOY C-276 IN FGD SYSTEMS
(14)

C-276 is the most widely used corrosion-resistant material in FGD. There is a lot of experience with C-276 in FGD, because it is used successfully since the 1980s.

Parts of the FGD system made of C-276 are:

- Outlet ducts
- Stack
- Reheat heat exchanger
- Absorber vessels

Figure 2-6 shows an absorber vessel in detail:

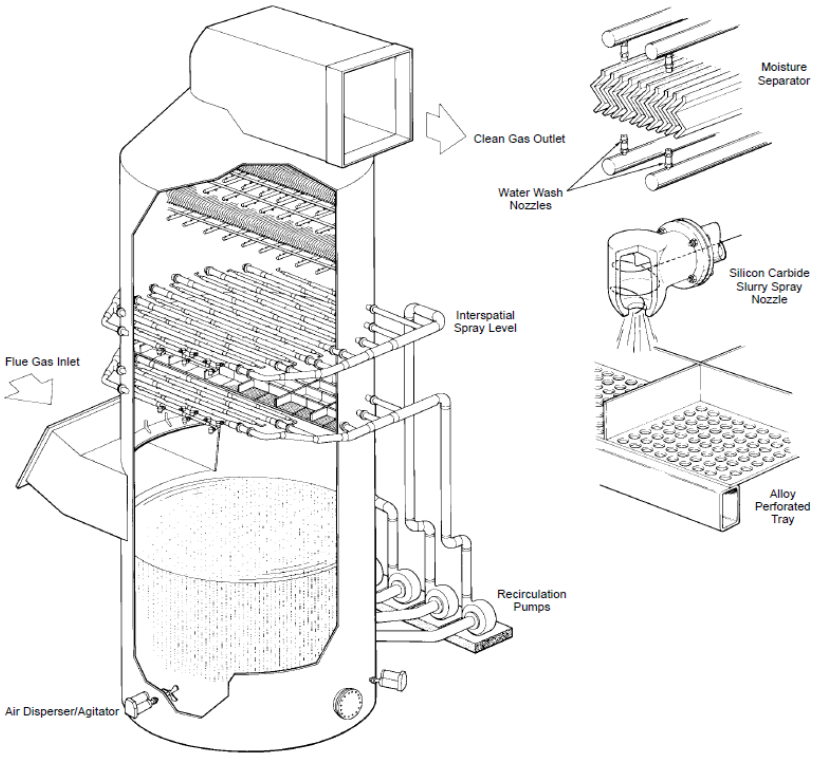

Figure 2-6: FGD absorber tower (15)

3 FLUX CORED ARC WELDING FCAW

3.1 PROCESS AND MACHINE

3.1.1 FUSION WELDING PROCESSES

(16)

Fusion of the base material is used to produce the weld. All standard welding processes except OAW can be used to weld C-276. The four major types of fusion welding processes are as follows:

- Gas welding:

  Oxyacetylene welding (OAW)

- Arc welding

  Shielded metal arc welding (SMAW)
  Gas-tungsten arc welding (GTAW)
  Plasma arc welding (PAW)
  Gas-metal arc welding (GMAW)
  Flux cored arc welding (FCAW)
  Submerged arc welding (SAW)

- High-energy beam welding:

  Electron beam welding (EBW)
  Laser beam welding (LBW)

- Electroslag welding (ESW)

Used for C-276

Not used for C-276

3.1.2 THE FCAW MACHINE AND WELDING AREA

FCAW is very similar to GMAW, except the electrode is different. The special properties of a flux cored welding wire are described in the chapter 3.2. In our case the welding machine was a Fronius CMT with a push-pull system, but the exact setup will be described later in chapter 3.4.2.1: Experimental setup.

Figure 3-1 shows the welding machine (schematic) and the enlarged welding area of FCAW.

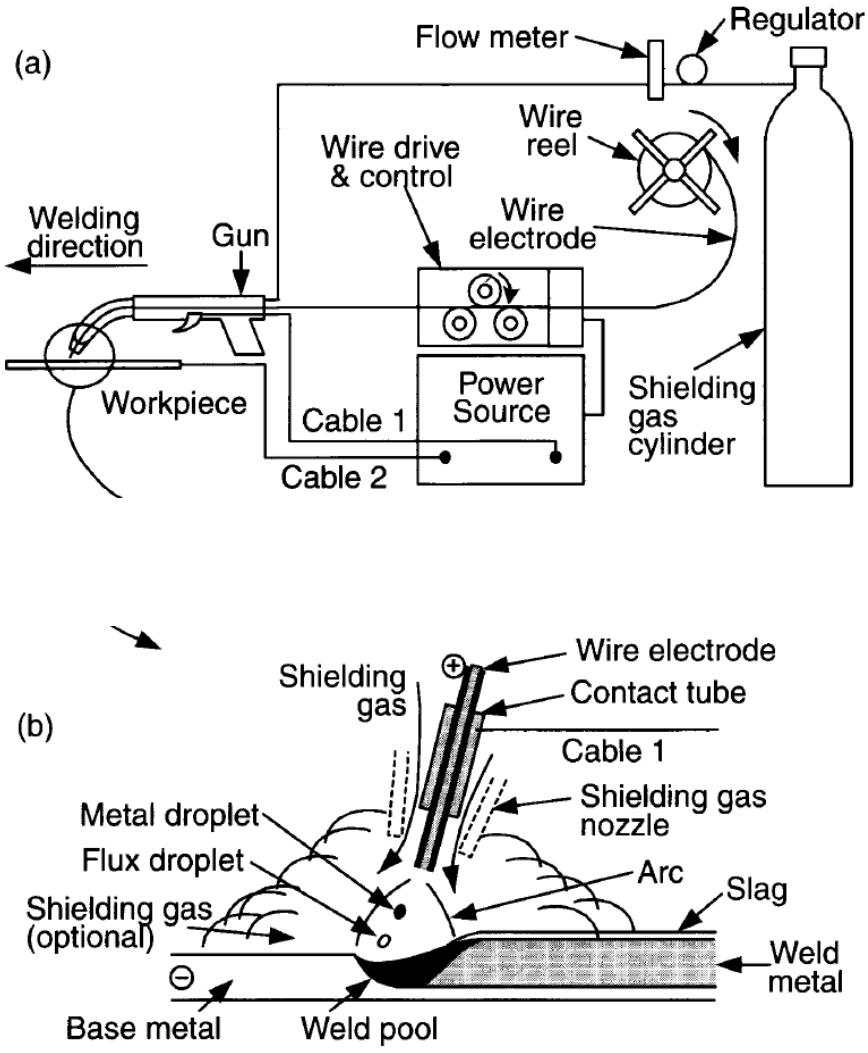

Figure 3-1 Flux core arc welding: (a) overall process; (b) welding area enlarged (16)

3.2 FLUX CORED WELDING WIRES IN GENERAL

3.2.1 HISTORICAL DEVELOPMENT

Already in 1908 Oscar Kjiellberg, who is also known as the inventor of the covered electrode, mentioned the possibility of filling a metal tube with a tried paste. This was the birth of the idea for a flux cored welding wire (17).
The Gas metal arc welding (GMAW) method was introduced in 1948 in the US and in 1953 in the Soviet Union. This was the starting point for the industrial application of flux cored wires. In 1954 the first flux cored welding electrodes were available on the market. In 1959 self shielding flux cored wires were used in the industry (18).
Today more than 10 percent of the welding consumables worldwide are flux cored wires.

3.2.2 FUNCTIONS OF THE FILLING

(19)

The wire filling has several functions. It contains alloying elements, builds up slag, works as deoxidizer, supports the ionization, contains alloying elements and some fillings are shielding gas builders.

3.2.2.1 ALLOYING ELEMENTS

Mechanical and metallurgical properties of the weld deposit can be influenced rather easily. Different alloys can be produced from the same metal tube by alloying with the filling. For this reason, flux cored wires are very flexible for production. For some very high strength electrode materials there is no other possibility than producing flux cored wires. Another advantage is that even small amounts of welding wires of a certain alloy can be produced economically by replacing only the flux.

3.2.2.2 SLAG BUILDERS

The slag influences the welding behaviour on the one hand and the mechanical properties of the welding deposit on the other hand. The viscosity and the solidification rate of the slag influences the welding behaviour. For positional welding a fast solidifying slag helps to control the liquid weld bath. The slag can be either rutile or basic.

A basic slag improves the purity of the weld metal but the appearance of the finished seam is rougher. The basic type also leads to bigger droplets compared to the rutile type. The main components are CaO, MgO and CaF_2.

The rutile type improves the deposition rate and the final welding seam is flatter than the basic type seam. It also causes smaller droplets compared to the basic type. The main component is TiO_2.

From the formation of the droplet to the final weld, the slag covers the metal and protects it from harmful external influences, such as oxygen.

Note that not every flux cored wire has slag building ingredients. The metal powder cored welding wires do not build up slag.

3.2.2.3 DEOXIDIZING ELEMENTS

This elements help to reduce the formation of harmful oxides inside the weld metal. It binds the oxygen and transfers the resulting oxide into the slag. Oxide or slag inclusions can deteriorate the properties of the weld metal, especially the impact strength (20).

3.2.2.4 IONIZATION SUPPORT

Substances that are easily ionized improve the stability of the electric arc. One of these substances is potassium.

3.2.2.5 SHIELDING GAS BUILDERS

Self shielding welding wires would not work without shielding gas builders. For every other flux cored welding wire, shielding gas builders play a subordinate role.

3.2.3 CLASSIFICATION OF FLUX CORED WIRES

Flux cored welding wires can be either classified according to their filling, or according to their cross-sectional form.

3.2.3.1 CLASSIFICATION ACCORDING TO FILLING

Basically there are two main types of flux cored wires. Flux cored wires are either slag building types or metal powder types.
The slag building types are further divided in four groups. All possible combinations of the following table are available:

Rutile	fast freezing slag	shielding gas necessary
	slow freezing slag	no shielding gas necessary

Basic	fast freezing slag	shielding gas necessary
	slow freezing slag	no shielding gas necessary

Table 3-1: Classification according to filling

3.2.3.2 CLASSIFICATION ACCORDING TO THE CROSS-SECTIONAL FORM

Several cross-sectional forms can be realized:

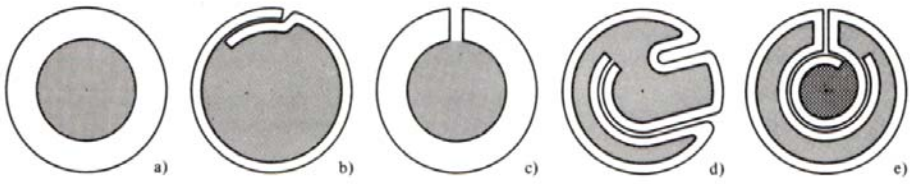

Figure 3-2: X-sections of flux cored wires (19)

3.2.4 FCAW COMPARED TO NORMAL GMAW

3.2.4.1 ADVANTAGES

- Less operator skill required
- Higher deposition rate, because of the higher current density
- Flexible in production
- Self shielding capability
- All position capability, because of the slag support
- Flat and smooth welding bead, because of the slag coverage
- Less pre cleaning of the base metal required
- Protection of the weld bath through shielding gas and slag → double protection
- Good wetting of the weld flanks → smaller V-groove angles possible
- Less shielding gas is necessary → lower costs for shielding gas

3.2.4.2 DISADVANTAGES

- Higher welding wire costs
- The flux can become humid → hydrogen cracking
- Degassing problems, because of the slag coverage → porosity
- Slag has to be removed in most cases

3.2.5 PRODUCTION OF FLUX CORED WIRES

For the production of a flux cored welding wire, several steps are necessary. Related to the cross-section design of the welding wire the production is more or less sophisticated. Following pictures shows a simplified production process of a flux cored welding wire.

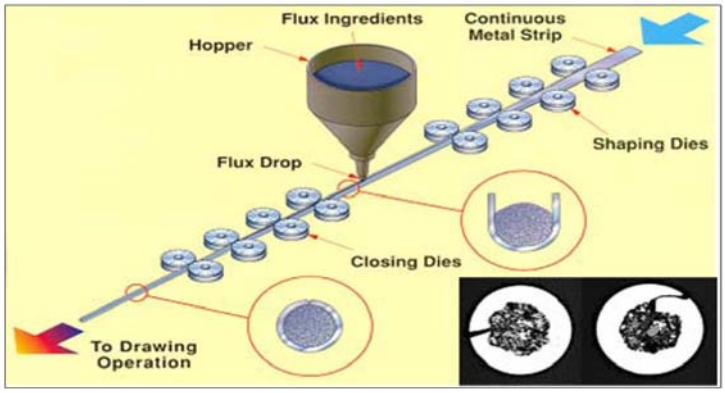

Figure 3-3: The production process of flux cored wires (21)

Necessary steps:

- The flux ingredients must be mixed homogeneously.
- The metal strip is formed to an u-shape by roller dies.
- The flux is inserted into the u-shape.
- Roller dies close the u-shaped metal strip.
- The raw flux cored wire goes to the next station, where it is drawn or rolled to the required diameter.
- If necessary, the wire is heat treated to dry the flux.
- If necessary the wire is heat treated to make it softer to avoid wire feed problems during welding.
- The wire is coated to avoid wire feed problems.
- The finished wire is packed in a water proof bag, to avoid the moistening of the flux.

3.3 WELDING OF NICKEL IN GENERAL

3.3.1 BASIC RULES FOR WELDING NICKEL ALLOYS

For the joining of nickel and nickel-based alloys some rules have to be followed to make sure, that the weld has the same mechanical and chemical properties as the base material:

- Nickel-based alloys must be at least welded “matched”.
- Depending on the designated operating temperature the base material must be in a solution- or soft-annealed state before welding.
- Mill scale has to be removed before welding.
- Weld flanks as well as both sides of the sheets have to be metallic bright in an interval of 25mm from the flank. There must not be grease or markers. A clean surface is very important.
- Cleaning agents must not contain sulphur or chlorides. Brushing and grinding tools must be made of stainless material.
- The weld preparation for butt joints has to be done according to certain rules (see Figure 3-4 Weld preparation for nickel and nickel alloys). That is because the viscosity of the nickel weld pool is bigger than the viscosity of molten steel.
- The weld pool has to be protected from gases, which can cause pores (N, O, and CO_2). Even in small amounts (>0,5% (2)) Nitrogen causes pores.

- The weld pool should not react with oxidizing gases, because this can cause a burn-off of alloying elements with affinity to oxygen, which can deteriorate the corrosion resistance of the weld.
- Heat tint must be removed after welding.

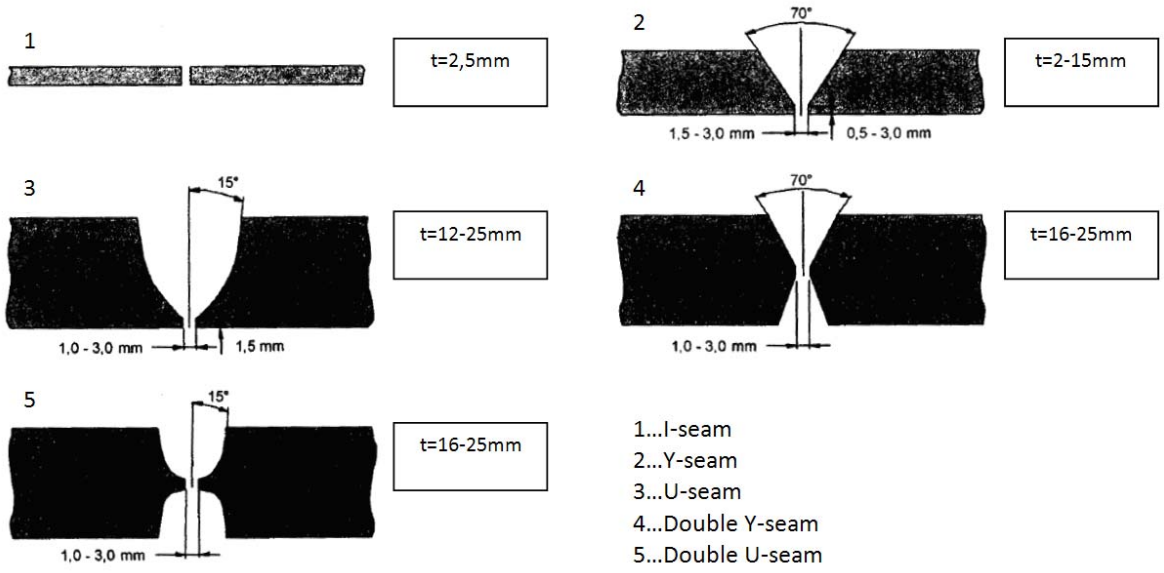

Figure 3-4 Weld preparation for nickel and nickel alloys (2)

3.3.2 SPECIFIC WELDING PROPERTIES OF NICKEL AND NICKEL-BASED ALLOYS

Some other specific properties except of those mentioned above have to be considered:

- Nickel has a low thermal conductivity connected with a strong thermal expansion ($14*10^{-6}$ 1/K) compared with ferritic steel ($12*10^{-6}$ 1/K).
- The nickel-nickel sulphide eutectics have a very low melting point (~640°C), which makes nickel very susceptible to hot cracks, if there is sulphur pollution (see Figure 3-5)
- The danger of pores in the weld because of nitrogen and oxygen absorption.
- The influence of heat input on disadvantageous precipitations.

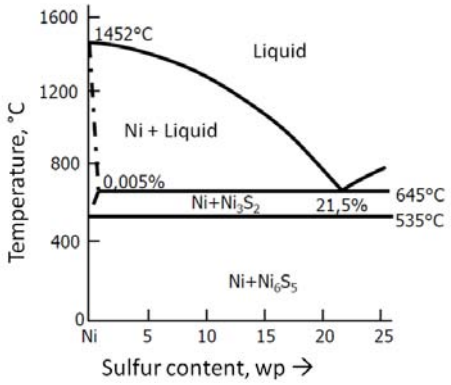

Figure 3-5: Nickel - Sulphur equilibrium (22)

3.3.3 SPECIAL RULES FOR WELDING WITH C-276 FLUX CORE

The C-276 flux cored wire builds up a slag coverage, which must be removed after welding. Slag remains can work as sponge in corrosive environments and therefore can be harmful.

Following rules are necessary to avoid the risk of hot cracking and the excessive precipitation of TCP phases and carbides:

- If a multipass is necessary, the interpass temperature must not exceed 150°C.
- The heat input per unit length is also limited. The values are different for each welding process. The formula for calculating the heat input (Equation 3-1) and a table with the limiting values for heat input per unit length (Figure 3-5) are given below.

3.3.3.1 HEAT INPUT PER UNIT LENGTH

The heat input per unit length is calculated as follows:

$$H = \frac{I \times U \times 60}{s \times 1000} \times \eta$$

Equation 3-1 (23)

H….Heat input per unit length [kJ/cm]

U….Arc voltage [V]

s….Travel speed [cm/min]

η….Thermal efficiency factor

It is not correct that all of the electric energy is heat input per unit length. There are always some heat losses which are depending on the thermal efficiency of the welding process. That is why an efficiency factor is necessary for calculating results that are a better description of the real heat input per unit length (24).

Process	SAW	SMAW	GMAW	GTAW
Efficiency factor	1	0.8	0.8	0.6

Table 3-2: Efficiency factors of different welding processes (23)

FCAW, which is special form of the GMAW process, has a slightly different efficiency factor than the normal GMAW process. Christoph Freytag measured the efficiency factors for FCAW wires and documented them in his thesis. For two different FCAW wires the results were as follows (25):

FCAW wire type	Efficiency factor min	Efficiency factor max
Böhler EAS 4M	0.81	0.84
Böhler UTP AF 7015	0.75	0.77

Table 3-3: Efficiency factors of different FCAW wires (25)

According to these values the efficiency factor of 0.8 from **Error! Reference source not found.** seems to be usable also for FCAW.

With Equation 3-1 and the efficiency factor, the heat input can be calculated and compared with following maximum values. The maximum values must not be exceeded.

Process	GMAW	GTAW	Hot wire GTAW	PAW	SMAW
max. Heat input [kJ/cm]	11	8	6	10	7

Table 3-4: Maximum values for heat input (26)

3.4 DROP TRANSITION

3.4.1 DROP TRANSITION FORCES

The electrode has two functions: It carries the arc and it is filler metal at the same time. Welding processes with permanent electrode (e.g. GTAW) are an exception. That means that the electrode has to be transferred into the weld pool on the work piece. At the tip of the electrode which is also the upper end of the arc, the electrode starts to melt and build drops which are transferred into the weld pool. Figure 3-6 describes all forces which are involved in the drop transition.

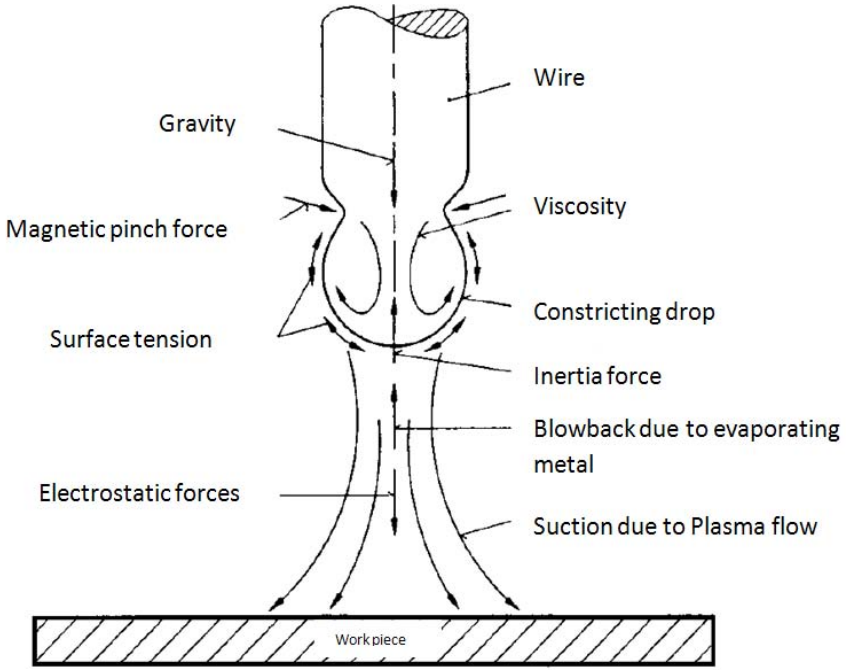

Figure 3-6: Forces involved in the drop transition (27)

3.4.1.1 THE PINCH EFFECT

A pinch is the compression of an electric conducting filament due to magnetic forces. This electromagnetic force is based on the Lorentz force. The radial component of the magnetic field is the pinch force. Figure 3-7 illustrates the pinch force on a welding electrode.

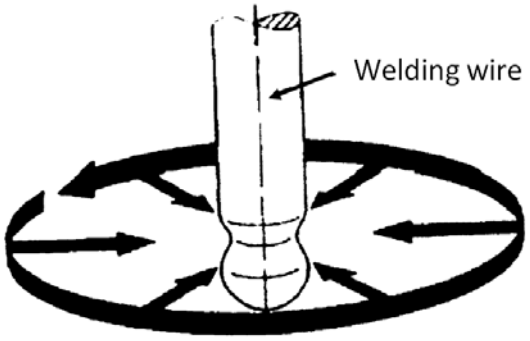

Figure 3-7: Effect of the pinch force (27)

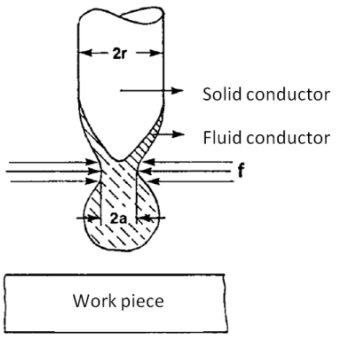

Figure 3-8: Pinch force in detail (28)

Figure 3-2 shows the pinch force in detail. The shaded area is the molten metal. The pinch force helps separating the drop from the welding wire. The pinch force can be calculated as follows:

$$f = \frac{5 \times m \times I^2}{\pi^2 \times a^2}$$

Equation 3-2 (28)

f……..Pinch force
m…….Magnetic permeability
a……..Liquid conductor radius
I……..Current

Except of the current all other values are almost constant, which leads to a simplified formula that shows the influence of the current.

$$f \approx \frac{I^2}{2}$$

Equation 3-3 (28)

The pinch force is influenced by the current to the power of two. Figure 3-9 shows the influence of different pinch forces on the drop transition.

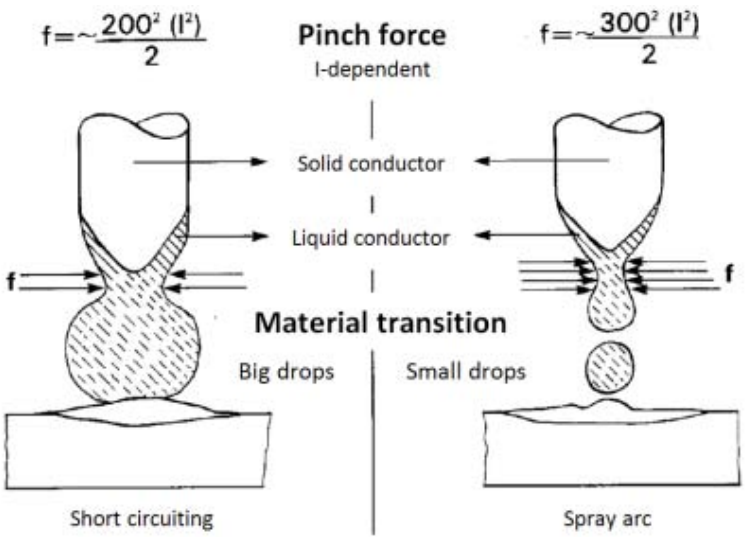

Figure 3-9: Current dependency of the pinch force (28)

3.4.1.2 SURFACE TENSION

Surface tension is like a thin elastic film that surrounds a liquid caused by intermolecular cohesion. Hence surface tension expresses the attempt of diminishing the surface of the liquid. It is the force that points to the inside of a liquid. It is described by the ratio of change in energy and change of surface area.

$$\sigma = \left(\frac{\Delta E}{\Delta A}\right)$$

Equation 3-4: Surface tension

σ….surface tension
E….Energy
A….Surface area

When the drop is formed at the end of the conductor, the surface has to grow. Hence a higher pinch force is needed if the surface tension is high. For liquids with high surface tension a higher current is necessary to form drops. For smaller surface tension a smaller welding current is sufficient to get a good material transfer.

Influencing parameters:

- Temperature: The surface tension decreases (linear) with increasing Temperature (29).
- Oxygen content: The surface tension of molten metal decreases with increasing Oxygen content (see Figure 3-10). Oxygen is a surface active element such as N and S. Surface active elements are decreasing the surface tension in general. Note that even small amounts of Nitrogen cause pores in Nickel.

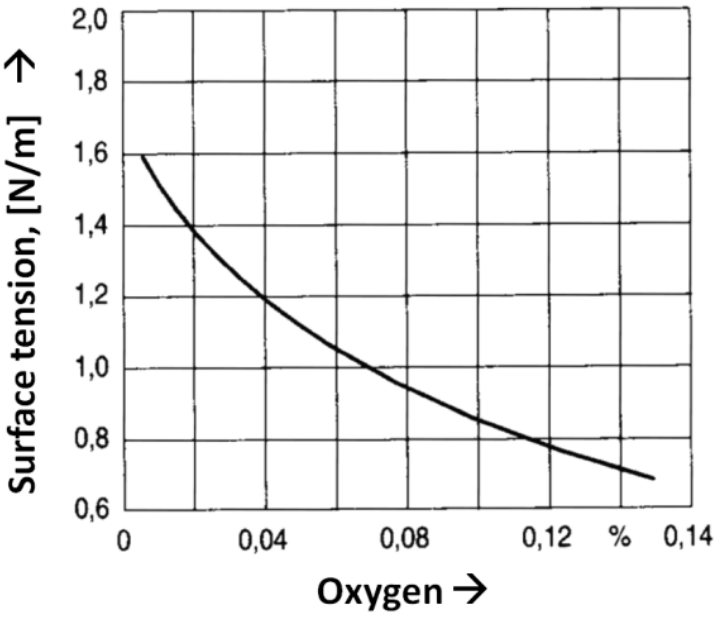

Figure 3-10: Influence of oxygen on the surface tension of molten metals (30)

3.4.1.3 VISCOSITY

Definition:

Viscosity is a measure of the ability of one layer of molecules to move over an adjacent layer of molecules (31).

If the viscosity of the molten metal is high the pinch force also has to be high to form a drop. The drops of flux cored wires are covered with slag, which usually has a higher viscosity than the molten metal at the same temperature.

Influencing parameters:

- Temperature: The viscosity decreases exponentially with increasing temperature. The Arrhenius relationship shown in following equation describes the connection between viscosity and temperature (31)

$$\eta = A \times e^{\left(\frac{E}{R \times T}\right)}$$

Equation 3-5 (31)

A.….Constant
E…..Activation energy
R…..Gas constant
T…..Temperature

- Chemical composition: The chemical composition of the weld metal as well as the composition of the slag is influencing the viscosity of the drop. Figure 3-11: Influence of the TiO2 (rutile) content on the viscosity of the molten slag Figure 3-11 shows as an example how the viscosity can change with different rutile content of the slag.

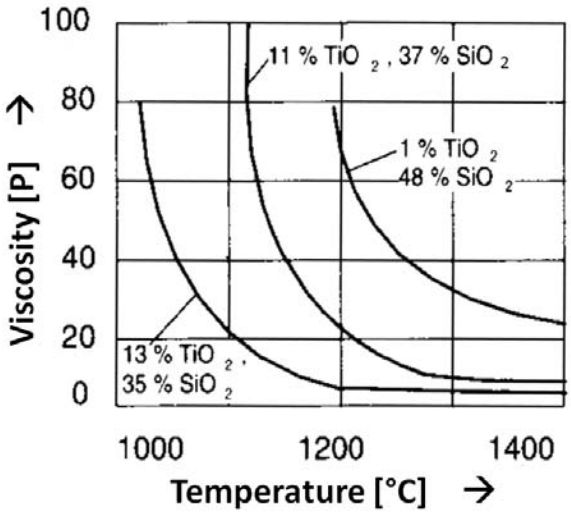

Figure 3-11: Influence of the TiO2 (rutile) content on the viscosity of the molten slag (30)

3.4.1.4 SUCTION FORCES DUE TO THE PLASMA FLOW

(29)

The arc on the weld pool side is broader than the arc on the electrode side, which leads to higher current density on the electrode side. Hence the lateral contraction of the magnetic field is bigger on the electrode side. This leads to a pressure difference inside the arc between weld pool and electrode which causes an axial force that accelerates the plasma. In addition to that the gases which enter the arc are abruptly heated up to temperatures up to 30000 K, which leads to a prompt expansion of the gases and this causes flow speeds in the arc that almost reach the speed of sound.

The plasma flow causes suction forces that can overcome gravity and help separate the drop from the electrode even in overhead position.

3.4.1.5 GRAVITY

(29)

For some welding processes like CO_2 welding the gravity force is very important. For the overhead position other forces have to be active to transfer the drop from the electrode into the weld pool.

3.4.1.6 FORCES THAT HINDER THE DROP TRANSITION

(29)

Another three forces have to be mentioned that hinder the drop transition. The first one is the inertia force. Force is needed to accelerate the drop. The other two are caused by the arc itself. The arc causes static forces which can lift up the drop. The second one is caused by evaporating metal. If the arc overheats the drop the metal starts to evaporate and blows back the drop.

3.4.1.7 CONCLUSION

Overall, the forces supporting the drop transition are stronger, so that depending on the arc form bigger or smaller drops can be transferred to the work piece. Especially for the C-276 PW welding wire this is very important, because it is developed for position welding.

3.4.2 *EXPERIMENTAL INVESTIGATIONS: DROP TRANSITION OF DIFFERENT C-276 FLUX CORED WIRES*

3.4.2.1 EXPERIMENTAL SETUP

The material transfer was filmed with a high speed camera. Following equipment and parameters were used:

- VKT high speed camera plus software
- Nikon lens: focal width 200
- 2500 W spotlight
- UV filter
- Recording rate: 2000 fps

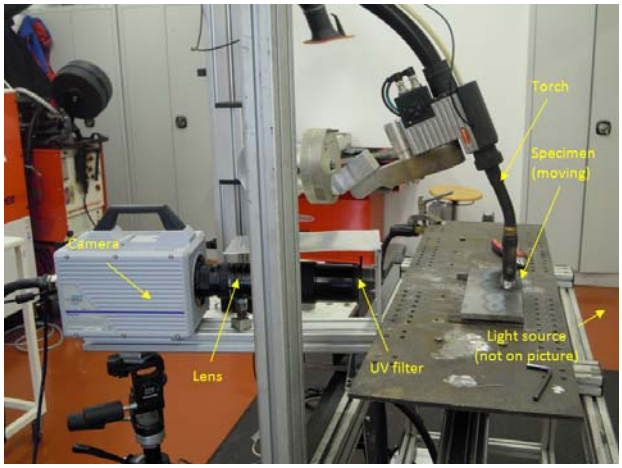

Figure 3-12: Experimental setup for filming the drop transition (TU Graz IWS welding laboratory).

3.4.2.2 DROP TRANSITION OF C-276 IN GENERAL

Exemplarily the drop transition of the C-276 wire is shown here as a picture series. The first picture describes the parts of the drop transition. The following picture series describes the dynamic process of the drop transition. Welding parameters see Table 3-5 page 34.

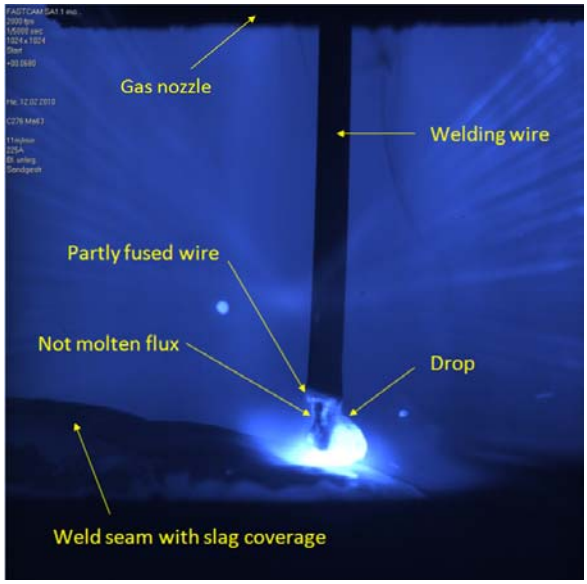

Figure 3-13: The drop transition

The whole drop transition process:

a) 0ms b) 3ms c) 6ms

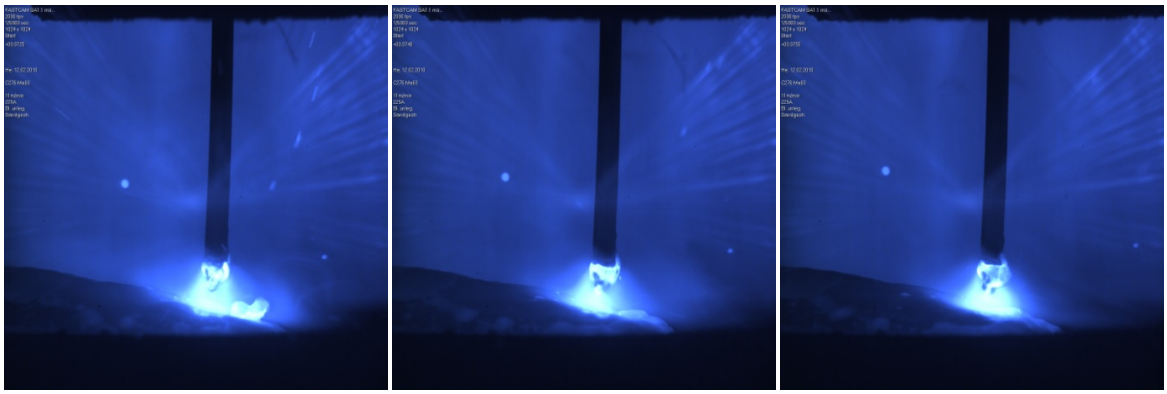

d) 9ms e) 12ms f) 15ms

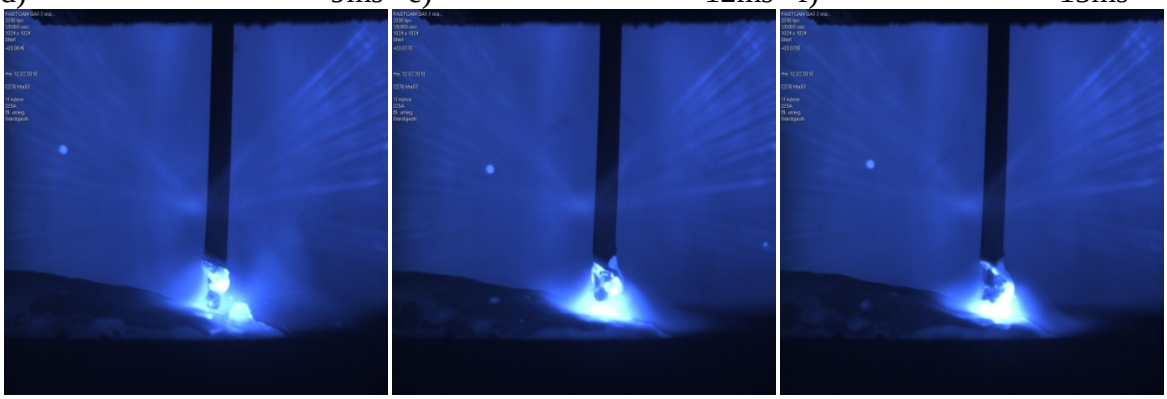

g) 18ms h) 21ms i) 24ms

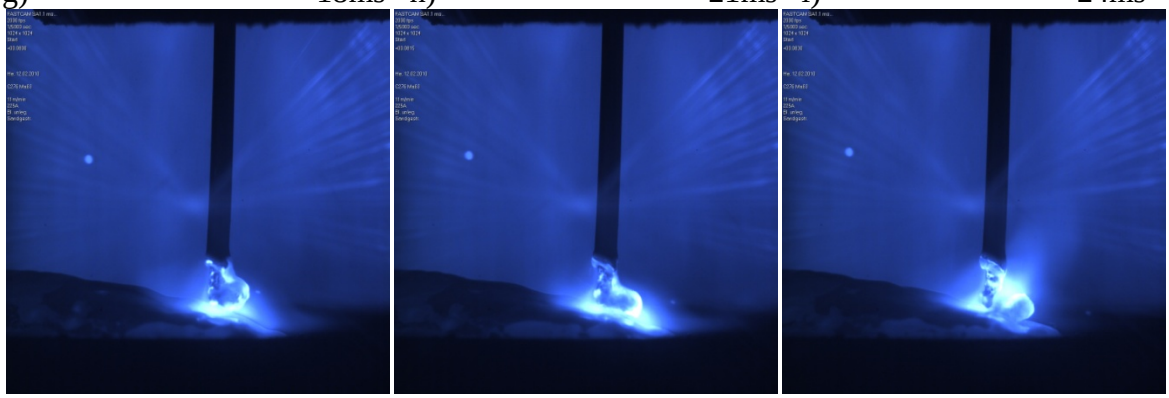

Figure 3-14: Picture series of the drop transition (Masse 63)

This picture series is from a welding trial with the Masse 63 test wire, which is representative for the other test wires and the competition.

It shows the drop transition of one big droplet. The bright dots which are moving away from the welding wire from picture to picture are spatters. The arc is not spatter free because it is an intermediate arc.

Another problem that can be seen here is that the viscosity of the drops is very high. Thus the drop is very big and therefore the drop transition and also the wetting of the base material is not ideal.
A solution would be to increase the welding current. This would increase the temperature on the one hand and the pinch force on the other hand (see 3.4.1 above). The problem is that this would lead to an increased hot cracking risk, because the solidification interval gets longer.
Another solution would be to change the chemical composition of the wire. Raising the oxygen content by for example adding rutile (see 3.4.1.3 above) would lower the viscosity. The problem is that more dimples or slag inclusions will occur. The dimples have a deteriorating effect on the corrosion resistance.

3.4.2.3 DESCRIPTION OF THE TESTED WIRES

Overall five different wires have been tested. All wires have been welded with the same parameters and the same shielding gas:

Travel speed [cm/min]	Wire feed speed [m/min]	Current [A]	Voltage [V]	Shielding gas	Shielding gas flow [l/min]
30	11	225	28.2	Corgon 18	15

Table 3-5: Welding parameters

All noticeable characteristics of each wire are described below. To quantify the drop transition behaviour the drops per second have been counted. It is not easy to count the drops, even with a high speed camera film, because the drop size changes with almost every drop. Still, this drop count is representative for the welding behaviour. The higher the drop count, the smaller the drops, the better the welding behaviour. Good drop transition and good wetting, which is a problem of welding nickel-based alloys, can only be achieved with small drops.
Compared with a normal spray arc, the drop transition is not very steady. The arc type is an intermediate arc for all the tested wires.

Stoody:

The C-276 welding wire from the company Stoody which is also sold under the name Midalloy ENiCrMo-4 is the competitive product. It was kind of a benchmark for Böhler. This analysis will show that the weldability of the analyzed Böhler prototype wires is better.

Counting the drops for one second was especially hard here, because the wire crashed into the weld pool without lighting an arc several times. The reason for this is a short interruption in the electric circle due to contact problems. The coating of the wire could be a reason for the contact problems. The coating should improve the wire feed behaviour.

a) 0ms b) 3ms c) 6ms

d) 9ms e) 12ms f) 15ms

Figure 3-15: Stoody high speed images: wire fracture due to cycle interruption

The result is a wire fracture and a lot of spatter. Some of the positions where the wire crashed can be identified in the final weld.

The drop rate in this case is 26 drops per second. Due to the wire fracture many drops are lost, because the fractured wire does not melt. If only the part where the wire does not crash is

counted and projected to one second the estimated drop count would be around **45 drops per second**, what is quiet coarse. From the tested wires this wire is the one with the worst drop transition.

Masse 63:

Masse 63 turned out to be one of the best. The drop rate is the biggest with **83 drops per second**. The drops are still very big, but compared to the other wires they are smaller. In some parts of the high speed film, the drop transition (frequency and drop size) is very steady, which is good. The problem with the interrupted current does not occur here. This is most probably because this is a prototype wire and therefore it is not coated at all.

Masse 68:

Masse 68 reached a drop count of **67 drops per second**. The drop transition is in the midfield compared to the rest of the wires. One remarkable phenomenon occurred. The wire melts long before it reaches the arc (picture on the right). This is probably because the C-276 band was not folded properly during manufacturing. One manufacturing step did probably go wrong (see chapter 3.2).

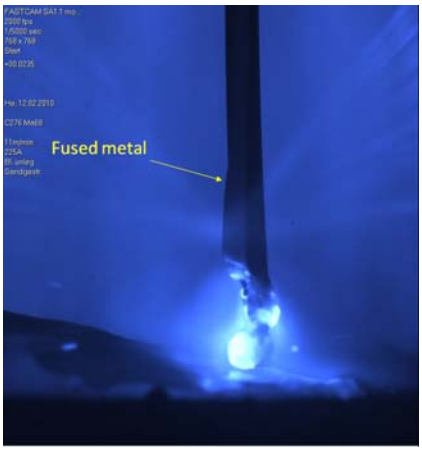

Figure 3-16: Masse 68 HSC captured

Figure 3-17: Wire cross-section Masse 68

Masse 73:

79 drops per second is the drop crate of Masse 73. This is the second best drop count. This test wire also showed some steady drop transition in some moments like Masse 63 did.
The same phenomenon as Masse 68 showed occurred here (picture on the right). The wire melts long before it reaches the arc. In this case it is not that grave compared to Masse 68. The reasons are the same. The test wire was probably not rolled correctly.

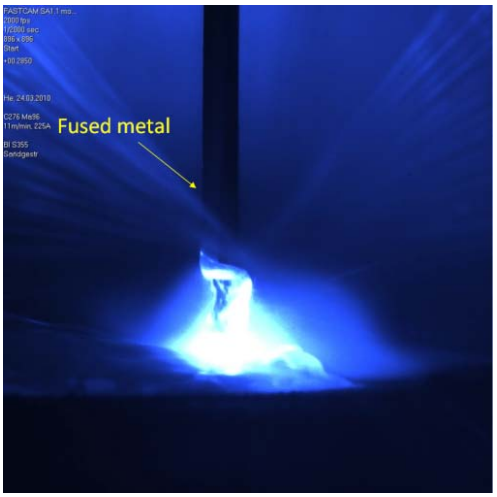

Figure 3-18:Masse 73 HSC captured

Figure 3-19: Wire cross section Masse 73

Masse 90:

This prototype wire shows the same problems as the Stoody wire does. The wire touches the weld pool and breaks or explodes if the arc reignites in this moment. It looks the same as in the picture series of the Stoody wire (see Figure 3-15) for that reason another picture series is not inserted here.
The problem here is probably also the coating. Masse 90 is the only wire of the Böhler test wires that has been stress relief heat treated and coated. Most probably the coating is too thick and therefore the electrical contact in the contact tip is sometimes interrupted and the wire crashes.

The drop count including the crashes is **44 drops per second**. The drop count only counted without crashes is about **70 drops per second**. This wire would certainly show a better welding behaviour with optimized coating.

Conclusion:

Following ranking from best to worst is the result for the melting and drop transition behavior:

- Masse 63
- Masse 73
- Masse 68
- Masse 90
- Stoody

It can be expected that the drop rate of Masse 90 could be improved if the coating is optimized. Masse 63 and Masse 73 are rather similar. There is only a slight difference between the first and second place.

The Stoody wire is the worst. The drop rate is low and the problem with the short circuiting does also occur.

It is very important to mention that this is the classification for this test only. In other categories like mechanical properties or slag coverage or weld appearance the classification could be completely different.

An overview is attached in the appendix and the high speed films are available on the enclosed CD.

4 PORE FORMATION AND NON METALLIC INCLUSIONS

(30)

4.1 DEFINITION OF THE TERM PORE

A pore is a cavity filled with gas. Pores are formed, if the gases cannot bubble out before the metal solidifies.

4.2 CAUSES FOR PORE FORMATION

- Gas evolution: Caused by metallurgical reaction during the cooling down of the weld pool gas can be formed. Usually this gas is CO.
- Decrease of solubility: During the cooling down of the weld the solubility of gases (N, H) decreases and pores are formed.
- Mechanical pore formation: Turbulences are the reason for pore formation.

Factors for the decrease of solubility:

- The decrease of solubility is temperature dependent. It's a directly proportional relationship. The lower the temperature the lower the solubility of the gas.
- Usually there is a big difference of solubility between different phases of a metal. Molten metal can dissolve a lot more gas than solid metal. That means, that the solubility drops, during the solidification of the metal.

The morphology of pores is dependent on:

- Formation mechanism
- Crystallization time / solidifying velocity
- Precipitation velocity
- Growth velocity
- Base material
- Chemical composition of the strip and the filling

4.3 PHYSICAL PRINCIPLES FOR THE PORE FORMATION

4.3.1 RELATIONSHIP BETWEEN FORMATION MECHANISM AND MORPHOLOGY

Chalmers (30) describes the pore formation in the area of the crystallization front. Three different modes are described (see Figure 4-1):

- The gases can escape if the gas bubbles rise faster than the crystallization front solidifies (Figure 4-1a)
- The crystallization front passes the gas bubbles and traps them if the solidifying velocity is bigger than the gas bubbles formation and movement (Figure 4-1b)
- A permanent gas feed of an already formed gas bubble causes an elongation of the bubble in the direction of the solidifying front. The result is a wormhole. (Figure 4-1c)
-

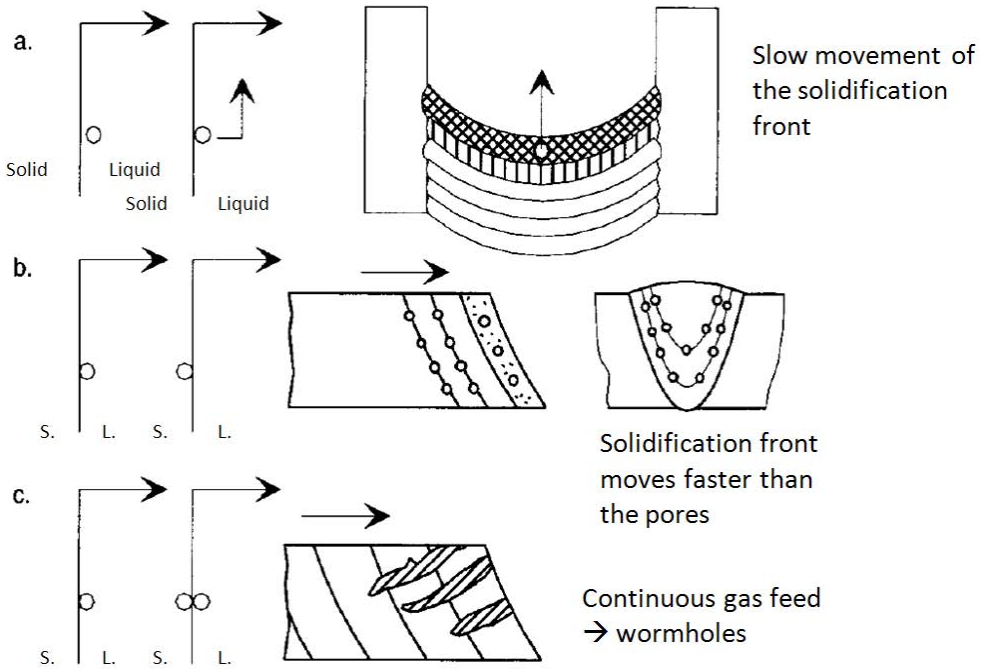

Figure 4-1: Principles of pore formation (30)

4.3.2 FORMATION OF A GAS BUBBLE / WETTING CONDITIONS

The form of a gas bubble is also dependent on the wetting conditions. The wetting angle θ is a parameter to describe the bubble formation. It is calculated with a relationship of interface tensions.

$$\cos\theta = \frac{\sigma_{sp/gas} - \sigma_{sp/fp}}{\sigma_{fp/gas}}$$

Equation 4-1: Wetting angle (30)

θ.....Wetting angle

$\sigma_{sp/gas}$....Interface tension solid phase – gas

$\sigma_{sp/fp}$.....Interface tension solid phase – fluid phase

$\sigma_{fp/gas}$.....Interface tension fluid phase – gas

At θ > 90° the fluid phase wets the solid phase badly (Figure 4-2a). The gas bubble starts to grow till θ < 90. The form of the bubble is oval now (Figure 4-2d and c). When the wetting angle reaches the value zero, the bubble separates from the solid phase.

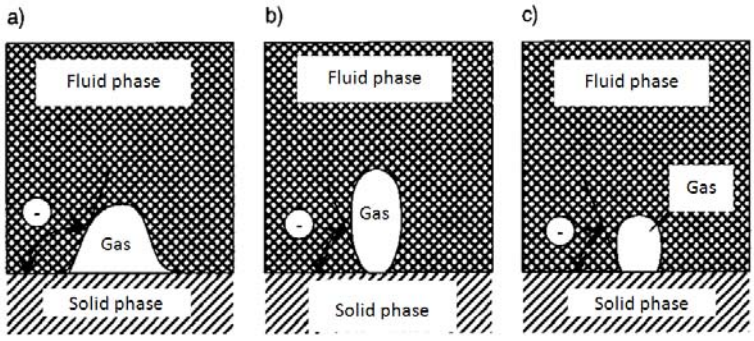

Figure 4-2: Gas bubble forms dependent on wetting condition (30)

The gas bubble is built up and separates from the crystallization front if the solidification is slow enough.

4.3.3 CRYSTALLIZATION VELOCITY

The gas bubble builds up and separates from the crystallization front if the crystallization is slow enough (Figure 4-3a). The gas cavity doesn't separate from the solid phase completely, if the crystallization velocity reaches a certain point (Figure 4-3b).

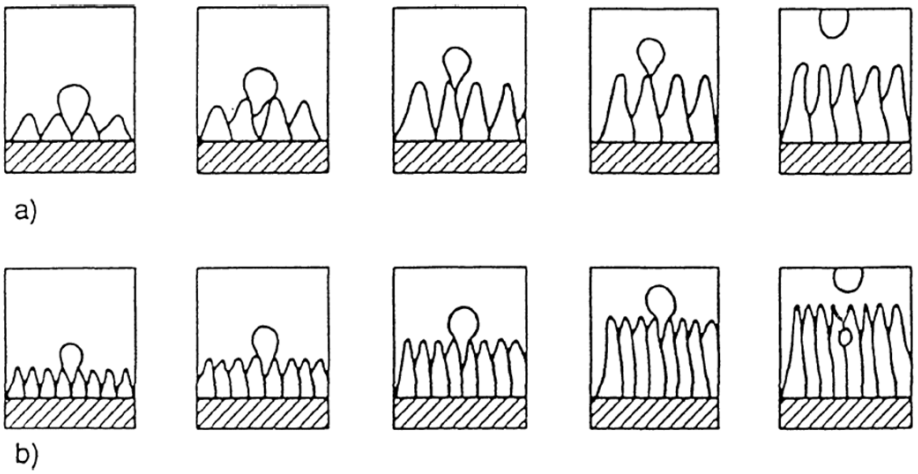

Figure 4-3: Formation of a gas bubble at different crystallization velocities (32)

4.3.4 PARTIAL PRESSURE

For the formation and growth of gas bubbles the inner pressure of the gas bubble has to be bigger than the outer hydrostatic pressure. That means that $\mathbf{p_{Gas}} >> \mathbf{p_{Outside}}$. The outside pressure is defined as follows:

$$p_{Outside} = p_{Atm} + h_1 + \rho_1 + h_2 + \rho_2 + \frac{2 \times \sigma}{r}$$

Equation 4-2: The partial pressure (30)

P_{Atm}....Atmospheric pressure
h_1.....Head of metal above the bubble
h_2.....Head of slag film above the bubble
ρ_1.....Density of the metal
ρ_2.....Density of the slag
σ.....Interface tension gas – liquid metal
r..... Bubble radius

The hydrostatic pressure of the metal and the slag can be neglected because it is very low. This leads to a simplified formula:

$$p_{Inside} \gg p_{Atm} + \frac{2 \times \sigma}{r}$$

Equation 4-3: Pressure inside the gas bubble (30)

P_{Inside}.....Pressure inside the gas bubble
σ.....Interface tension gas – liquid metal
r.....Bubble radius

That means the pressure inside the bubble at the beginning of its formation has to be high, because the bubble radius influences the pressure indirectly proportional.
On the other hand the interface tension between the molten metal and the gas should be as low as possible. Elements that lower the surface tension (see chapter 3.4.1.2, page 28) would not only have an advantageous effect on the drop transition, but also on the degassing of the weld pool.

4.4 AVOIDANCE OF PORE FORMATION IN GENERAL

Pore formation can be avoided by:

- Proper deoxidation of the weld pool.
- Reduction of the N and H solubility by reducing the partial pressure of these gases inside the arc.
- A proper weld pool form can also improve the degassing.
- Welding inside a vacuum chamber.

4.5 NON-METALLIC INCLUSIONS

A non metallic inclusion is formed since it cannot be separated from the weld metal because of certain crystallization- and cooling circumstances during welding. Inclusions which are formed inside the weld pool are called endogenous inclusions. Inclusions which come from the slag (slag inclusions) are called exogenous inclusions.

4.5.1 TYPES OF NON METALLIC INCLUSIONS

- Oxides: FeO, MnO, Cr_2O_3, SiO_2, Al_2O_3, **TiO_2**, $FeO \cdot Fe_2O_3$, $FeO \cdot Al_2O_3$, $FeO \cdot Cr_2O_3$, $MgO \cdot Al_2O_3$, $2FeO \cdot SiO_2$;
- Sulphides: FeS, MnS, Al_2S_3, CaS, MgS, Zr_2S_3, $FeS \cdot FeO$, $MnS \cdot MnO$;
- Nitrides: ZrN, TiN, AlN, CeN
- Phosphates: Fe_3P, Fe_2P

The morphology of non-metallic inclusions depends on:

- Chemical composition of the base material
- Chemical composition of the welding wire
- Coagulation of the inclusions (the ability of the inclusions to unite and grow)
- The velocity of the separation from the fluid weld metal
- The mobility of particles inside the weld pool / viscosity of the weld metal
- The melting temperature and the density of the non-metallic phases
- The turbulence in the weld pool (Marangoni current)

4.5.2 THE COAGULATION

Coagulation, which is also known as the “Ostwald ripening”, describes the growth of precipitates. In this case the precipitates would be the non-metallic inclusions. This phenomenon is also applicable for the pore growth.

Larger particles are energetically more favoured than smaller particles, because of their lower volume to surface ratio. The system tries to minimize its interface energy (also known as interface tension) by forming big particles out of many small ones.

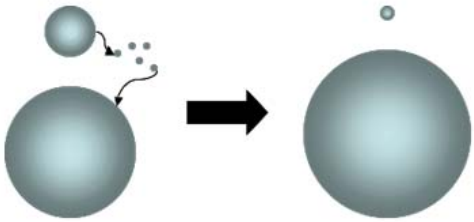

Figure 4-4: Basic principle of the Ostwald ripening

The coagulation properties of non-metallic inclusions are a result of several factors:

- Melting temperature of the non-metallic particles
- Difference between melting temperature of the weld pool and melting temperature of the particles: This is very important for the mobility of the particles. The higher the mobility the better the coagulation of the non-metallic particles. The non metallic particles are not many and small in our case, which means that the coagulation worked well on the surface but the small particles which are included in the solidified weld in the weld pool could not coagulate.
- Interface tension between molten weld metal and particles: This is the basic factor for the coagulation. The higher the interface tension the better the coagulation.
- Viscosity of the weld pool: The viscosity of the weld pool also influences the mobility of the particles. The bigger the viscosity of the weld pool, the worse the coagulation of the particles.

4.6 EXPERIMENTAL INVESTIGATIONS OF: PORES, DIMPLES AND SLAG INCLUSIONS

With the applied welding parameters (see Table 3-5, page 34), no big pores in the weld could be detected. All the tested wires show the same irregularities. Inside the weld there are some very fine pores that are surrounded with slag (~50µm).

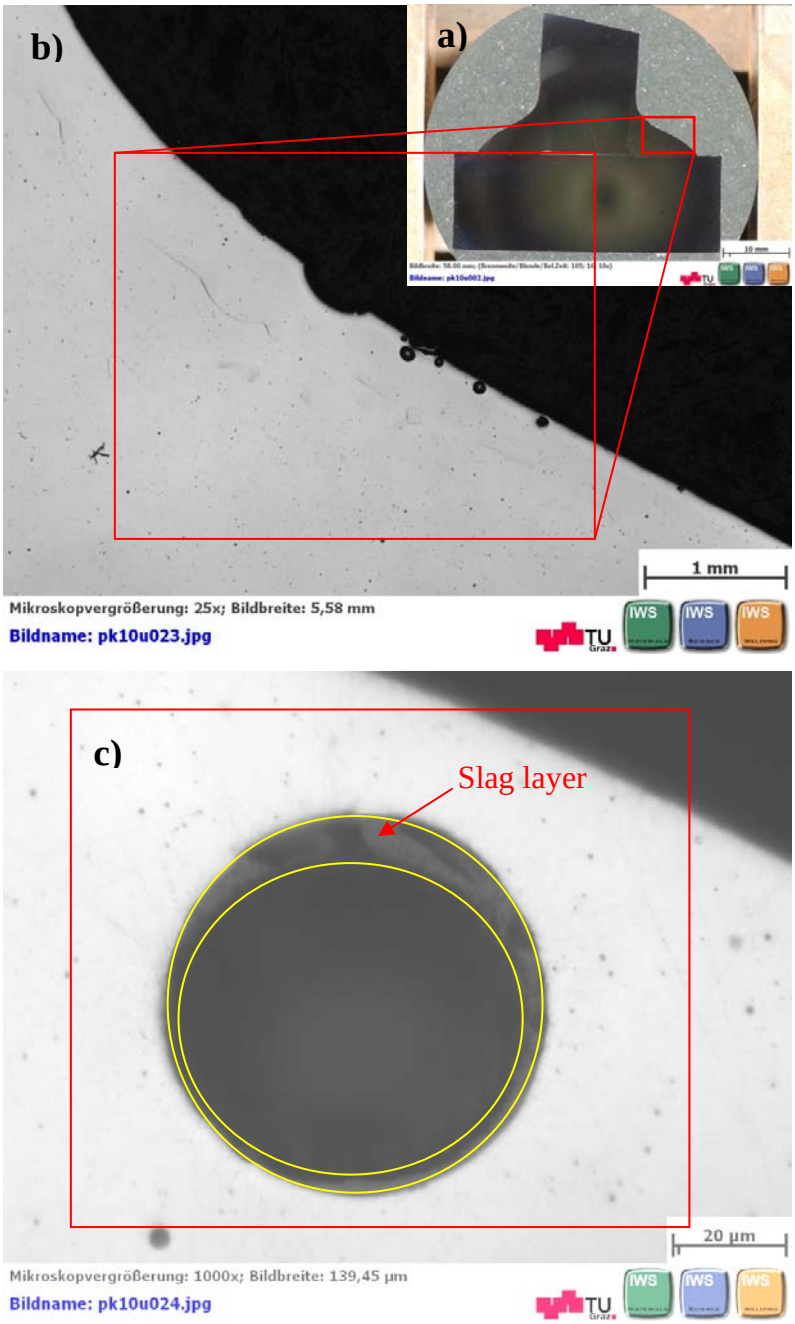

Figure 4-5: Masse 63: Dimples pores and slag inclusions in a fillet weld (S355 base material)

4.6.1 PORES AND SLAG INCLUSIONS

In Figure 4-5 the dimples and pores can be observed in a fillet weld welding trial with the test wire Masse 63. In Figure 4-5c the pore surrounded with slag can be observed. The narrow black seam is the slag. That indicates that the gas inside the pore most probably is carbon monoxide (see chapter 4.2) that was formed due to a metallurgical reaction during cooling-down of the weld. Some of the gas was deoxidized with the deoxidizing elements and formed the slag seam the other part remained as gas pore inside the weld pool.
The very small black dots in Figure 4-4c are very fine dispersed non metallic inclusions, i.e. slag inclusions. Most of the slag coagulates on the surface and the rest of it remains inside the weld pool.

Reasons for pores and slag inclusions (see chapter 4.2, page 39):

- Slag viscosity
- Weld metal viscosity
- Amount of deoxidizing elements (slag builders)
-

4.6.2 THE DIMPLE PROBLEM

The dimples on the surface are imprinted gas bubbles. One half of the gas bubble is imprinted into the weld and the other half of the bubble is imprinted in the slag coverage (see Figure 4-6). These dimples are on the one hand not very advantageous in respect to corrosion, on the other hand wires that cause such dimples are sometimes not accepted by the customer. The dimples turned out to be one of the biggest problems of developing C-276 flux-cored wire.

The reason for the dimples is a simple one. Since this slag should freeze fast to achieve good position weldability there is not enough time for degassing. The gas gets trapped between the weld and the slag coverage.

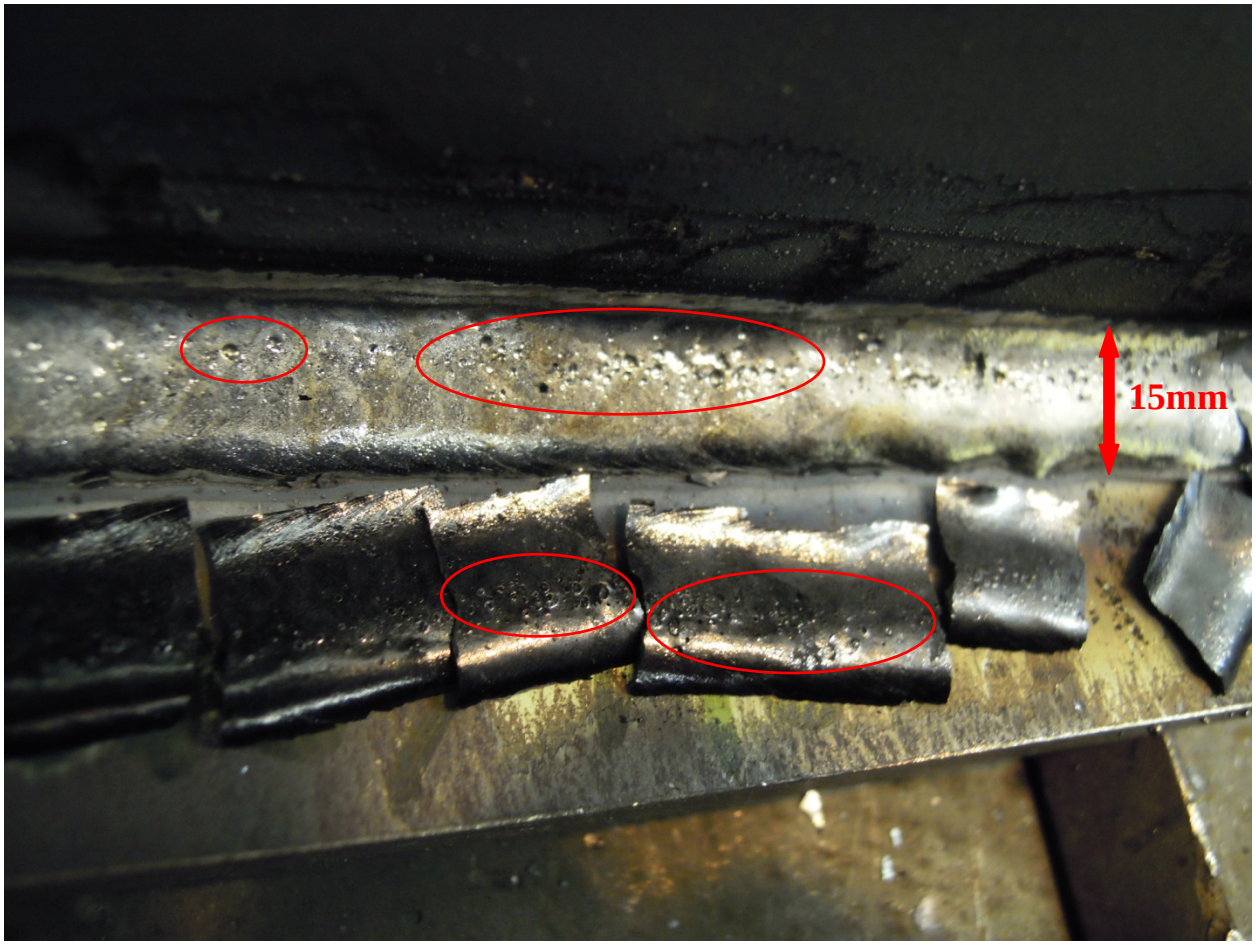

Figure 4-6: Dimples on a fillet weld (Masse 68)

Figure 4-6 shows the dimples very well. The slag coverage has already been removed. As already mentioned one part of the bubble is imprinted in the weld, the other half in the slag coverage.

4.6.2.1 SOLUTION APPROACHES:

- Better degassing with more deoxidizing elements
- Decreasing the weld metal viscosity
- Decreasing the surface tension of the weld metal
- Decreasing the amount of slag coverage
- Changing the slag viscosity

Better degassing with more deoxidizing elements:

Degassing would certainly decrease the amount of dimples and pores, but it would increase the slag inclusions inside the weld, because more slag is built. Another effect is that there is less oxygen in the weld metal and therefore the viscosity increases, which makes the weldability worse (see chapter 3.4.1.3, page 29)

Böhler Welding already tried to deoxidize with adding aluminium and titanium to the filling of the C-276 flux cored wire. The result was a wire with very bad welding behaviour. There was almost no wetting of the weld flanks. The resulting weld was a sequence of big solidified drops (Weiß, Böhler 2010).

Decreasing the weld metal viscosity:

As already mentioned the viscosity is dependent on temperature and the chemical composition. Since the slag influences the drop viscosity, especially the oxygen content decreases the viscosity of the drop, which is surrounded with slag (see Figure 3-11, page 30). A weld metal with lower viscosity has a positive effect on the welding behaviour (drop transition) and it would also be easier for the gas to escape in a more fluid weld pool than in a very viscous weld pool (see chapter 4.3.2, page 40).

The other way would be to raise the temperature. Raising the temperature means raising the welding parameter (current). The energy input per unit length is limited to 11 kJ/cm for GMAW (see 3.3.3.1, page 25). The reason for this limit is the hot cracking risk. With the applied parameters (see Table 3-5, page 34) the limit is not reached. The average heat input for the fillet weld on Figure 4-6: Dimples on a fillet weld (Masse 68) was 9,2 kJ/cm. Raising the parameters would be a good idea to improve the dimple situation.

On the other hand, with respect to hot cracking susceptibility it is the best to keep the parameters as low as possible.

Decreasing the surface tension of the weld metal:

The surface tension, also known as interface tension, influences the wetting conditions as well as the critical pressure that is necessary for pore growth (see Equation 4-3, page 43).
With a smaller wetting angle the pore forms faster. The interface tension between gas and molten C-276 weld metal is directly proportional to the wetting angle (see Equation 4-1, page 41). That means if the surface tension of the molten C-276 weld metal could be lowered the gas would bubble out faster.
The surface tension is dependent on the temperature and the content of surface active elements (see chapter 3.4.1.2, page 28). The dilemma with raising the temperature and the oxygen content has already been explained in the chapter “Decreasing the weld metal viscosity” on page 49. It is exactly the same problem here.
Other surface active elements like nitrogen or sulphur are also very critical. Already very low nitrogen content in nickel causes pores (see chapter 3.4.1.2, page 28). Sulphur forms a low melting eutectic that will certainly cause hot cracks (see Figure 3-5, page 24).

Decreasing the amount of slag coverage:

Another idea for solving the dimple problem is to decrease the slag coverage. Less slag means a lower barrier for the gas bubbles.
As already mentioned in chapter 3.2.2.2 (page 19) the slag builders have the important role of protecting the weld from oxidizing gases. Decreasing slag builders means worse protection of the weld. With less slag the position weldability also becomes worse.
Several tests with different slag amounts carried out by Böhler Welding (Mr. Weiß) showed that the lowest amount possible with respect to protection and position weldability reached the best results (Weiß, Böhler 2010)

Changing the slag viscosity:

This topic is explained in the next chapter, because it was analyzed more in detail.

5 SLAG VISCOSITY

As already mentioned above, the slag viscosity gets special attention. At the TU Bergakademie Freiberg measurements to quantify the viscosity of different prototype wires were carried out.
The results of these measurements are diagrams with viscosity over temperature. These diagrams can be used to find out more about the solidification velocities and viscosity levels at different temperatures.
The slag viscosity is directly connected to the slag inclusions and dimple formation.

5.1 DEFINITION OF VISCOSITY

A basic definition of viscosity has already been given in chapter 3.4.1.3 on page 29. The most common used unit is [Pa.s].
The viscosity of a slag is expected to be a function of the structure of its elements, for example the degree of polymerization of the melt (31). Some elements break up the grid structure of the slag and therefore it freezes slower.

5.2 BASICITY: A MEASUREMENT FOR SLAG VISCOSITY

(20)

There is a connection between the basicity of the slag and its viscosity. It should help to predict the viscosity and the solidification path of the slag.

The slag constituents are divided into three groups:

- Amphoteric oxides: These oxides are either network builders or network breakers in together with a real network builder or breaker.
- Network builders: These oxides improve the polymerization. They tend to build big molecule units.
- Network breakers: Network breaking oxides tend to break up the intermolecular connections.

Network breakers which have a rather high basicity cause a low viscosity at high temperatures (liquid state), see Figure 5-5 on page 57, but the solidification is rather fast. Fast freezing slags contain network breakers. That means that slags with high basicity are fast freezing slags.
In contrast slow freezing slags contain network builders. That means that slow freezing slags are acidic.
In the table below important slag constituents for nickel-based flux cored wires are listed with their optical basicity. With measuring or knowing the basicity of the slag constituents the overall basicity index can be calculated and the solidification behaviour can be estimated.

In the dissertation of Rudolf Vallant (20) the equation for calculating the basicity index for nickel based flux cored wire slags was adapted:

$$B.I. = \frac{CaF_2 + CaO + MgO + Na_2O + K_2O + 0.5 \times (MnO + Fe_2O_3 + Cr_2O_3)}{SiO_2 + 0.5 \times (Al_2O_3 + TiO_2 + ZrO_2 + Nb_2O_5)}$$

Equation 5-1: The adapted basicity index equation after Bauné (20)

A B.I. < 1 means the slag is acidic. Values between 1 and 1.2 are neutral and a B.I. > 1.2 means the slag is basic.

Network builders	**Opt. basicity Λ**	**Network breakers**	**Opt. basicity Λ**
SiO_2	0.48	K_2O	1.40
		Na_2O	1.20
amphoteric oxides		Li_2O	1.05
Nb_2O_5	0.61	CaO	1.00
Al_2O_3	0.65	MnO	0.95
TiO_2	0.65	MgO	0.85
ZrO_2	0.86	Cr_2O_3	0.69
		Fe_2O_3	0.69
		CaF_2	*0.43 / 0.67*

Table 5-1: Classification of oxides (relevant for the welding slag) and recommended optical basicities (20).

It has to be mentioned that this way of determining the slag viscosity is only able to predict trends, because the slag systems are very complex and the temperature changes are very dynamic and not homogeneous. The real slag viscosity and the solidification can only be determined exactly with a viscometer measurement.

5.3 CORRELATION SLAG INCLUSIONS - VISCOSITY

The size of the slag inclusions is dependent on the coagulation. The coagulation itself is dependent on the melting temperature of the slag and the viscosity of the slag compared with the melting point and viscosity of the weld metal. The higher the slag viscosity, the higher the interface tension between slag and molten weld metal, i.e. the better the coagulation. Good coagulation is advantageous if the slag particles don not get trapped in the weld metal. Figure 5-1 and Figure 5-2 show cross sections of Alloy 625 flux core welds. Alloy 625 shows similar welding characteristics and problems as Alloy C-276 that is why these pictures are also representative.

Figure 5-1: Alloy 625 multipass in overhead (PE) position

The white dots in figure 5-1 above are slag inclusions. They are not in the middle of the layers, but on the upper side. The slag coagulates on the lower side (welding side) and on the upper side of the weld. The particles are trapped here, because the slag freezes very fast and the weld metal has a high viscosity. The reason for the upper position of the slag inclusions in the weld is that the slag has a lower density compared to the weld metal, i.e. buoyancy force.

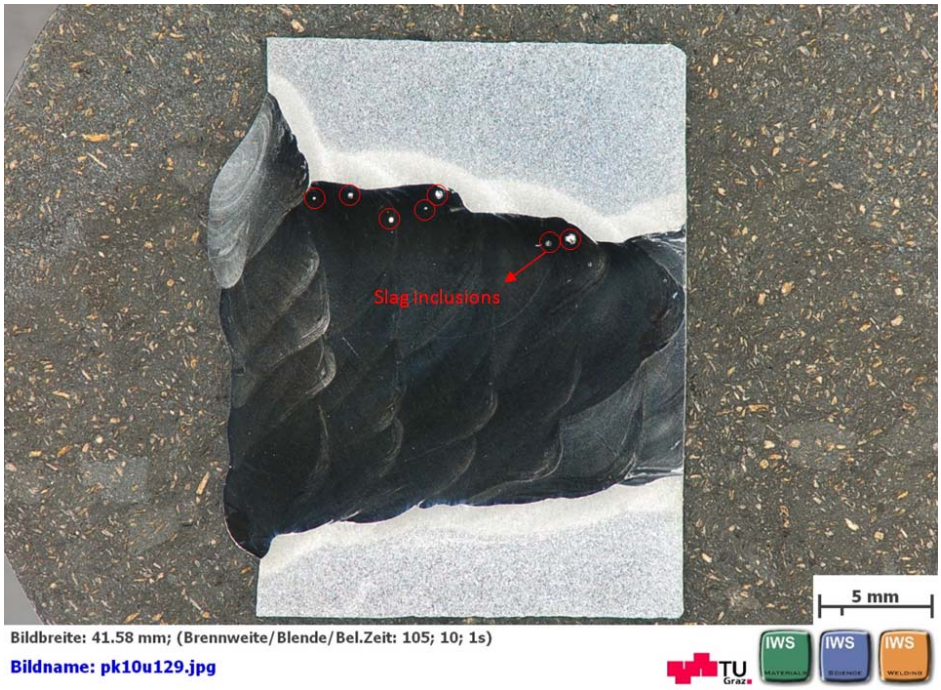

Figure 5-2: Alloy 625 multipass in horizontal vertical position (PC)

The weld in horizontal vertical position (PC) has the slag inclusions mainly in the layers on the upper side. The weld x-sectional shape of the affected layers is different than the shape of the other layers. The surface of the affected layers faces to the lower side. That means that the lighter slag has problems to coagulate on the surface, because the surface direction is slightly opposed to the gravity direction. The other layers have a weld surface which is slightly inclined to the upper side, which makes it easier for the slag to coagulate completely on the surface. Therefore there are no slag inclusions in these layers.

5.4 CONNECTION DIMPLES - VISCOSITY

What is more important concerning the development of the C-276 flux core is the dimple problem. Welding wires for position welding usually have a very fast freezing slag. The slag works as weld pool support, i.e. that the slag always has to be solid before the weld metal solidifies. The solidification interval of the slag is very important in respect to the dimple formation. The slower the slag freezes, the longer the time for the gas to bubble out. That means that a short solidification interval causes more dimples. On the other hand the shorter the solidification interval, the better the position weldability.

5.5 MEASURING METHOD

(31)

Following methods are applied for determining the viscosities of slags:

- Capillary method: The time required for a liquid to flow through a capillary tube is determined.
- Falling body method: The time for a body to fall because of gravity or to be dragged upwards through the melt is determined.
- Rotation method: Described below
- Oscillating method: Described below

At the TU Bergakademie Freiberg two slag viscometers are available. One works with the rotation method, the other uses the oscillating method.

5.5.1 VIBRATION VISCOMETER

The setup of a vibration viscometer is shown in Figure 5-3. The rotating cylinder on the picture is a rotating cylinder. The cylinder oscillates with the same amplitude in both directions. With increasing viscosity the energising current has to increase too to reach the same amplitude. That means that the energising current is directly proportional with the viscosity. The energising voltage, which is proportional to the energising current, is measured and with this value the viscosity is calculated.

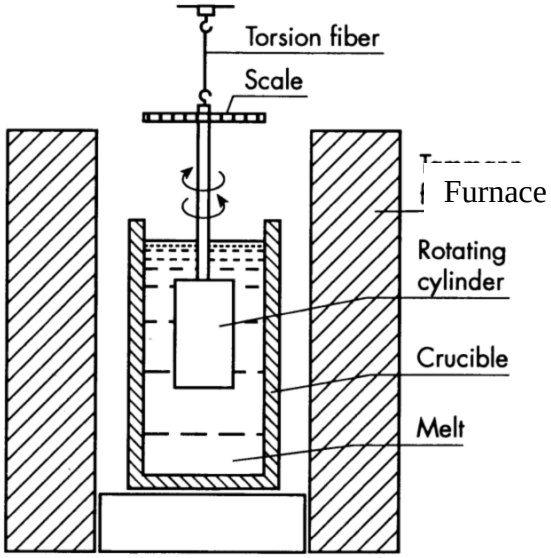

Figure 5-3: Oscillating viscometer (31)

5.5.2 ROTATION VISCOMETER

The rotation viscometer is also shown in Figure 5-4. The rotating cylinder in the picture below is a molybdenum cylinder in our case. This viscometer works similar to the vibration viscometer. The energising current is directly proportional to the torque. The higher the necessary torque is to reach a certain number of revolutions the higher the energising current. The energising voltage, which is proportional to the energising current, is measured and the slag viscosity is calculated.

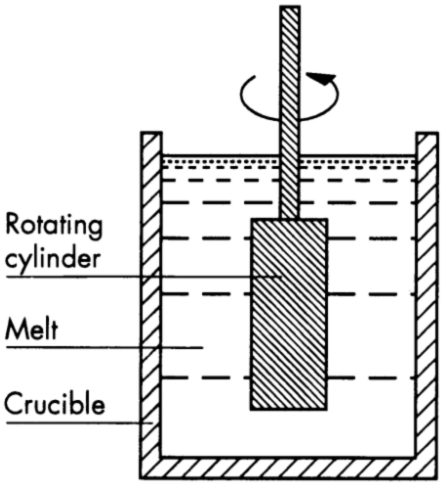

Figure 5-4: Rotation viscometer (31)

5.5.2.1 EXPERIMENTAL MEASUREMENT AT TU BERGAKADEMIE FREIBERG

All our measurements have been carried out with a rotation viscometer. The slag was heated up in the molybdenum crucible and then the molybdenum paddle was inserted and started to stir. A very important thing is the protection of the crucible and the paddle from atmospheric gases. The chamber where the crucible is placed is filled with inert gas to avoid the oxidation of the molybdenum parts.

With the cooling rate of 20 K/s the slag was cooled down till solidification and the viscosity was measured.

5.6 SLAG VISCOSITY CURVES AND THE INFLUENCE ON WELDING BEHAVIOUR

(20)

In this chapter the important characteristics of viscosity curves are explained, to describe the influence of the slag viscosity on welding behaviour.

A typical viscosity curve is given below to explain what the main characteristics are.

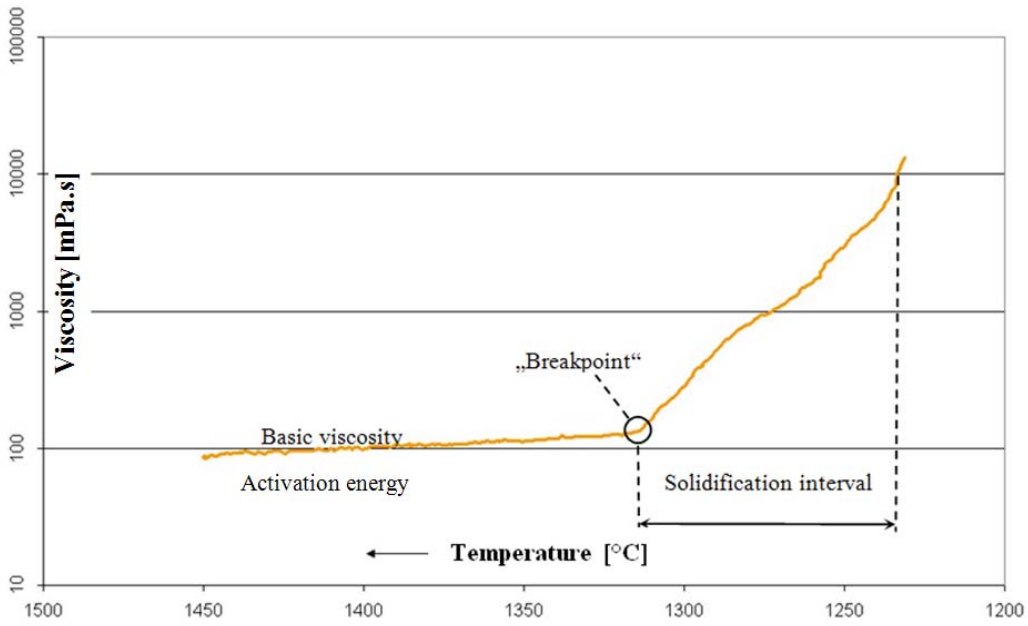

Figure 5-5: Typical viscosity-temperature curve of a slag remelt (20)

5.6.1 BASIC VISCOSITY

The basic viscosity is the viscosity of the slag in the thin fluid state i.e. without precipitation of particles or crystallites. This characteristic influences mainly the slag coverage in the downhand position (PA). The lower the basic viscosity, the worse the slag coverage in the middle of a butt weld or bead on plate weld welded in downhand position.
The increase of viscosity with decreasing temperature can be described with the Arrhenius law (see chapter 3.4.1.3, page 29) until the “breakpoint” temperature is reached.

5.6.2 THE BREAKPOINT

The breakpoint marks the temperature where the slag starts to solidify. At this temperature particles and/or crystallites start to precipitate and grow. Fast freezing slag precipitates are mainly crystallites. Slow freezing slags significantly change the mobility of the silicon grid.

5.6.3 THE SOLIDIFICATION INTERVAL

The solidification interval is the temperature difference between breakpoint and the absolute solidified slag. The viscosity of 10000 [mPa.s] marks the point of absolute solidification in our case. This interval is the most important parameter, because it is used to classify the slags (fast freezing/slow freezing). A short interval means it is a fast freezing slag and a long solidification interval means it is a slow freezing slag. Everything in between is called intermediate freezing slag.

5.6.4 VISCOSITIES OF DIFFERENT FLUIDS

To make it easier to imagine the viscosity values given in the diagrams here are some viscosities of different fluids.

Fluid	Water (20°C)	Motor oil (25°C)	Honey
Viscosity [mPa.s]	1	100	10000

Table 5-2: Fluid viscosities

5.6.5 CHARACTERISTIC SLAGS

Figure 5-6 shows characteristic types of slags. (3) is a very fast freezing slag, (2) is an intermediate freezing slag and (1) is a slow freezing slag.

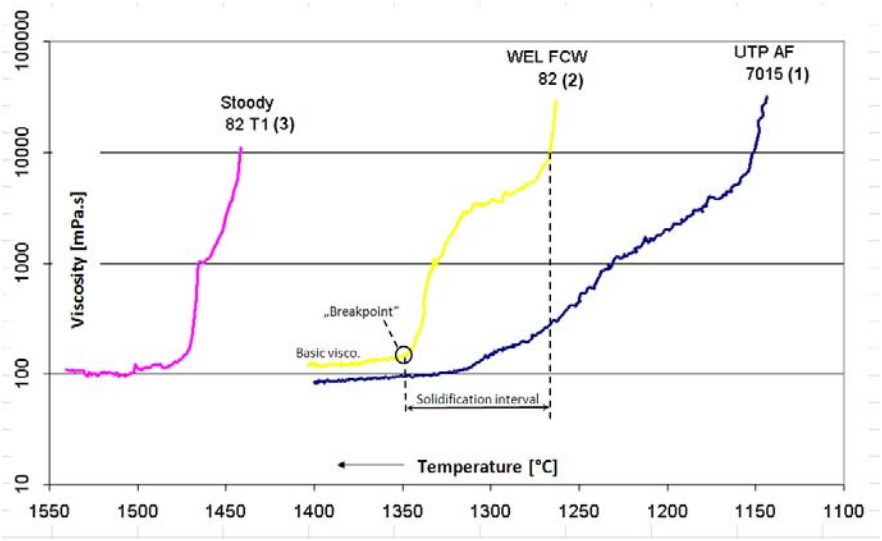

Figure 5-6: Viscosity-temperature curve of different nickel based flux cores (20)

The basic viscosity of slag (3) is rather low and the solidification interval is very small (~ 40°C), i.e. that the slag flows to the edge of the weld in downhand position. It has to be mentioned that not only the viscosity influences this phenomenon, but also the flow (Maragoni flow) in the molten weld metal. The latter depends on several factors like chemical composition, but this topic is not to be described in detail within this thesis. In the middle of the weld the slag coverage is poor and as a consequence the weld metal oxidizes. As already mentioned for position welding the short solidification interval is advantageous. Due to the short solidification interval it is more likely that undesired surface dimples appear (see chapter 5.4, page 55). It is a typical fast freezing slag for position welding.

Slag (1) also has a low basic viscosity, but it solidifies completely different. The breakpoint is at 1325 °C and the solidification interval is approximately 160 °C. That means that this slag can not be used for position welding, because it will not support the weld metal due to the long solidification interval. On the other hand, there are no dimple problems reported with this kind of

slag (Weiß, Böhler 2010). Due to the slow freezing of the slag, the gas (pores) has enough time to escape. This is a classical slow freezing slag for downhanded welding.

Slag (2) is an intermediate freezing slag. It starts to solidify at 1350°C and the solidification interval is 80°C. Remarkable is also the solidification path of this slag. It freezes fast at the beginning, slows down in the middle of the solidification interval and finishes freezing fast again. This S-curved solidification enables fair position weldability as well as good downhand weldability. The dimple problem, which occurs with fast freezing slag and viscous weld metals (nickel based, high alloyed, duplex), could probably be handled with such kind of slag.

5.7 EXPERIMENTAL RESULTS

Three different C-276 welding wires have been analyzed with respect to slag viscosity. Therefore the slag of the C-276 welding trials has been collected and sent to the TU Bergakademie Freiberg for the viscosity measurements.

Following C-276 welding wire slags have been tested:

- Stoody C-276
- Masse 90 with C-276 VDM strip
- Masse 90 with C-276 Arcelor Mittal strip

The difference between the two prototype wires (Masse 90) is the metal strip. The chemical composition of the strips is different but the flux composition is exactly the same.

In addition other slags from other wires have been tested. All results are attached in the appendix. In this chapter only the C-276 slags will be discussed in detail.

5.7.1 C-276 WELDING WIRES

5.7.1.1 STOODY C-276

The slag from this wire shows following characteristics:

Stoody C-276	Basic viscosity [mPa.s]	Breakpoint [°C]	Solidification interval [°C]
	10	1405	15

Table 5-3: Stoody C-276: characteristic solidification parameters of the slag

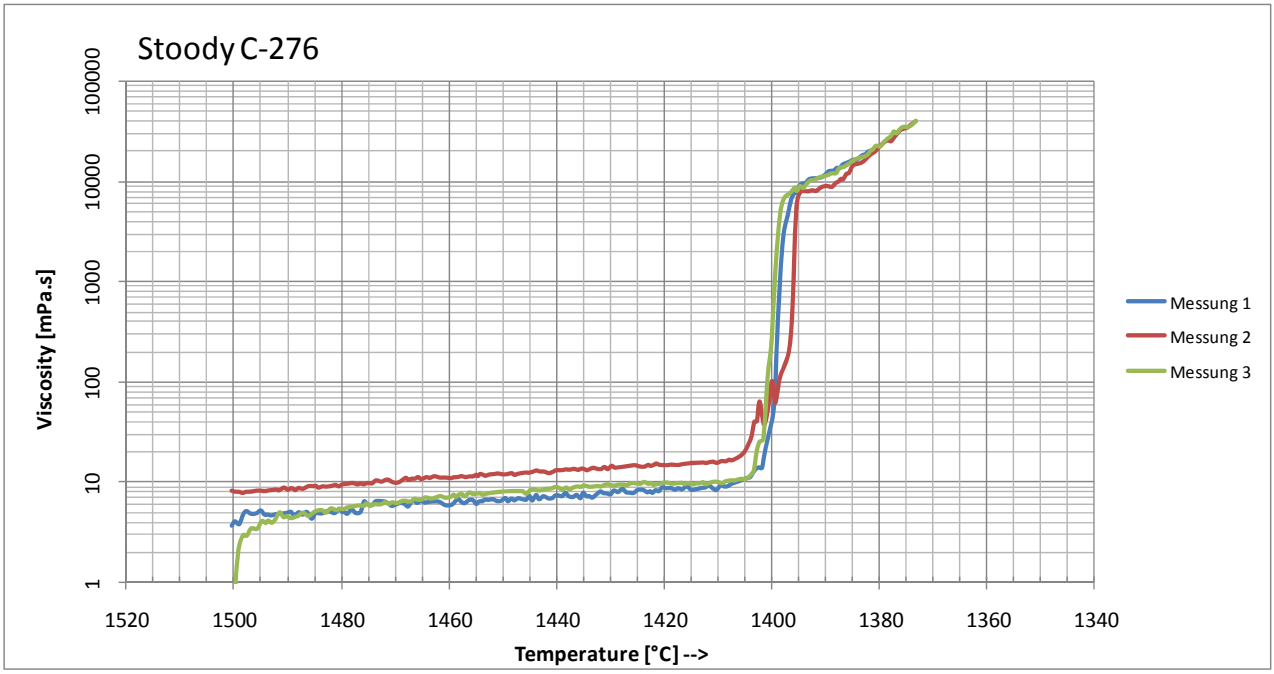

Figure 5-7: Viscosity-temperature curve of Stoody C-276

Interpretation:

This slag shows the typical position slag solidification curve (see chapter 5.6, page 57). It is a fast freezing slag with a basic viscosity which is very low (>10mPa.s). There are more dimples in the downhand position (PA) welds compared to the other two test wires (Masse 90). This is in agreement with the described theory from above (see chapter 5.6, page 57). The gas has no time to escape and forms dimples.

The breakpoint is an intermediate one compared with the other two slags.

5.7.1.2 MASSE 90 WITH VDM STRIP

The slag from this wire shows following characteristics:

Ma 90 with VDM strip	Basic viscosity [mPa.s]	Breakpoint [°C]	Solidification interval [°C]
	150	1430	65

Table 5-4: Masse 90 VDM strip: characteristic solidification parameters of the slag

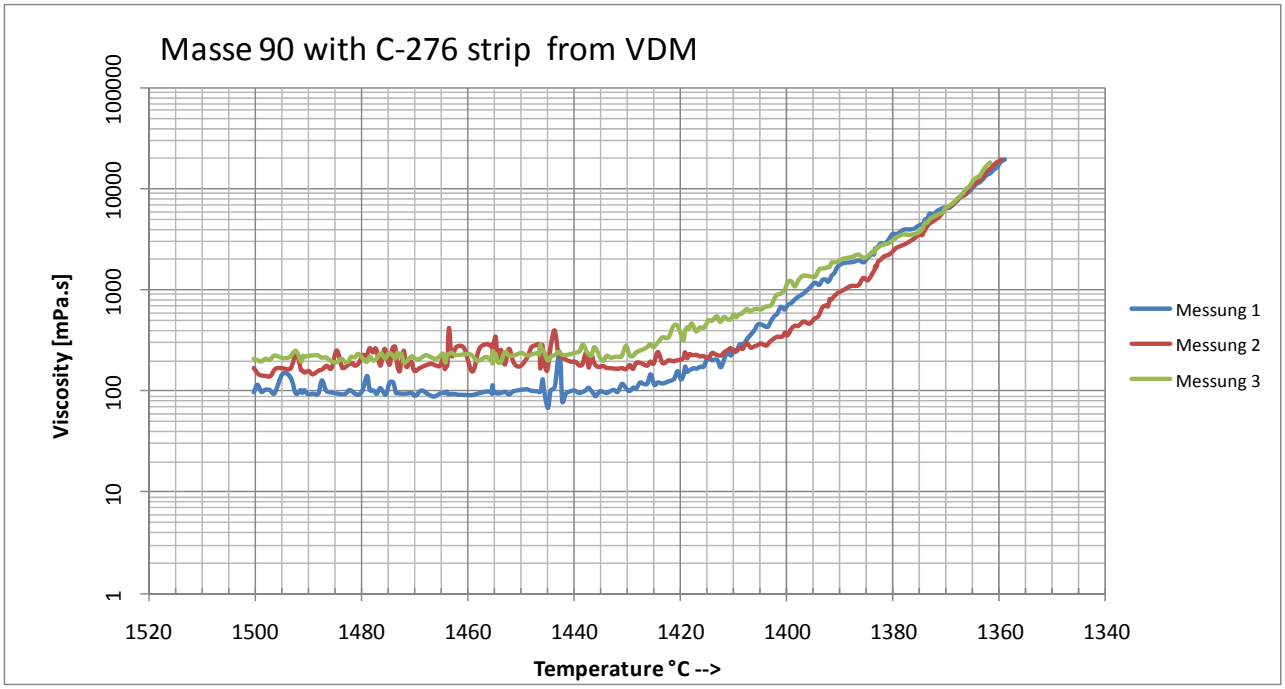

Figure 5-8: Viscosity-temperature curve of Masse 90 with VDM strip

Interpretation:

This measurement shows some scatter. The basic viscosity is the highest and the solidification interval is the longest compared to the other two C-276 slags. It shows the characteristics of a slow freezing slag which are higher basic viscosity and a longer solidification interval.

The number of dimples was the lowest compared to the other two welds. That is probably because the gas pore has more time to bubble out due to the longer solidification interval.

5.7.1.3 MASSE 90 WITH ARCELOR MITTAL STRIP

The slag from this wire shows following characteristics:

Ma 90 with Arcelor strip	Basic viscosity [mPa.s]	Breakpoint [°C]	Solidification interval [°C]
	35	1395	40

Table 5-5: Masse 90 Arcelor Mittal strip: characteristic solidification parameters of the slag

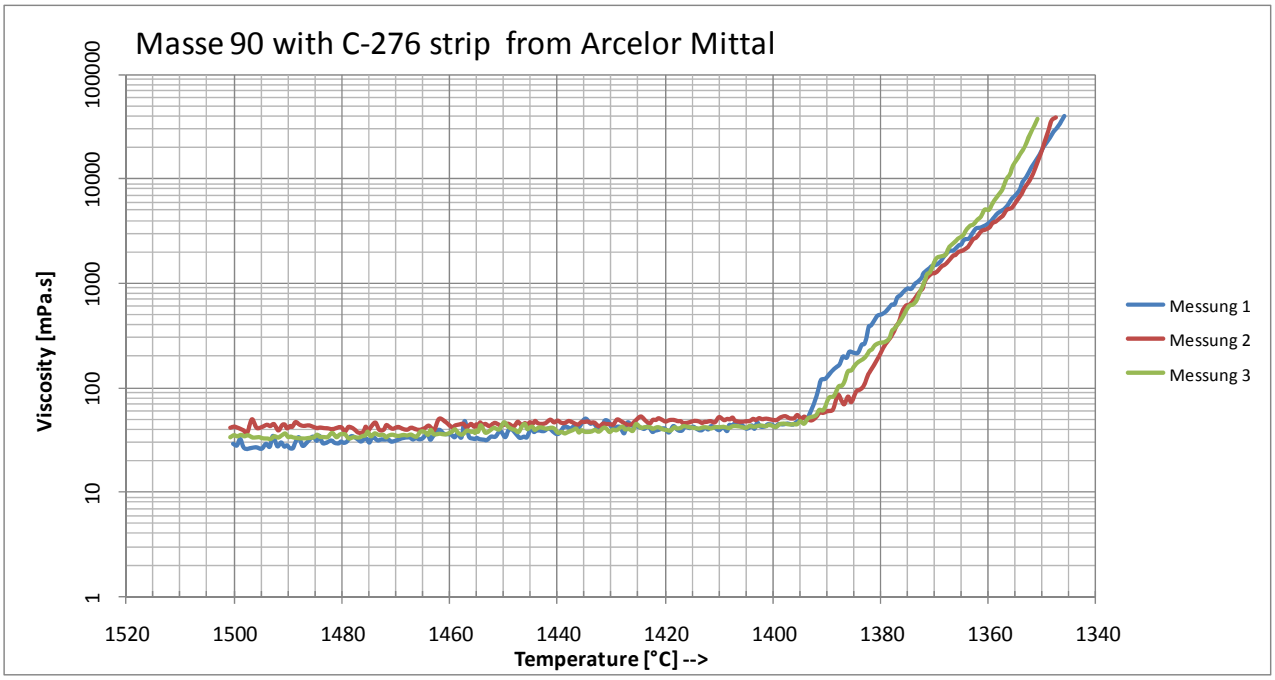

Figure 5-9: Viscosity-temperature curve of Masse90 with Arcelor Mittal strip

Interpretation:

This slag has the lowest breakpoint. The basic viscosity is lower compared to Masse 90 with the VDM strip. The solidification interval is 20°C shorter than the one of Masse 90 with VDM strip. It is an intermediate freezing slag. It is certainly not a typical slag for position welding.

On these weld a little more dimples appeared than on the welds of the other Masse 90. This is probably because the solidification interval is shorter.

5.8 METAL SOLIDIFICATION – SLAG SOLIDIFICATION

In this chapter the solidification of the metal is compared with the slag solidification. Three wires have been analyzed: Stoody, Masse 90 with VDM strip and Masse 90 with Arecelor Mittal strip. The upper graph is a Scheil simulation of the weld metal. This simulation is explained later in chapter 6.2. It describes the solidification of the weld metal. The graph below is the slag solidification curve measured at the TU Bergakademie Freiberg. The red lines on the right side (see Figure 5-10) mark the solidification interval of the slag. The red line at the 1300°C mark is just for orientation.

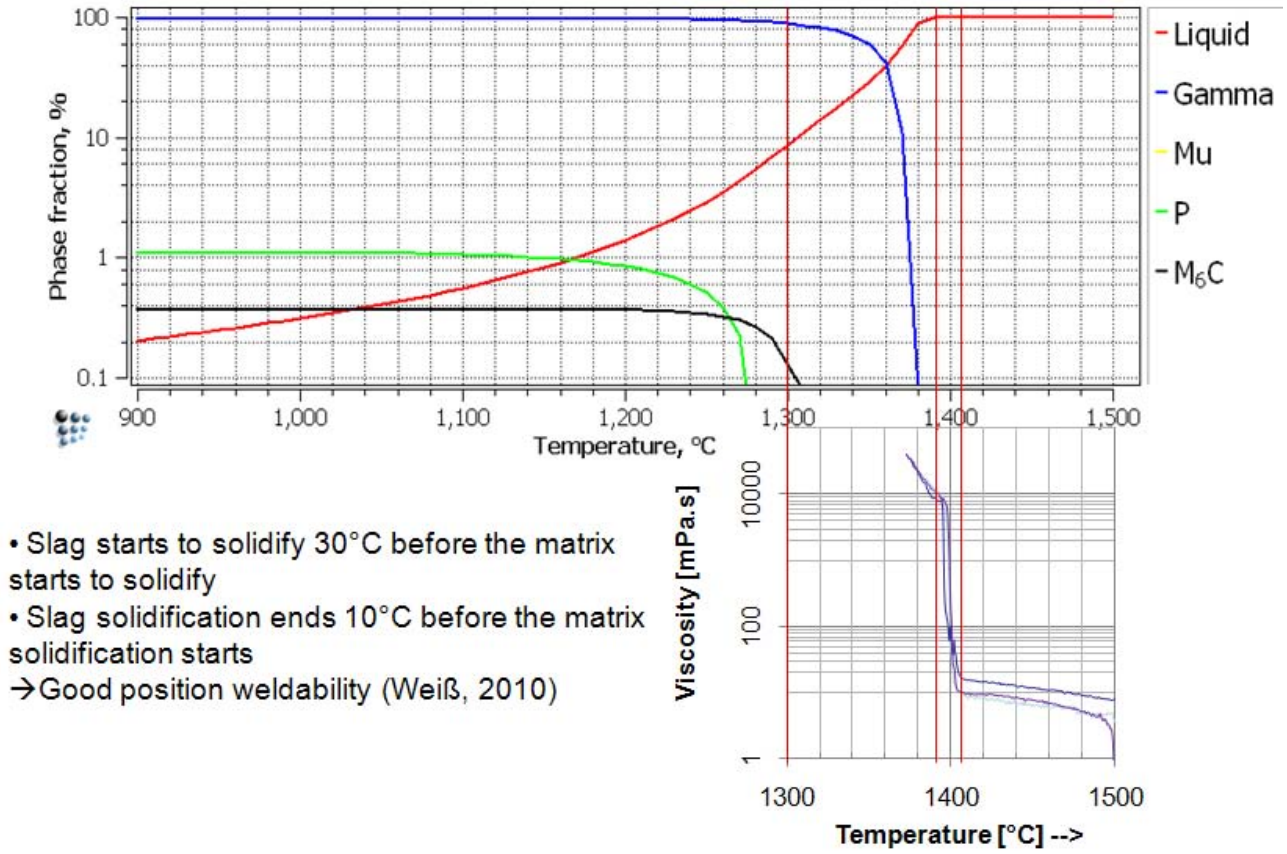

Figure 5-10: Stoody: solidification of the weld metal compared to the slag solidification

The Stoody comparison shows the ideal combination for position welding, but there is no possibility for the pores to bubble out. This wire shows the most dimples.

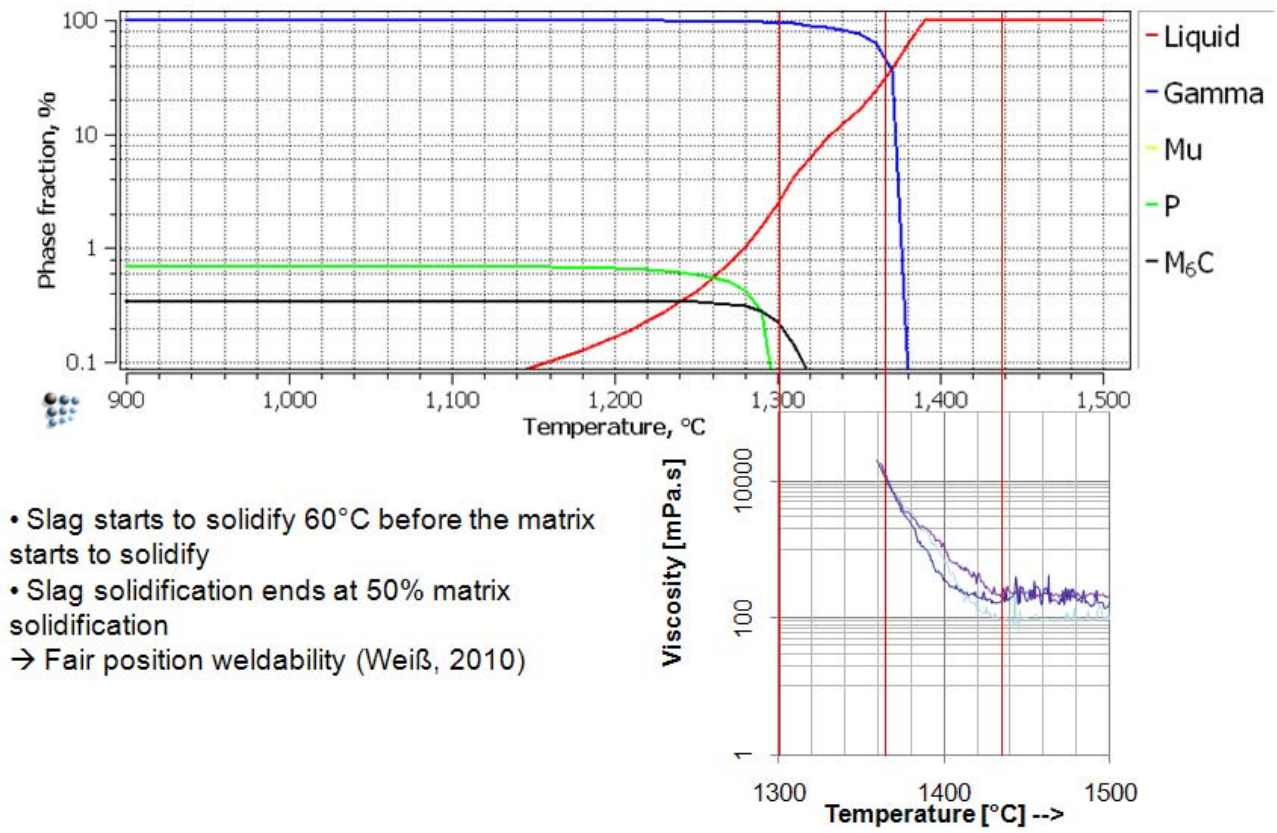

Figure 5-11: Ma90 VDM strip: solidification of the weld metal compared to the slag solidification

The slag of Masse 90 with VDM strip starts to solidify rather early compared to the other two wires. There is more time for metallurgical reactions. The position weldability is fair (Weiß, 2010), because the slag solidifies rather slowly for a position slag.

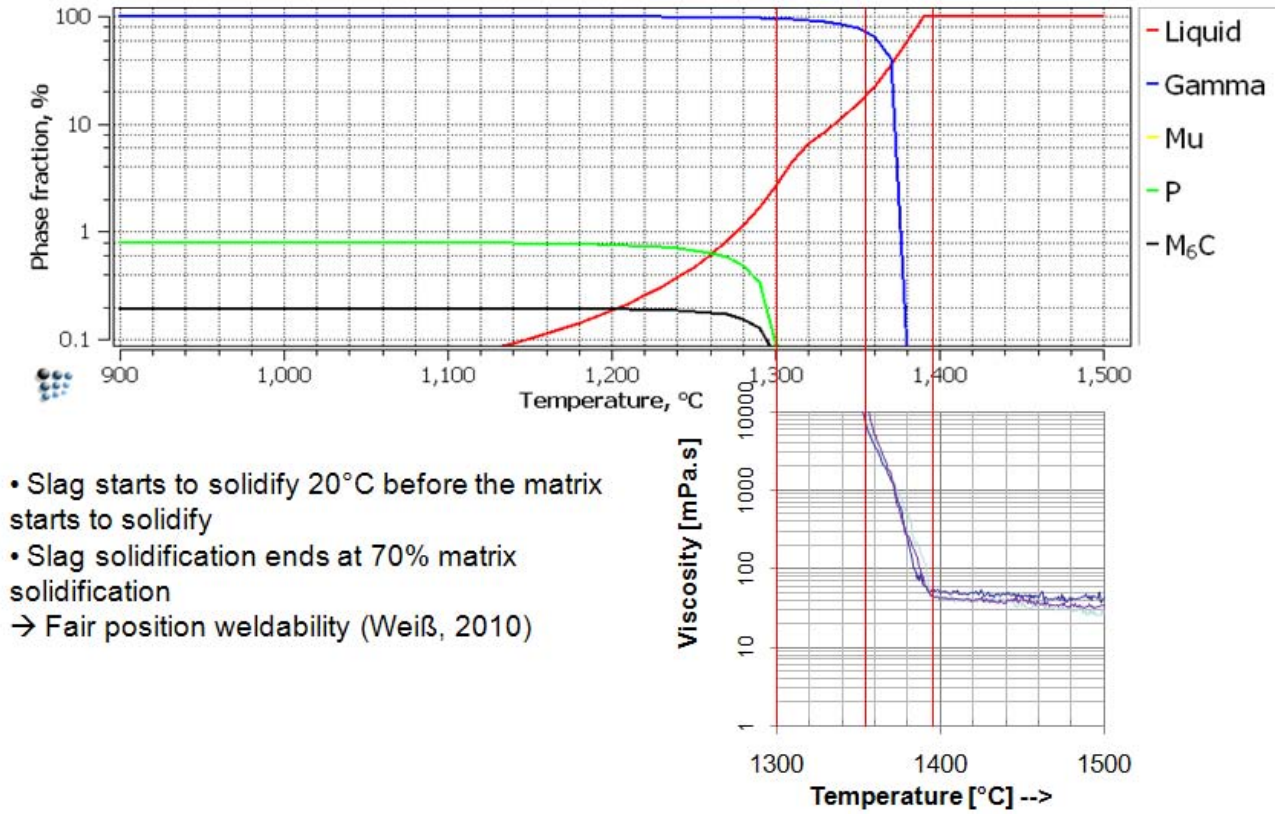

Figure 5-12: Ma90 AM strip: solidification of the weld metal compared to the slag solidification

This comparison shows that the slag solidifies rather fast, but too late compared to the weld metal. That is exactly what should be avoided. The slag solidification should start earlier (at higher temperatures) and the solidification interval should be longer (broader temperature range). The result with respect to dimple formation would be better with the same position welding behaviour.

5.9 CONCLUSION

According to the welding trials of Böhler Welding (Weiß) the classification in respect to dimple formation is as follows: Masse 90 with VDM strip showed the lowest number of dimples, Masse 90 with Arcelor Mittal strip showed a medium number of dimples and Stoody C-276 showed the most dimples. This correlates with the solidification interval, i.e. the shorter the interval the more dimples appear.

The number of dimples seems to correlate with the time for the pore to bubble out. This is in agreement with the theory described above (see chapter 5.6, page 57).

The breakpoint most probably also has an influence on the dimple formation, because it determines the temperature where the solidification starts, but it is not as important as the influence of the solidification interval, otherwise Masse 90 with VDM strip would show more dimples.

The Masse 90 slags do not show the solidification behaviour of a typical slag for position welds. According to Mr. Weiß the solidification interval is at the lowest limit for position welds, i.e. that a slower freezing slag would not be applicable for position welds.

Since the solidification interval is the key to the solution of the dimple problem this is bad news. A slower freezing slag would leave enough time for the pore to escape, but it cannot support the molten metal. Thus the physical limit of the slag viscosity for adequate position welding behaviour is reached. From this point of view the dimple problem can most probably not be solved completely.

Another possibility would be the use of two different slag systems. One for position welds and one only for downhand position welds. But that would lead to two different wires, which wouldn’t be very handy. This solution would probably not be accepted by the customer.

6 MATCALC SIMULATION

In this chapter three different calculations are carried out with MatCalc version 5.31.:

- Equilibrium calculation
- Scheil calculation
- Precipitation simulation in the HAZ (Heat affected zone)

It starts very simple with the equilibrium calculation and becomes more accurate for the welding process with the Scheil- and kinetics- calculation

For each calulation method the physical preconditions are explained. This explanation is followed by the simulation results for the different compositions and an interpretation of the results. The different simulation compositions of the weld metal are given in Table 6-1 to Table 6-4. The minimum, medium and maximum values are based on the AWS classification for ENiCrMo4 weld metal, since this product is developed for the american market. The calculations should show tendencies in phase formation with changing composition. The four main elements that are changed for each simulation are Chrome, Iron, Molybdenum and Tungsten. Hence in each calculation there are four comparisons of different compositions. Each comparison should show the influence of one of the alloying elements mentioned above.
The first composition is the minimum composition. Then the chrome content is set to a medium value and finally to a maximum value. The other alloying elements are not changed. That should show the influence of Chromium on the phase formation.
This is carried out for the other three main alloying elements as well.

6.1 THE EQUILIBRIUM CALCULATION

Physical preconditions and reasons:
The precondition for an equilibrium calculation is an infinite slow cooling rate. The more dynamic the process, the less the reality will match with an equilibrium calculation. FCAW is a very dynamic welding process, i.e. fast heating and cooling rates.

However the reason why this calculation is carried out, is because tendencies in phase formation can be seen even with a simple equilibrium calculation. Another reason is that alloy C-276 includes many alloying elements, and therefore cannot be represented with a simple ternary system. With Matcalc it is possible to calculate the phase fractions for each temperature.

In the following calculation, the Chromium content is changed according to Table 6-1: Cr composition variants.

6.1.1 CHROME COMPOSITION VARIANTS

Limits	C	Co	Cr	Fe	Mo	Ni	Si	W	Al	Ti
minimum	0.015	0.2	14.5	4.0	15.0	balance	0.20	3.0	0.03	0.08
medium	0.015	0.2	15.5	4.0	15.0	balance	0.20	3.0	0.03	0.08
maximum	0.015	0.2	16.5	4.0	15.0	balance	0.20	3.0	0.03	0.08

Table 6-1: Cr composition variants

Minimum composition:

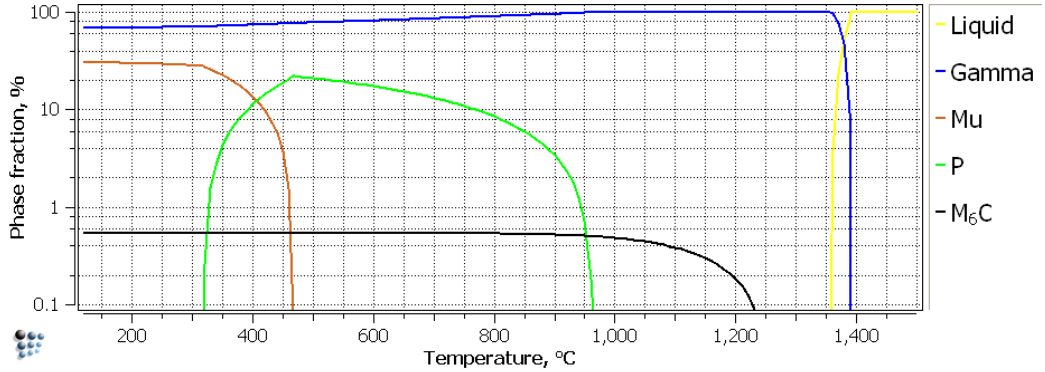

Figure 6-1: Equilibrium minimum composition

Medium Cr content:

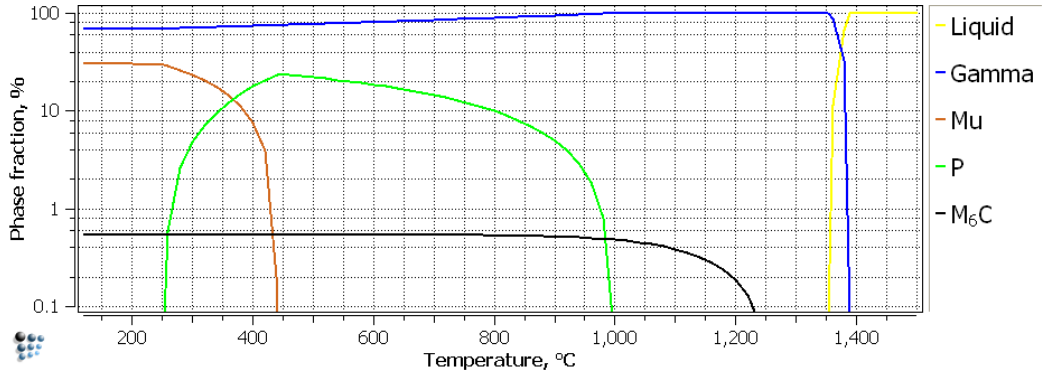

Figure 6-2: Equilibrium medium Cr content

Maximum Cr content:

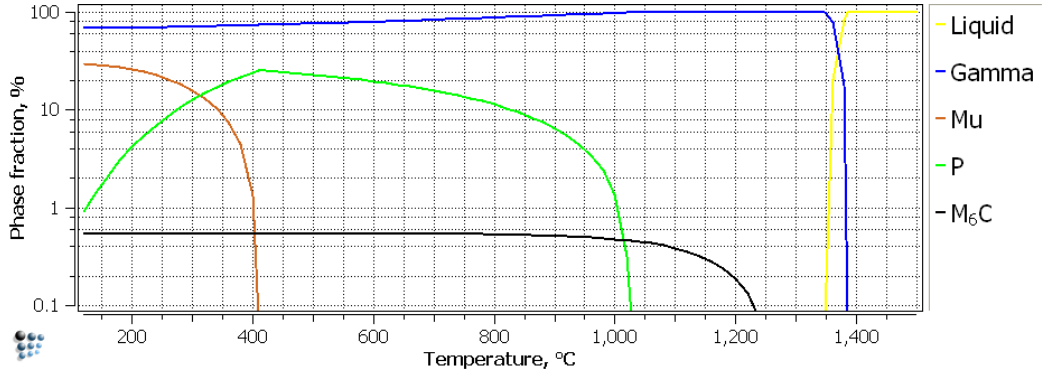

Figure 6-3: Equilibrium maximum Cr content

Interpretation:

It can be seen that the occuring phases are liquid, γ, P, μ and M_6C. This matches with the literature (see chapter 2.2, page 5). The liquid phase, the M_6C carbide and the γ matrix do hardly change with rising Cr content. With rising chrome content the solidification temperature moves slightly to lower temperatures, but this should be discussed later with the Scheil-calculation, because this is more accurate for calculating solidifaction intervals.
What also can be observed is that the μ-phase is a long time transformation product of the P-phase. The P-phase fraction starts to decrease when the μ-phase fraction starts to increase. This matches with the literature as well (see chapter 2.2, page 5)
The most important tendency that can be observed is that the P-phase becomes stable over a bigger temperature range with rising chrome content. With the lowest Cr content it starts to precipitate at about 950°C and with the maximum Cr content it starts to precipitate at about 1030°C.
Another important tendency is, that the maximum phase fraction of the P-phase increases with increasing Cr content. The reason for that is, that the highly alloyed nickel matrix is over saturated and therefore some part of the alloying elements form intermetallic phases instead of forming a solid solution with the nickel.

Consequences:

The P-phase and the μ-phase, which are connected to each other, both have a negative effect on the weld. As already mentioned in this thesis, this phases are brittle and they both have a higher molybdenum and chromium content. Concerning corrosion these elements should be distributed homogeneously in the weld metal.
Since these phases can also cause hot cracking, a lower chromium content is advantageous concerning the weldability.
By lowering the Cr content the welding behaviour will become better on the one hand, but on the other hand, the corrosion resistance will be declined.

6.1.2 *IRON COMPOSITION VARIANTS*

Limits	C	Co	Cr	Fe	Mo	Ni	Si	W	Al	Ti
minimum	0.015	0.2	14.5	4.0	15.0	balance	0.20	3.0	0.03	0.08
medium	0.015	0.2	14.5	5.5	15.0	balance	0.20	3.0	0.03	0.08
maximum	0.015	0.2	14.5	7.0	15.0	balance	0.20	3.0	0.03	0.08

Table 6-2: Fe composition variants

Minimum composition:

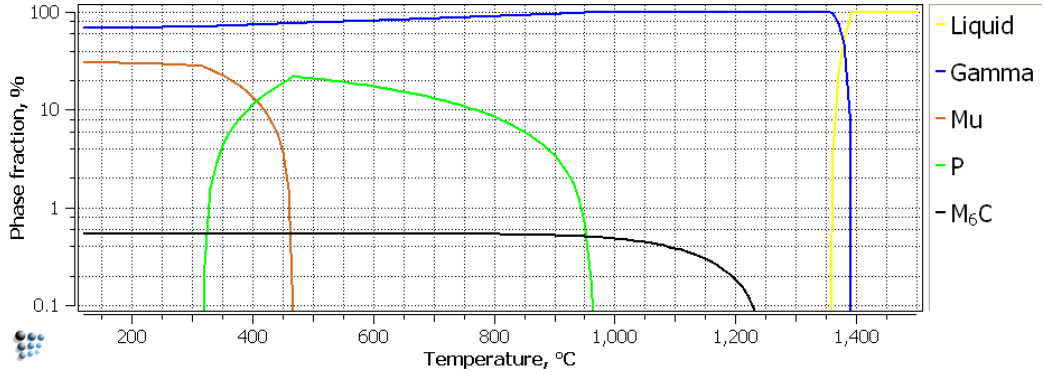

Figure 6-1: Equilibrium minimum composition

Medium Fe content:

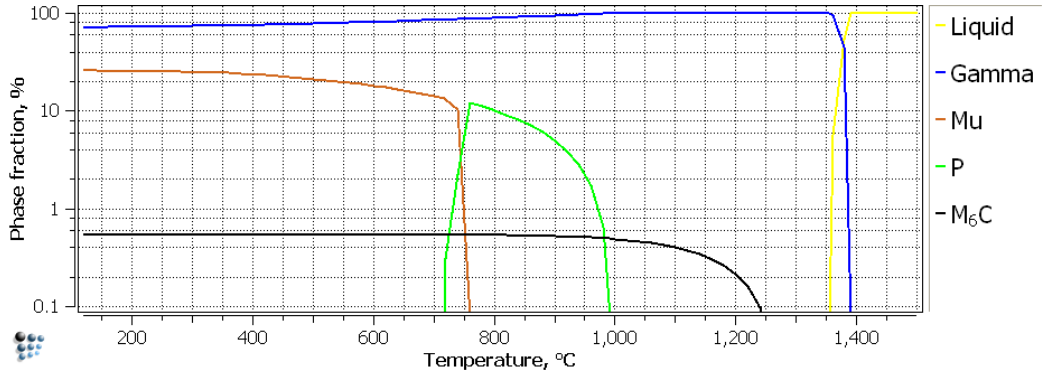

Figure 6-4: Equilibrium medium Fe content

Maximum Fe content:

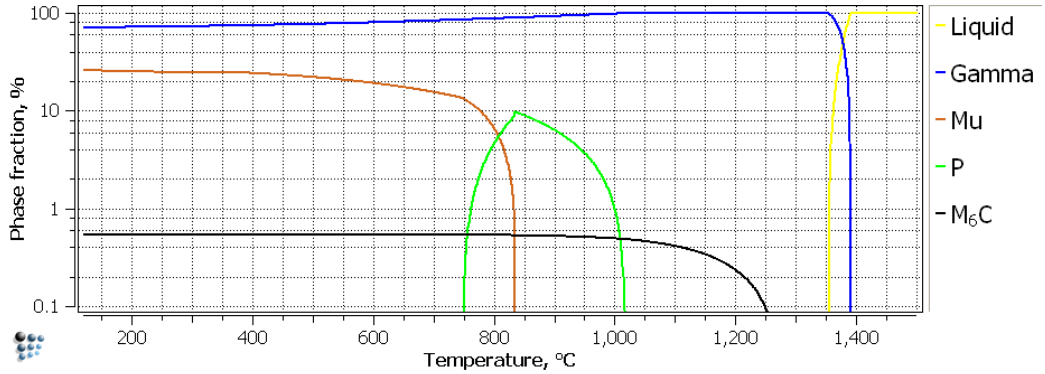

Figure 6-5: Equilibrium maximum Fe content

Interpretation:

First of all the abrupt narrowing of the P-phase is noticeable if the Fe content increases. This occurs, because the P-phase and the μ-phase are rather similar. Anyway, for the discussion of the welding behaviour, it does not make any difference, because both phases have the same effect and the μ-phase always starts to precipitate where the P-phase starts to decrease.
The changing Fe content has two effects: The M_6C carbide becomes stable over a bigger area. It precipitates at higher temperatures with increasing Fe content.
The second effect is that the P-phase and μ-phase area also becomes stable over a bigger temperature range. With increasing Fe content the P- and μ-phase precipitate at higher temperatures.

Consequences:

M_6C carbides as well as P-phase and μ-phase precipitations should be avoided, that is why a lower Fe-content is preferable.

6.1.3 *MOLYBDENUM COMPOSITION VARIANTS*

Limits	C	Co	Cr	Fe	Mo	Ni	Si	W	Al	Ti
minimum	0.015	0.2	14.5	4.0	15.0	balance	0.20	3.0	0.03	0.08
medium	0.015	0.2	14.5	4.0	16.0	balance	0.20	3.0	0.03	0.08
maximum	0.015	0.2	14.5	4.0	17.0	balance	0.20	3.0	0.03	0.08

Table 6-3: Mo composition variants

Minimum composition:

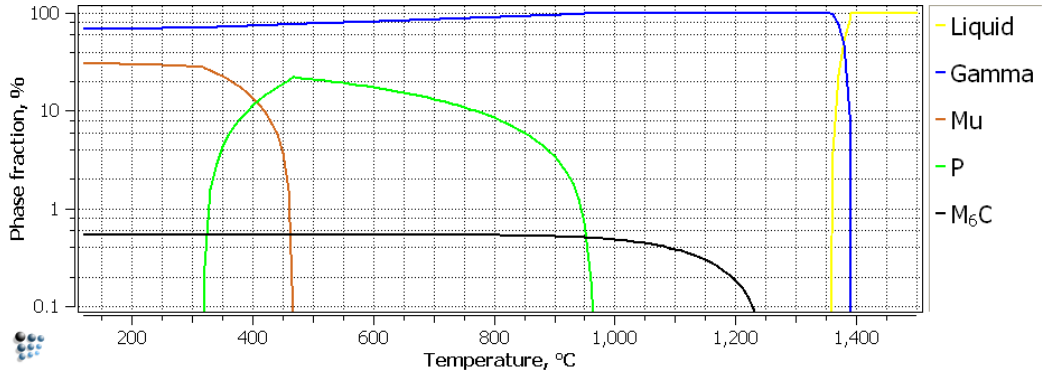

Figure 6-1: Equilibrium minimum composition

Medium Mo content:

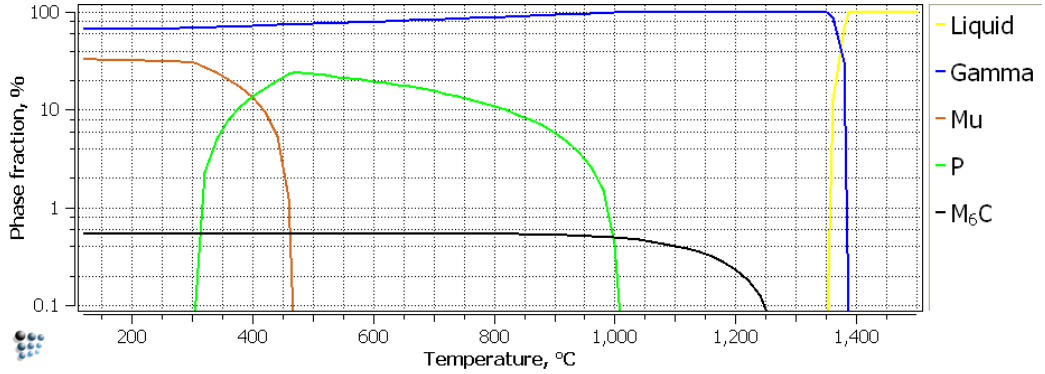

Figure 6-6: Equilibrium medium Mo content

Maximum Mo content:

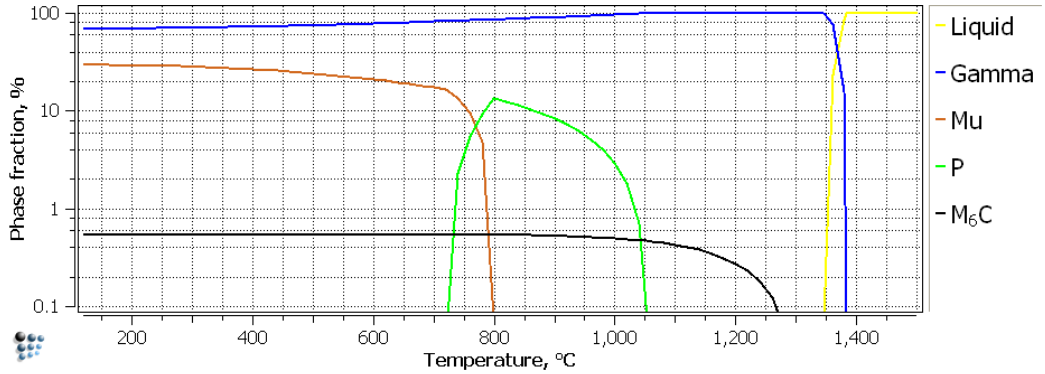

Figure 6-7: Equilibrium maximum Mo content

Interpretation:

Molybdenum has almost the same effect on phase precipitation as Cr. One exception is that Mo also has the effect of stabilizing the M_6C carbide at higher temperatures, which Cr does not have. With increasing Mo content the temperature range and the amount of P-phase and μ-phase are increasing.

Consequences:

The consequences on corrosion and welding behaviour are also similar to the ones of Cr. On the one hand, the corrosion resistance becomes better with higher molybdenum content, if it does not segregate to much. On the other hand the welding behaviour regarding hot cracking becomes worse with the increased precipitation of intermetallic phases.

6.1.4 *TUNGSTEN COMPOSITION VARIANTS*

Limits	C	Co	Cr	Fe	Mo	Ni	Si	W	Al	Ti
minimum	0.015	0.2	14.5	4.0	15.0	balance	0.20	3.00	0.03	0.08
medium	0.015	0.2	14.5	4.0	15.0	balance	0.20	3.75	0.03	0.08
maximum	0.015	0.2	14.5	4.0	15.0	balance	0.20	4.50	0.03	0.08

Table 6-4: W composition variants

Minimum composition:

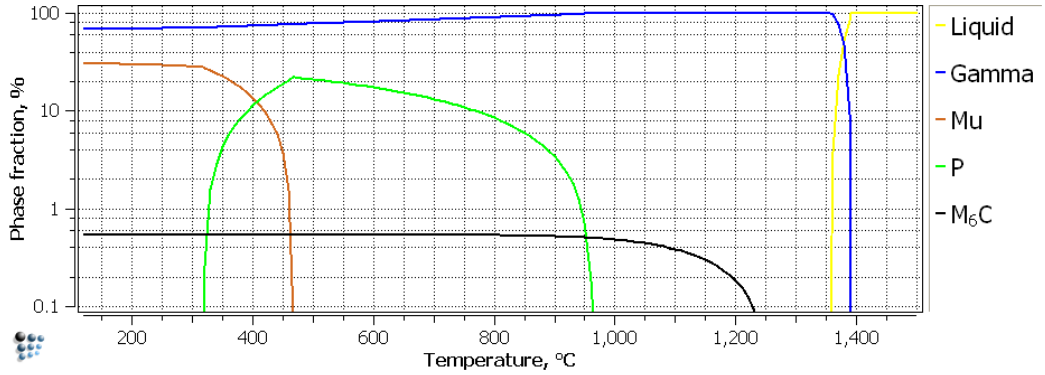

Figure 6-1: Equilibrium minimum composition

Medium W content:

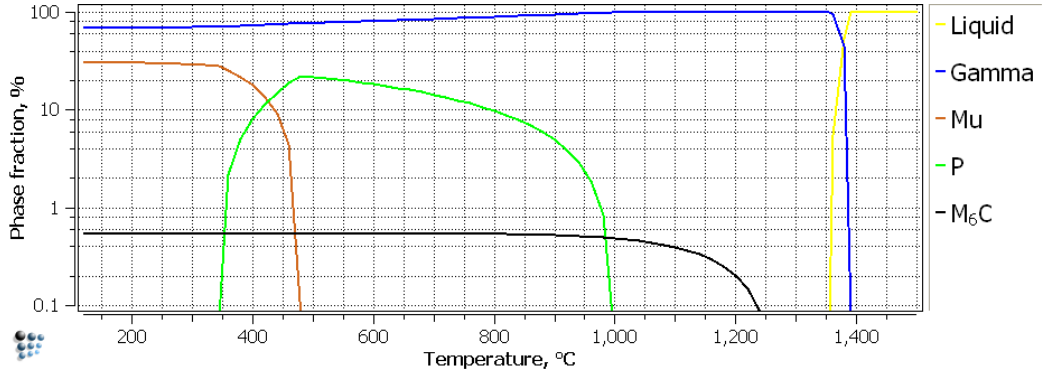

Figure 6-8: Equilibrium medium W content

Maximum W content:

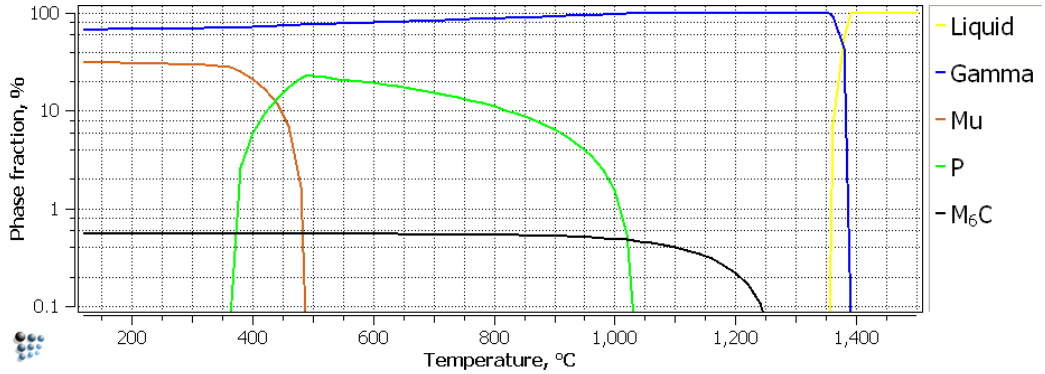

Figure 6-9: Equilibrium maximum W content

Interpretation:

Tungsten shows the same tendencies as molybdenum. The M_6C carbide and the P-phase areas are broadened to higher temperatures with increasing W content. The amount of precipitated P-phase also increases with increasing tungsten content.

Consequences:

Tungsten can be beneficial in certain corrosive environments and it is a good solid solution strengthener, but it also increases the precipitation of intermetallic phases and carbides. This results of the simulation match with the literature mentioned in the chapter 2.4 on page 9.

6.2 THE SCHEIL GULLIVER CALCULATION

The Scheil-Gulliver method allows calculating the fraction as well as the composition of a phase during solidification.

The boundary conditions for this calculation are:

- Equilibrium at the solidification front
- A complete mixing in the liquid phase

The assumption that there is an equilibrium at the solidification front allows the usage of an equilibrium calculation. Unlike the case of equilibrium solidification, the solute cannot diffuse back into the solid and the solute rejected by the growing solid has to go into the liquid. As a consequence the compostition of the liquid changes faster compared to the equilibrium solidification (16). This makes the Scheil calculation more accurate for predicting the solidification of the weld pool compared to the equilibrium simulation.

The undercooling rates are very small, i.e. the Scheil method is only an instrument to determine tendencies for the weld pool solidification.

Still the Scheil method can especially help finding out about tendencies for hot cracking susceptibility of different alloy composition because it descirbes the solidification interval. It shows all the phases that are precipitated during the solidification.

The same simulation method as for the equilibrium calculation is used here. Cr, Fe, Mo and W contents have been varied for each calculation to find out which phases precipitate during solidification. The composition variants are given in Table 6-1 to Table 6-4 for each of the elements.

6.2.1 CHROME COMPOSITION VARIANTS

Limits	C	Co	Cr	Fe	Mo	Ni	Si	W	Al	Ti
minimum	0.015	0.2	14.5	4.0	15.0	balance	0.20	3.0	0.03	0.08
medium	0.015	0.2	15.5	4.0	15.0	balance	0.20	3.0	0.03	0.08
maximum	0.015	0.2	16.5	4.0	15.0	balance	0.20	3.0	0.03	0.08

Table 6-1: Chrome composition variants

Minimum composition:

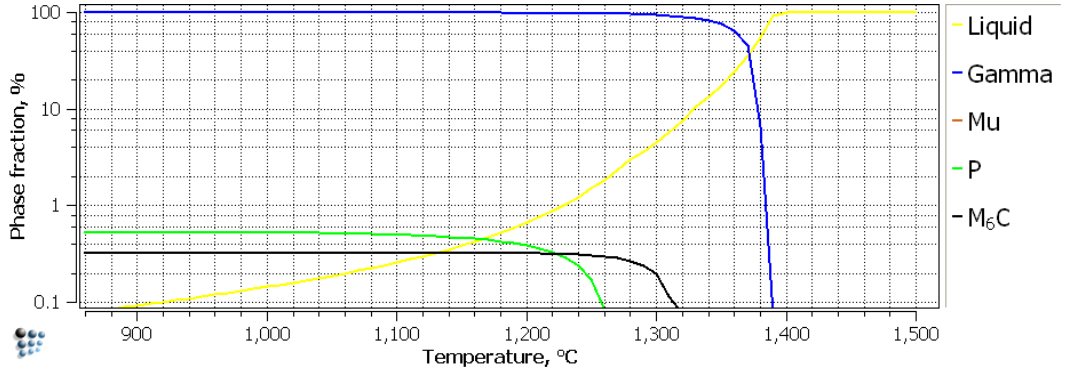

Figure 6-10: Scheil minimum composition

Medium Cr content:

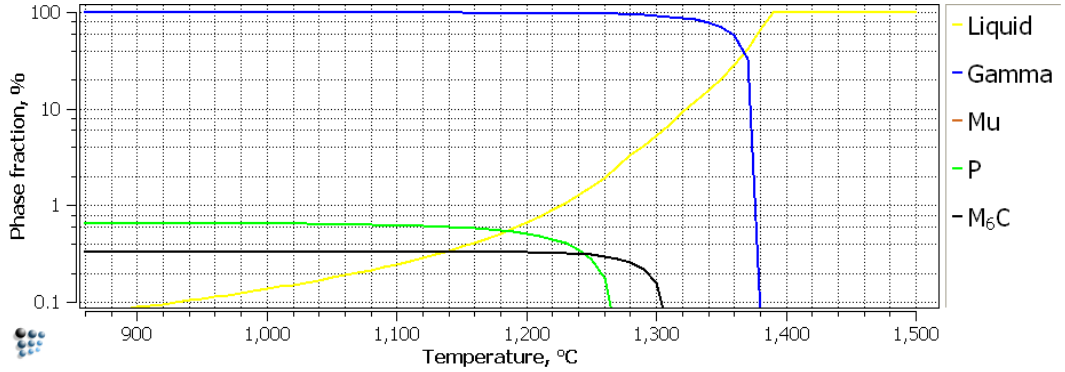

Figure 6-11: Scheil medium Cr content

Maximum Cr content:

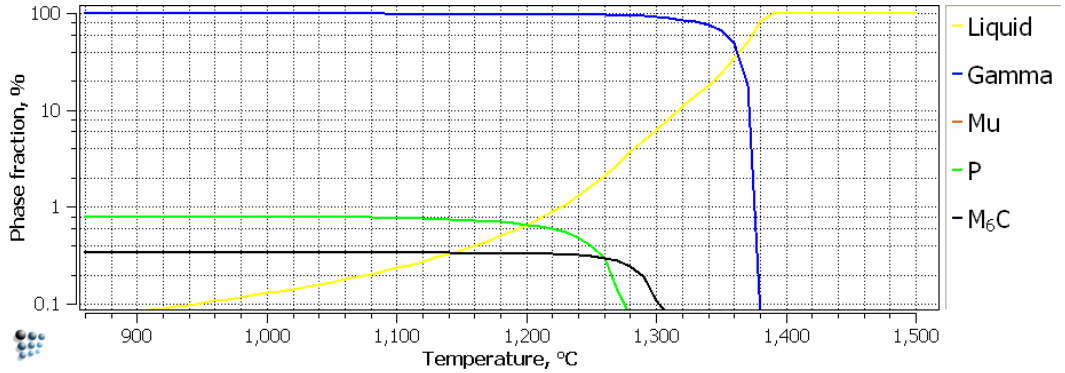

Figure 6-12: Scheil maximum Cr content

Interpretation:

The most important influence of increasing Cr is on the P-phase. It starts to precipitate at higher temperature with increasing chrome content. Also more P-phase is precipitated with increasing Cr. These results match with the equilibrium calculation and the literature in chapter 2.4 on page 9.
The μ-phase is not precipitated at all. At higher temperatures this phase is never stable.

Another important result is, that the solidification interval becomes shorter with more Cr, because γ nucleates at lower temperatures and the liquid-phase disapears at higher temperatures, which should reduce the hot cracking susceptibility.
As the carbides and the P-phase are precipitated before the solidification is finished, this should increase the risk of hot cracking. The hot cracking susceptibility also increases with a bigger amount of precipitated P-phase. That is because these hard and brittle phases can not deform plastically very well during solidification and that leads to cracks.

The M_6C carbides are not influenced much by changing the Cr content. This matches with the equilibrium simulation in chapter 6.1 on page 68.

Consequences:

On the one hand increasing Cr has an advantageous effect, because it shortens the solidification interval. On the other hand it has a disadvantageous effect, because more P-phase is precipitated. It is hard to determine which effect has more influence on hot cracking. The increasing P-phase content has not only the disadvantage of increased hot cracking susceptibility, it also makes the weld more brittle. Hence the recommondation in this case is similar to the one of the equilibrium calculation: Keeping the Cr content as low as possible in regard to welding behaviour is better. Regarding corrosion behaviour the Cr content should be high.

6.2.2 *IRON COMPOSITION VARIANTS*

Limits	C	Co	Cr	Fe	Mo	Ni	Si	W	Al	Ti
minimum	0.015	0.2	14.5	4.0	15.0	balance	0.20	3.0	0.03	0.08
medium	0.015	0.2	14.5	5.5	15.0	balance	0.20	3.0	0.03	0.08
maximum	0.015	0.2	14.5	7.0	15.0	balance	0.20	3.0	0.03	0.08

Table 6-2: Fe composition variants

Minimum composition:

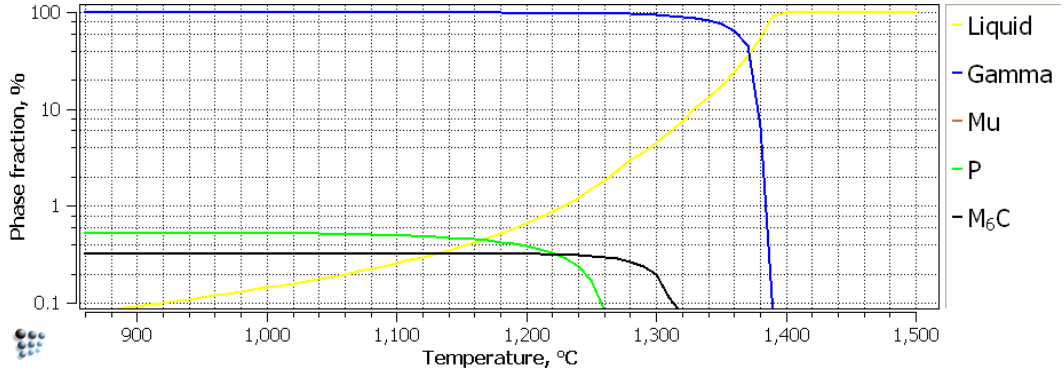

Figure 6-10: Scheil minimum composition

Medium Fe content:

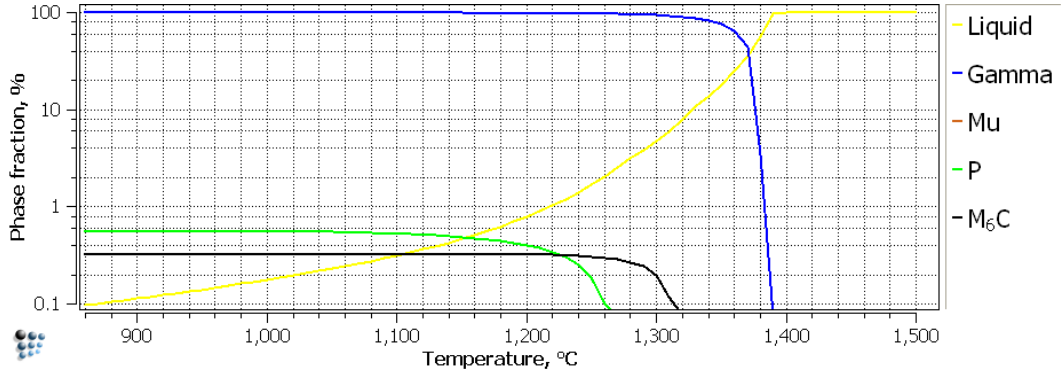

Figure 6-13: Scheil medium Fe content

Maximum Fe content:

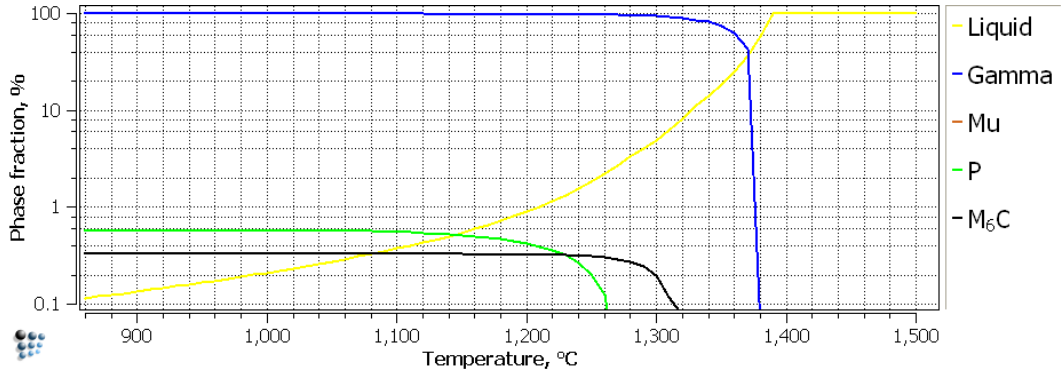

Figure 6-14: Scheil maximum Fe content

Interpretation:

The P-phase and the M_6C carbides are not influenced much by increasing iron content. Precipitation temperature and precipitated amounts stay almost the same for the three different compositions.

The matrix phase starts to precipitate at slightly lower temperatures with increasing iron content. The liquid solidifies at much lower temperatures with increasing iron content.

Consequences:

Since the solidification range is broadened with increasing iron content, because the liquid phase exists at lower temperatures, the hot cracking suceptibility is increased with growing iron content.

The hard and brittle carbides and intermetallic phases are not influenced much, which is positive regarding hot cracking. These phases are still precipitated before all the liquid is solidified, which has the negative effect of increasing hot cracking susceptibility.

6.2.3 *MOLYBDENUM COMPOSITION VARIANTS*

Limits	C	Co	Cr	Fe	Mo	Ni	Si	W	Al	Ti
minimum	0.015	0.2	14.5	4.0	15.0	balance	0.20	3.0	0.03	0.08
medium	0.015	0.2	14.5	4.0	16.0	balance	0.20	3.0	0.03	0.08
maximum	0.015	0.2	14.5	4.0	17.0	balance	0.20	3.0	0.03	0.08

Table 6-3: Mo composition variants

Minimum composition:

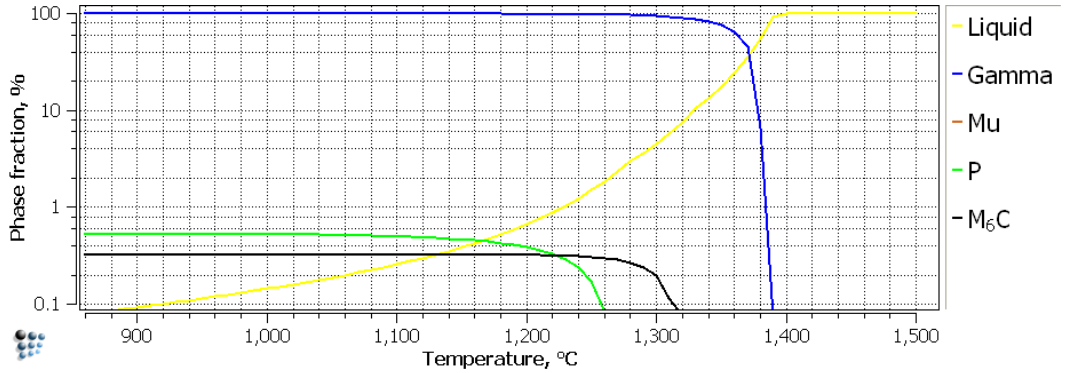

Figure 6-10: Scheil minimum composition

Medium Mo content:

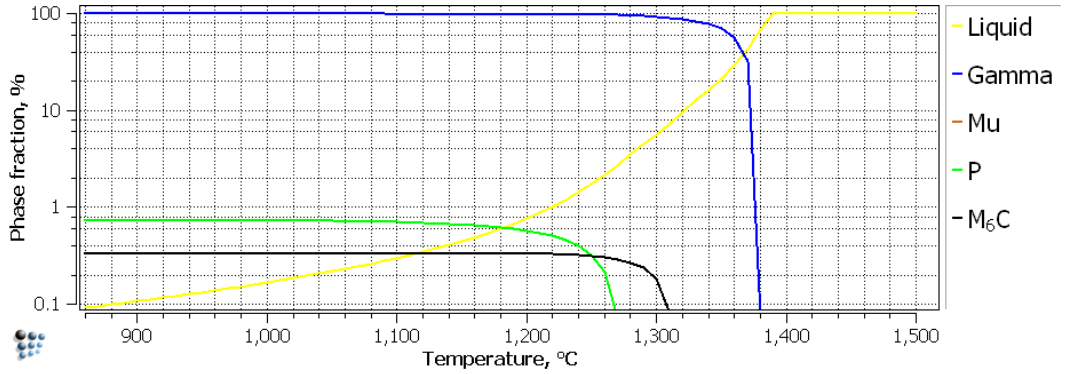

Figure 6-15: Scheil medium content

Maximum Mo content:

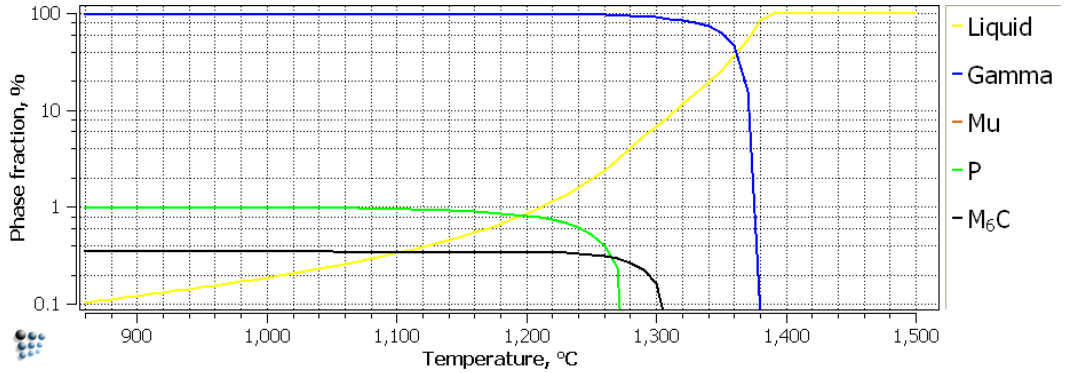

Figure 6-16: Scheil maximum Mo content

Interpretation:

The γ matrix phase starts to nucleate at a little lower temperatures with increasing molybdenum content. Compared to the matrix the liquid solidifies at much lower temperatures with increasing Mo content.

Increasing molybdenum increases the P-phase fraction and stabilizes it at higher temperatures. The P-phase is precipitated earlier with increasing Mo content. That matches with the equilibrium charts calculated above (see chapter 6.1).

The final amount of M_6C carbides stays the same in all three calculations. With increasing Mo content the carbide precipitation is shifted to lower temperatures.

Consequences:

The solidification interval is bigger and the amount of precipitated P-phase increases with increasing Mo-content. Both make the C-276 weld metal more suceptible to hot cracking. That's why molybdenum should be kept as low as possible to get a good welding behaviour. It has probably the worst influence on the welding behaviour.

With respect to corrosion, the Mo content should be as high as possible. It is the same ambivalence like for chrome content. It is suggested to first improve the welding behaviour to get a crack free weld and then to look after the corrosion behaviour of the weld. A cracked weld isn't very resistant to corrosion anyways.

6.2.4 *TUNGSTEN COMPOSITION VARIANTS*

Limits	C	Co	Cr	Fe	Mo	Ni	Si	W	Al	Ti
minimum	0.015	0.2	14.5	4.0	15.0	balance	0.20	3.00	0.03	0.08
medium	0.015	0.2	14.5	4.0	15.0	balance	0.20	3.75	0.03	0.08
maximum	0.015	0.2	14.5	4.0	15.0	balance	0.20	4.50	0.03	0.08

Table 6-4: W composition variants

Minimum composition:

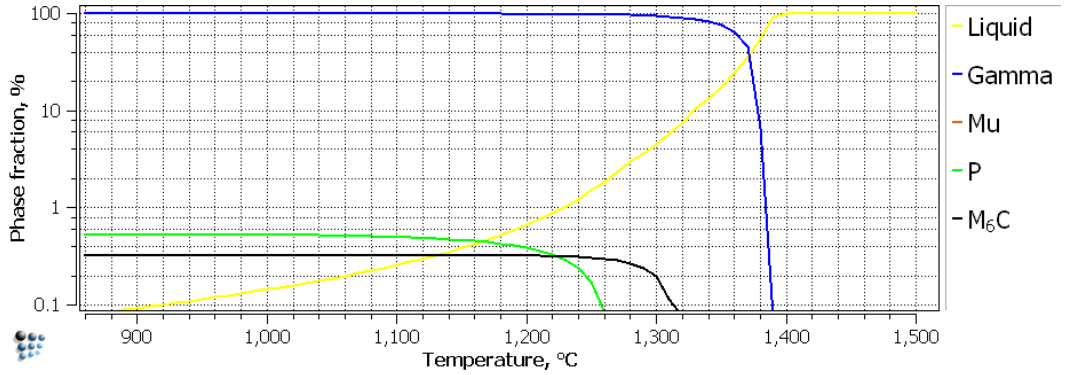

Figure 6-10: Scheil minimum composition

Medium W content:

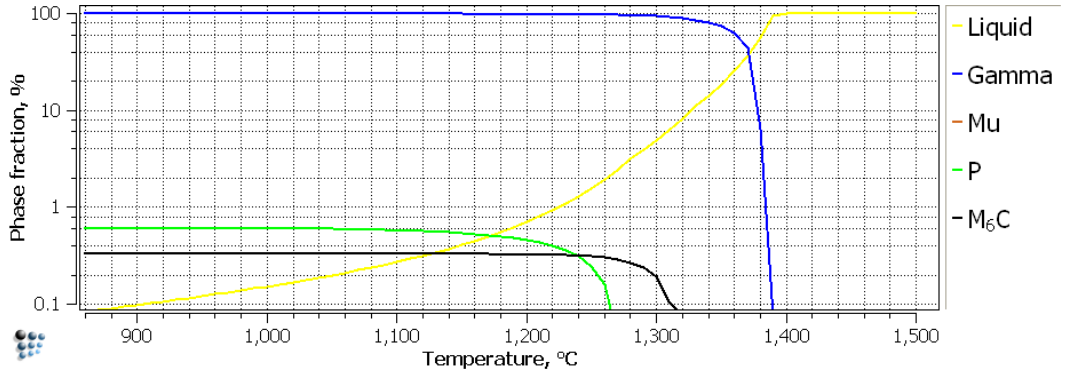

Figure 6-17: Scheil medium W content

Maximum W content:

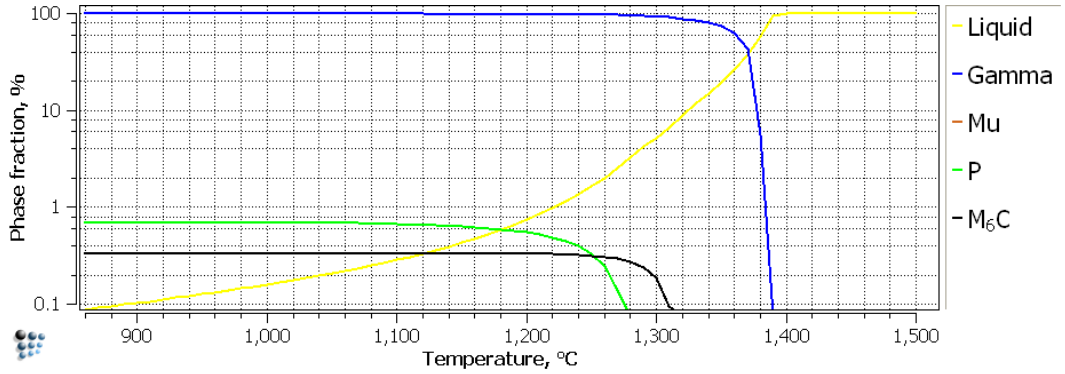

Figure 6-18: Scheil maximum W content

Interpretation:

The liquid solidifies at lower temperatures with increasing tungsten content. The matrix phase nucleates at the same temperature for all three compositions. That means the solidification interval becomes a little bit longer with increasing W content.
The P-phase is stabilized at higher temperatures and the final amount is slightly increased with rising W content.
The carbide precipitation is not influenced in this case.

Consequences:

Tungsten does not influnence the solidification as much as the other three main alloying elements (Cr, Fe, Mo). Still it has a slightly deteriorating effect on the final weld metal, because more intermetallic phase is precipitated with increasing W.
The beneficial effect of tungsten in respect to corrosion resistance has already been mentioned in chapter 2.4.4 on page 10.

6.3 THE PRECIPITATION SIMULATION IN THE HAZ

With Matcalc, heat treatments of different materials can be simulated too. The results are for example the phase fractions of the different precipitates. That is the main application. Since welding is a very short heat treatment with the different temperature zones in the HAZ this tool can also be used to predict the precipitates. From the amount of precipitates in the HAZ the hot crack susceptibility can be predicted. Mr. Tösch a former developer of welding wires at Böhler, stated that 2 to 3 percent unfavourable phase precipitates (P, Mu and M_6C) can cause hot cracking, depending on the alloy. This will be applied in the interpretation of the simulation results.

The major inputs in the previous simulations (Equilibrium and Scheil calculations) were the different alloy compositions. For the precipitation simulation another input is necessary, which is the heat treatment. The temperature cycle in the HAZ is the heat treatment input for Matcalc here.

To get this temperature cycle a simulation of a C-276 weld with the program Sysweld was carried out. A point for the calculation of the temperature cycle has been chosen. This calculation point is in the orange area, where the base material is not yet molten. Figure 6-19 shows the result of the calculation:

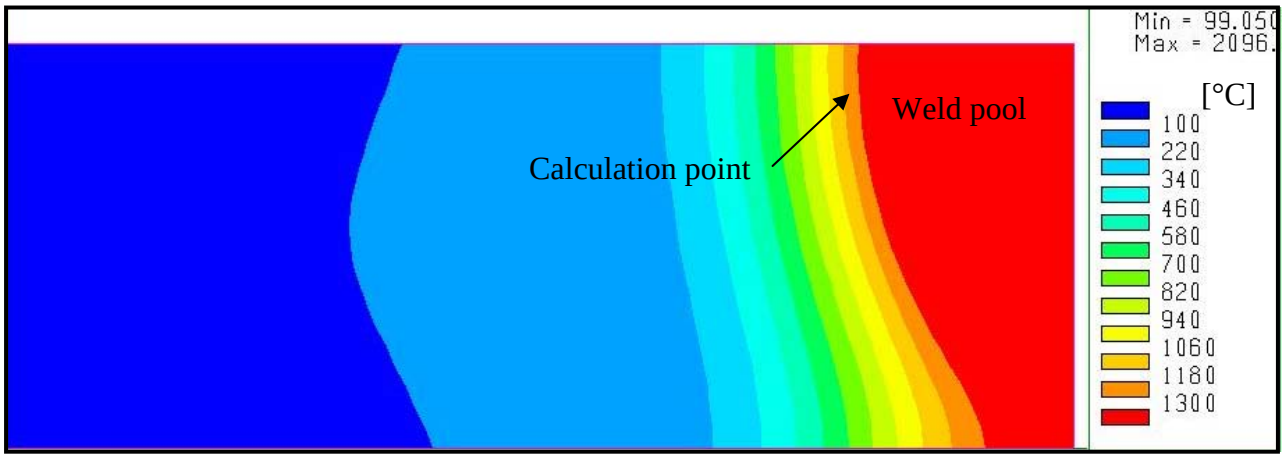

Figure 6-19: Cross section of the weld pool and the base material with calculated with Sysweld

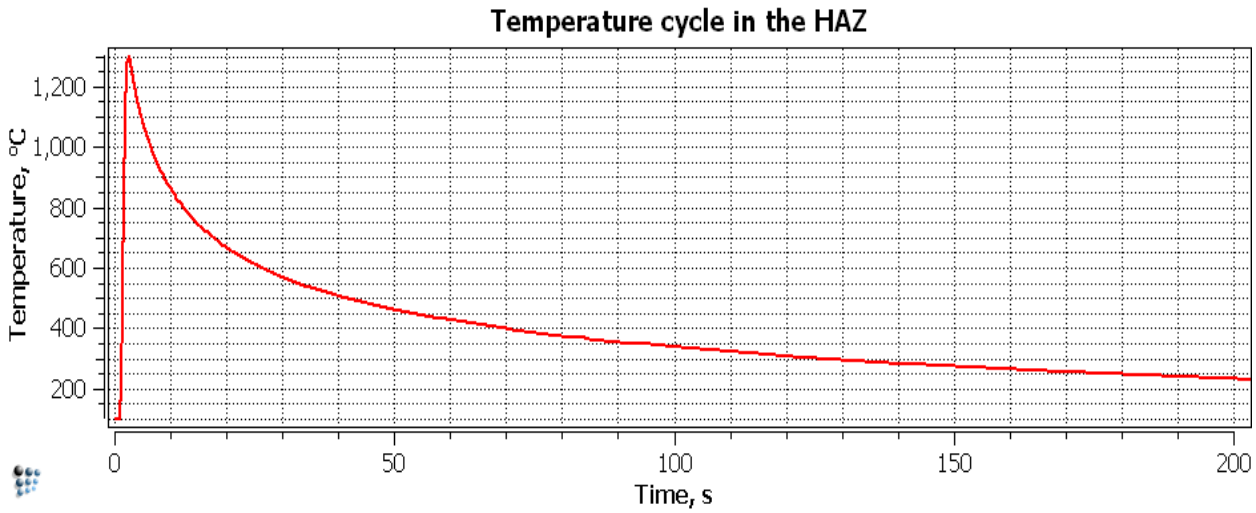

Figure 6-20: Calculated temperature cycle in the HAZ

Figure 6-19 shows the result of the Sysweld simulation (already transferred to Matcalc). An area in the HAZ cross section where the maximum temperature is 1300°C was chosen (see Figure 6-19). The higher the temperature, the higher the hot crack susceptibility, because there is more energy available to form unfavourable phases. The thermal expansion and contraction, which are necessary prerequisites for hot cracking, are also bigger with higher temperature. Higher temperatures should not be applied for this simulation because the melting range of alloy C-276 (1325°C – 1370°C) must not be exceeded as Matcalc can only calculate the precipitation kinetics correctly if the alloy remains in solid state.

The simulation mode is not the same as for the other two simulations, because only the minimum composition and the maximum composition for each of the four variable alloying elements (Cr, Fe, Mo, W) have been carried out. In addition to that a maximum composition simulation, which means the maximum value for each alloying element has been carried out.

A table on top of each page shows the alloy composition of each simulation.

6.3.1 CHROME COMPOSITION VARIANTS

Limits	C	Co	Cr	Fe	Mo	Ni	Si	W	Al	Ti
minimum	0.015	0.2	14.5	4.0	15.0	balance	0.20	3.0	0.03	0.08
maximum	0.015	0.2	16.5	4.0	15.0	balance	0.20	3.0	0.03	0.08

Table 6-5: Cr composition variants

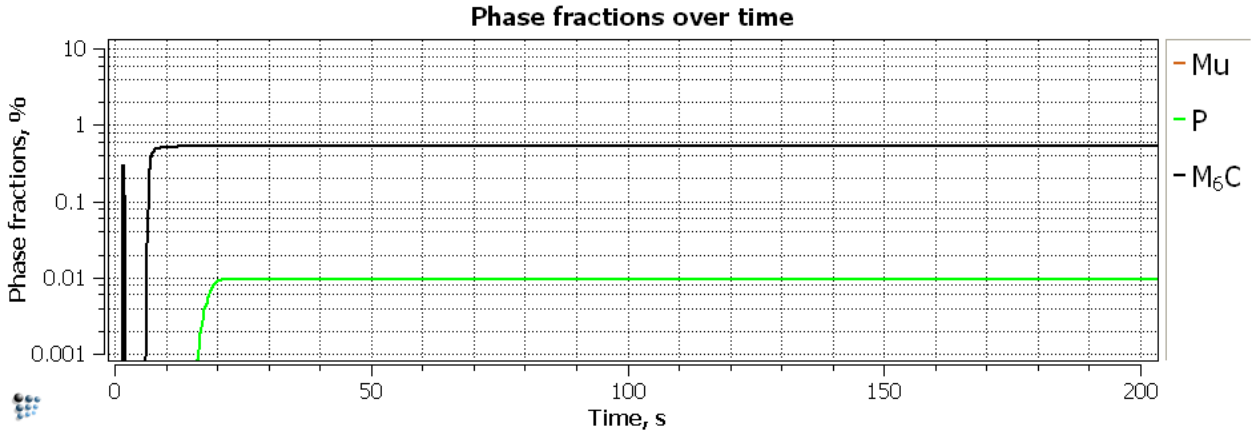

Figure 6-21: Kinetics minimum composition

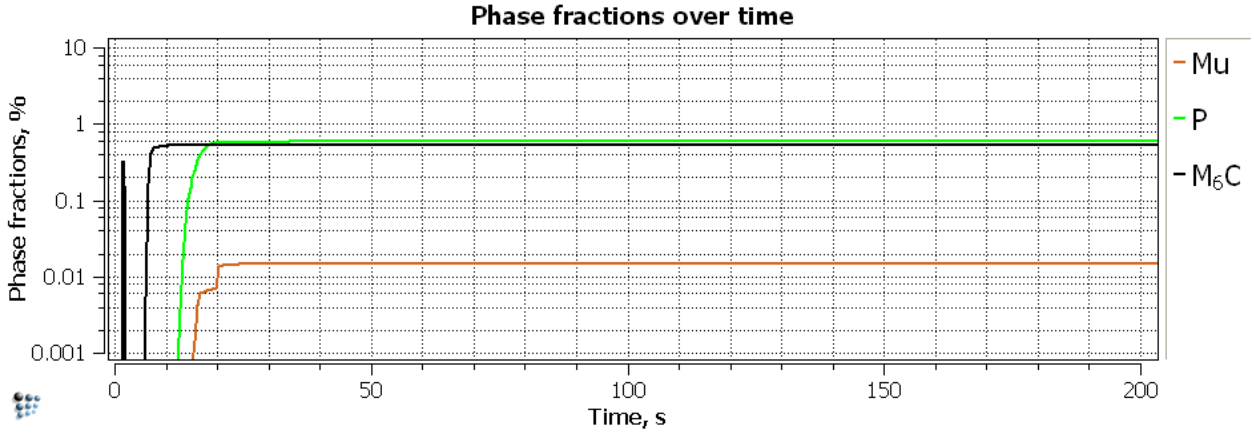

Figure 6-22: Kinetics maximum Cr content

Interpretation:

The M_6C carbide amount does not change with the Cr composition. It is always around 0.6 %. The P-phase fraction instead increases from 0.01% to 0.6% with more Cr added to the alloy. The μ-phase starts to precipitate, but with a value of about 0.015 % it can be neglected.

Consequences:

Raising only the Cr content does not increase the hot crack susceptibility in the HAZ much, because the overall content of disadvantageous phases is below 2% (Tösch).

6.3.2 *IRON COMPOSITION VARIANTS*

Limits	C	Co	Cr	Fe	Mo	Ni	Si	W	Al	Ti
minimum	0.015	0.2	14.5	4.0	15.0	balance	0.20	3.0	0.03	0.08
maximum	0.015	0.2	14.5	7.0	15.0	balance	0.20	3.0	0.03	0.08

Table 6-6: Fe composition variants

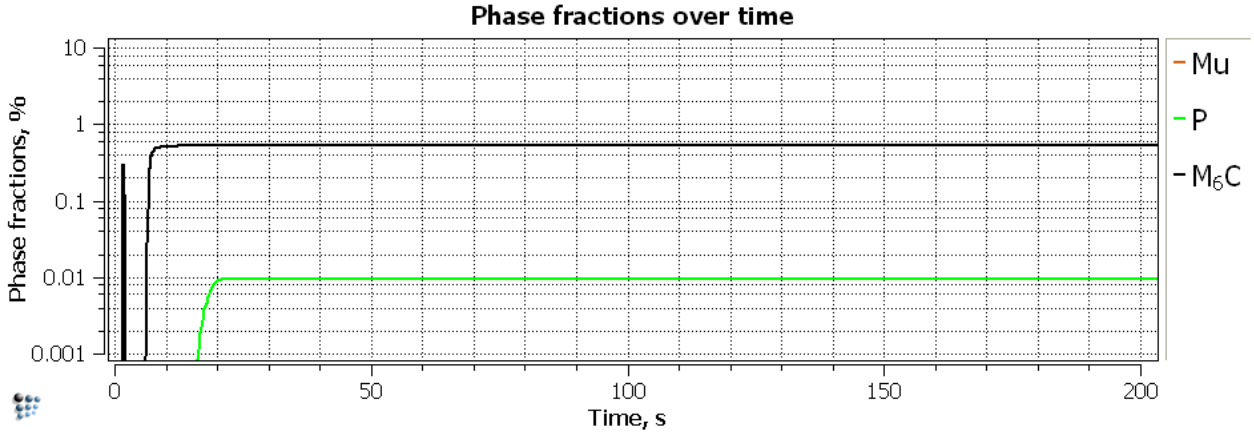

Figure 6-23: Kinetics minimum composition

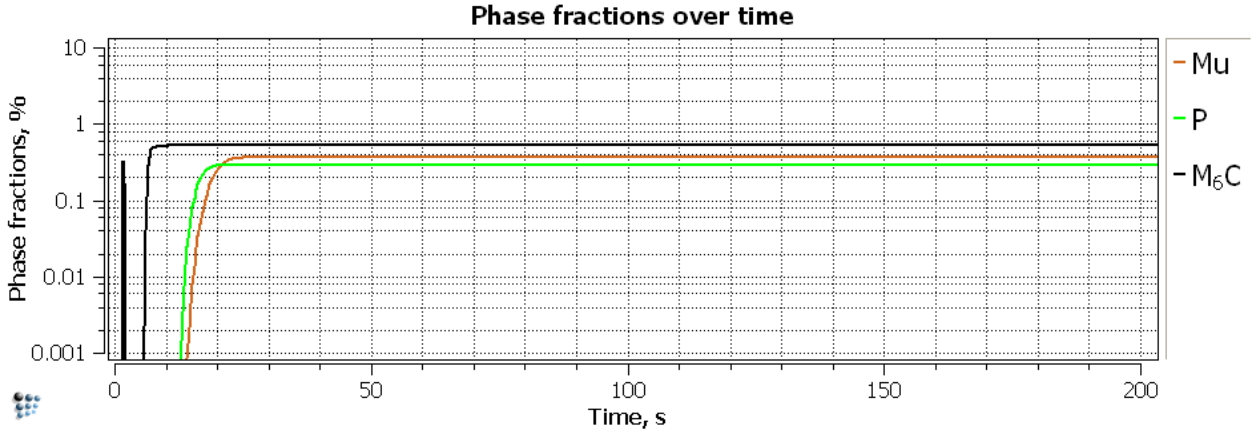

Figure 6-24: Kinetics maximum Fe content

Interpretation:

The M_6C carbide amount is always the same for all the kinetic simulations. It is limited because the carbon content is limited to 0.015 weight percent for all compositions. Increasing the Fe content increases the amount of P-phase and μ-phase to 0.3% and to 0.4%, respectively.

Consequences:

The P-phase and μ-phase precipitates are not enough to increase the hot cracking risk much, because the overall amount is below 2% (Tösch).

6.3.3 *MOLYBDENUM COMPOSITION VARIANTS*

Limits	C	Co	Cr	Fe	Mo	Ni	Si	W	Al	Ti
minimum	0.015	0.2	14.5	4.0	15.0	balance	0.20	3.0	0.03	0.08
maximum	0.015	0.2	14.5	4.0	17.0	balance	0.20	3.0	0.03	0.08

Table 6-7: Mo composition variants

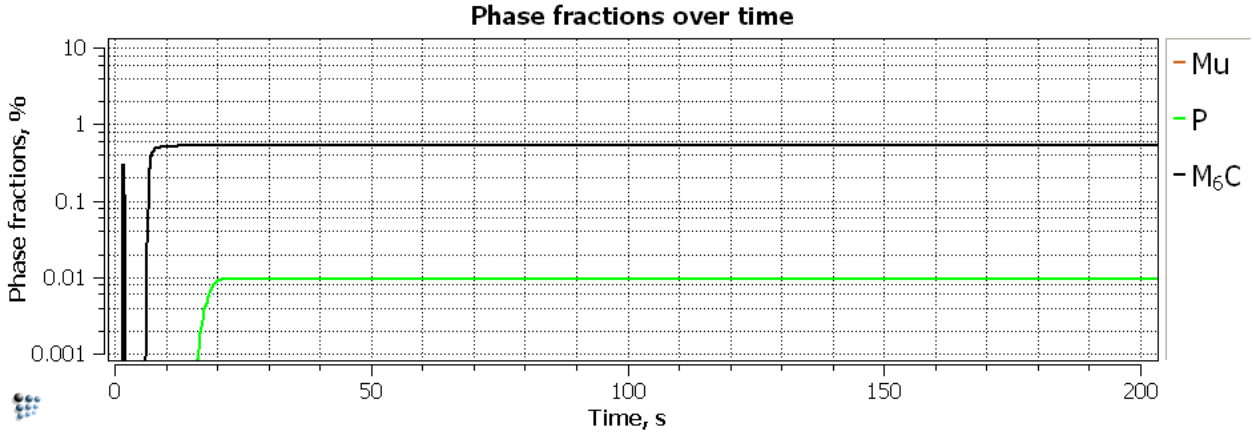

Figure 6-25: Kinetics minimum composition

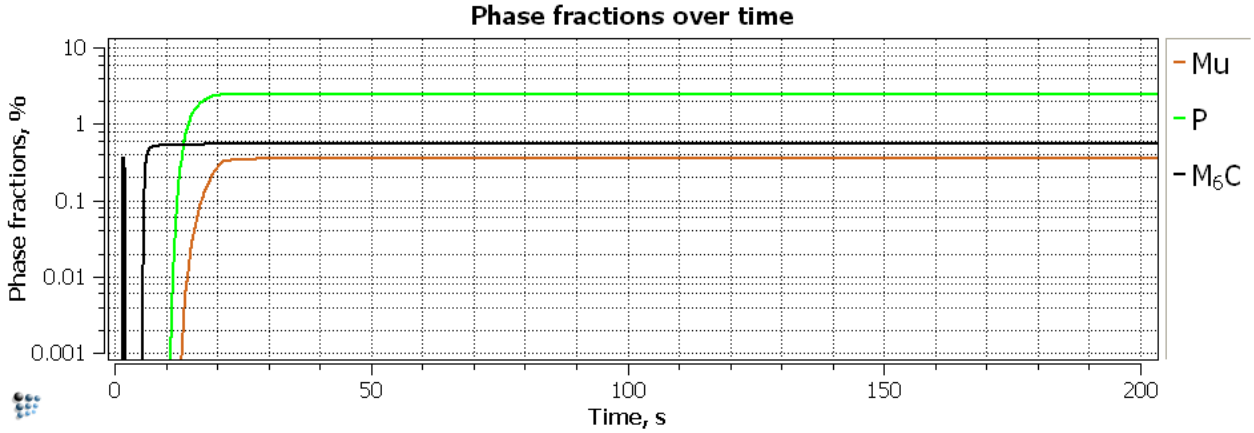

Figure 6-26: Kinetics maximum Mo content

Interpretation:

Increasing molybdenum from minimum to maximum composition increases the P-phase amount from 0.01% to over 2 percent. The μ-phase increases from zero to 0.4%.

Consequences:

Molybdenum seems to have the strongest influence on the hot crack susceptibility in these simulations. That matches with the previous simulations and with the results of the EDX analysis in chapter 6.4 on page 94. A P-phase content of 2% in the HAZ is over the limit that means hot cracking is possible in this case.

6.3.4 *TUNGSTEN COMPOSITION VARIANTS*

Limits	C	Co	Cr	Fe	Mo	Ni	Si	W	Al	Ti
minimum	0.015	0.2	14.5	4.0	15.0	balance	0.20	3.00	0.03	0.08
maximum	0.015	0.2	14.5	4.0	15.0	balance	0.20	4.50	0.03	0.08

Table 6-8: W composition variants

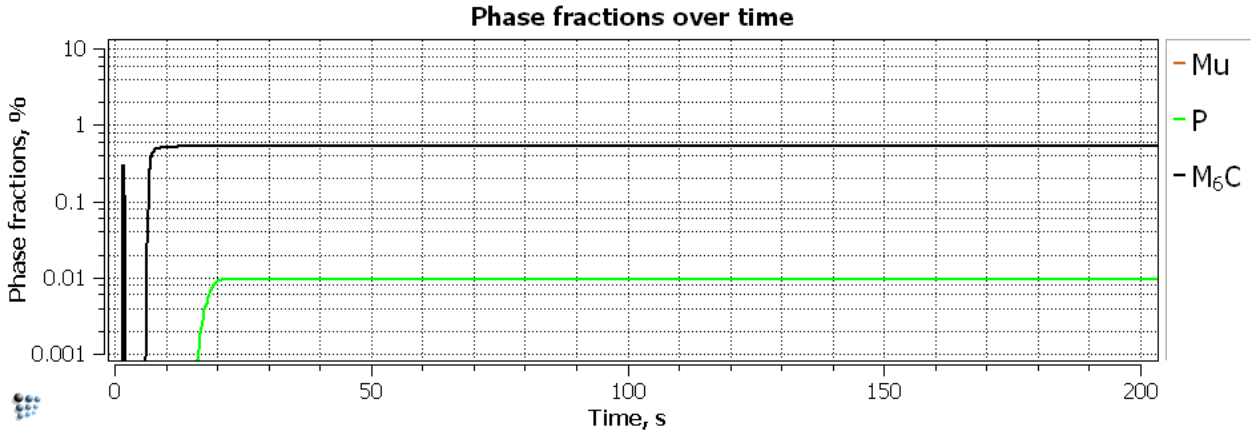

Figure 6-27: Kinetics minimum composition

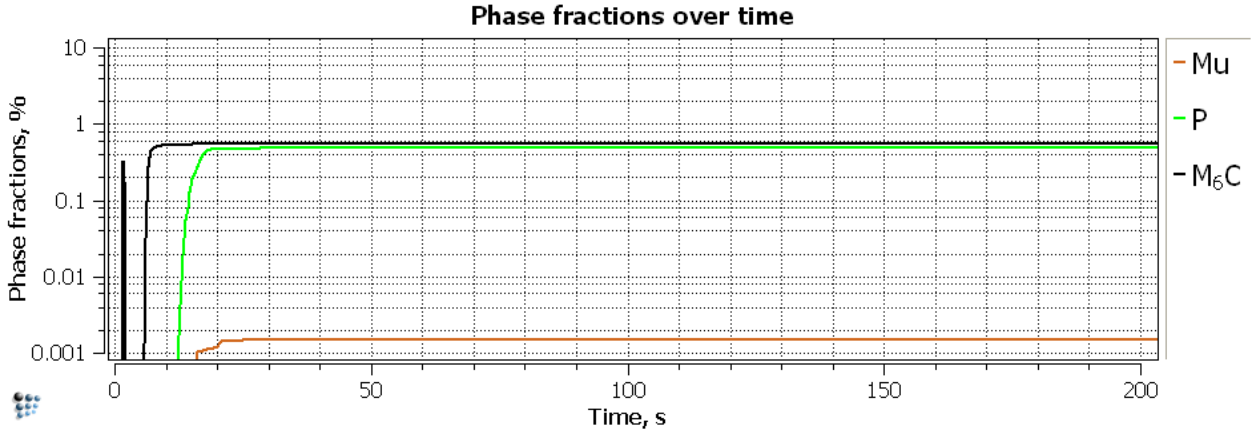

Figure 6-28: Kinetics maximum W content

Interpretation:

Increasing tungsten results in a P-phase amount of 0.4%. The μ-phase amount can be neglected because it is less than 0.01%.

Consequences:

The increasing tungsten amount alone does not really make the base material susceptible to hot cracking. The overall amount of the unfavourable phases is about 0.6%, which is far below the critical value of 2%.

6.3.5 *MINIMUM AND MAXIMUM COMPOSITION OF ALL VARIABLE ALLOYING ELEMENTS*

Limits	C	Co	Cr	Fe	Mo	Ni	Si	W	Al	Ti
minimum	0.015	0.2	14.5	4.0	15.0	balance	0.20	3.00	0.03	0.08
maximum	0.015	0.2	16.5	7.0	17.0	balance	0.20	4.50	0.03	0.08

Table 6-9: Minimum and maximum composition

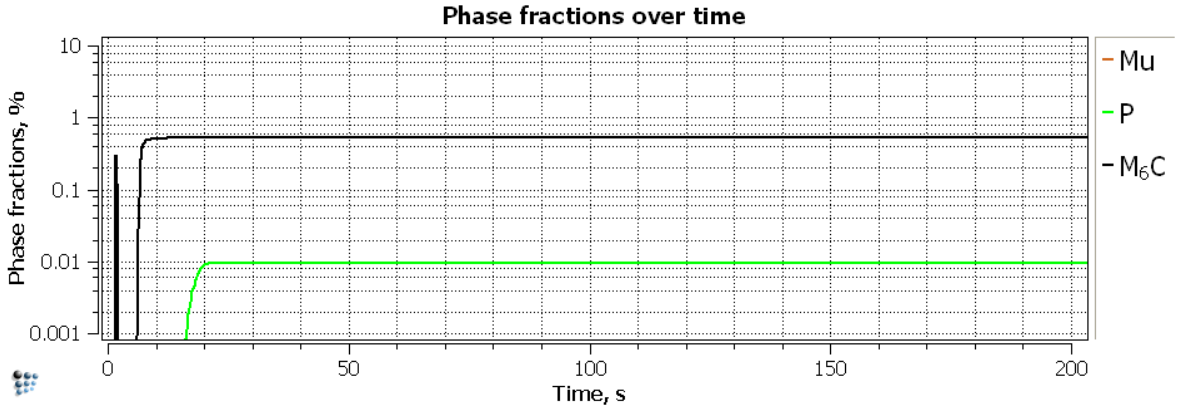

Figure 6-29: Kinetics minimum composition

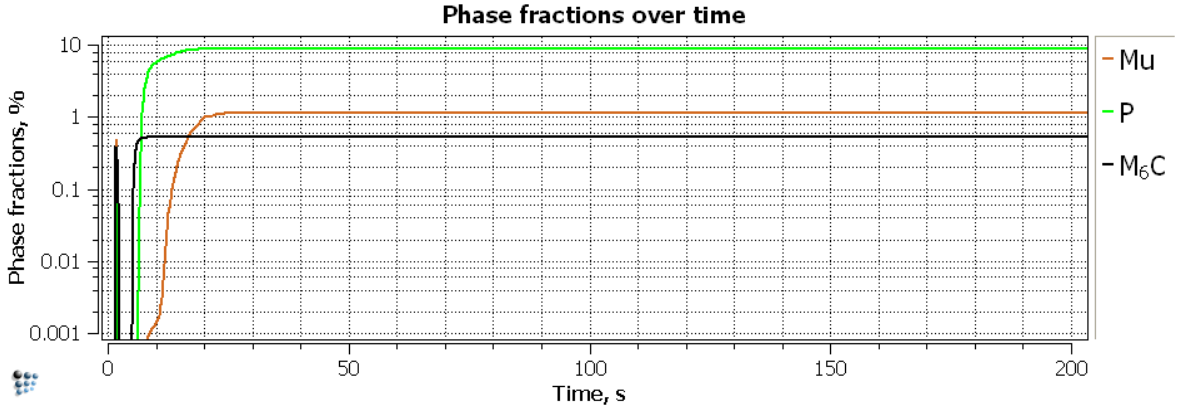

Figure 6-30: Kinetics maximum content of all variable alloying elements

Interpretation:

This simulation shows what happens if all alloying elements reach the maximum level. The P-phase precipitate amount reaches 10% and the μ-phase amount crosses the 1% border.

Consequences:

This composition is very hot cracking susceptible. The reason for the strong intermetallic phase precipitation is a reduced solubility of the alloying elements in a reduced amount of nickel. Reduced nickel amount means less matrix phase.

6.4 SEM DOCUMENTATION OF THE WELD METAL

As a proof that the P- and µ-phase really precipitate in a C-276 weld a cross section of a weld was examined (Masse 68) with the SEM. In addition to that an EDX image was taken. It was not possible to find out the exact composition of the examined phases for a comparison with the Matcalc results with the available resources, but for a proof of the existence of the P or µ phase this EDX-analysis is sufficient.

The calculated composition (Matcalc: Scheil calculation) of the P-phase shows following result:

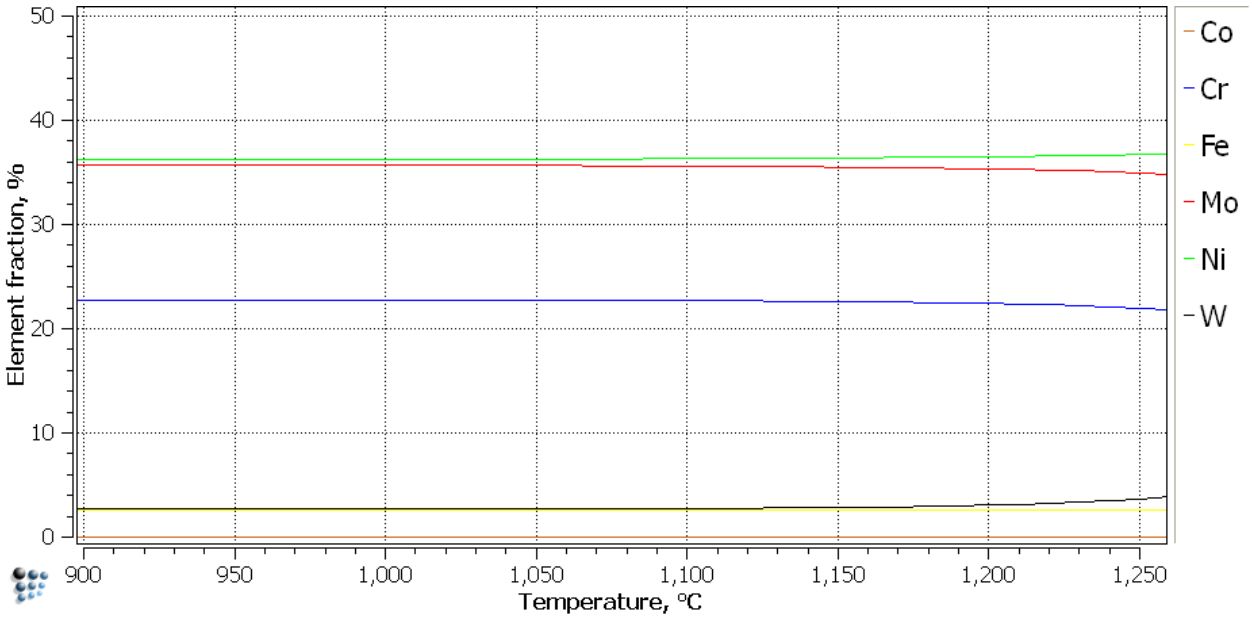

Figure 6-31: P-phase composition over temperature of Masse 68

The P-phase shows strongly elevated molybdenum content as mentioned in chapter 2.2.2 on page 5. In the EDX analysis of the weld cross-section this elevated molybdenum content can be observed.

Figure 6-32 and Figure 6-33 prove the existence of the P-phase in the weld metal. Figure 6-32 shows a BSE (Backscatter electron mode) image of unetched C-276 weld metal. The black dots in this picture are slag inclusions and the light areas are intermetallic phases.

Molybdenum is a rather heavy element compared to the other elements, thus it appears brighter in the BSE image.

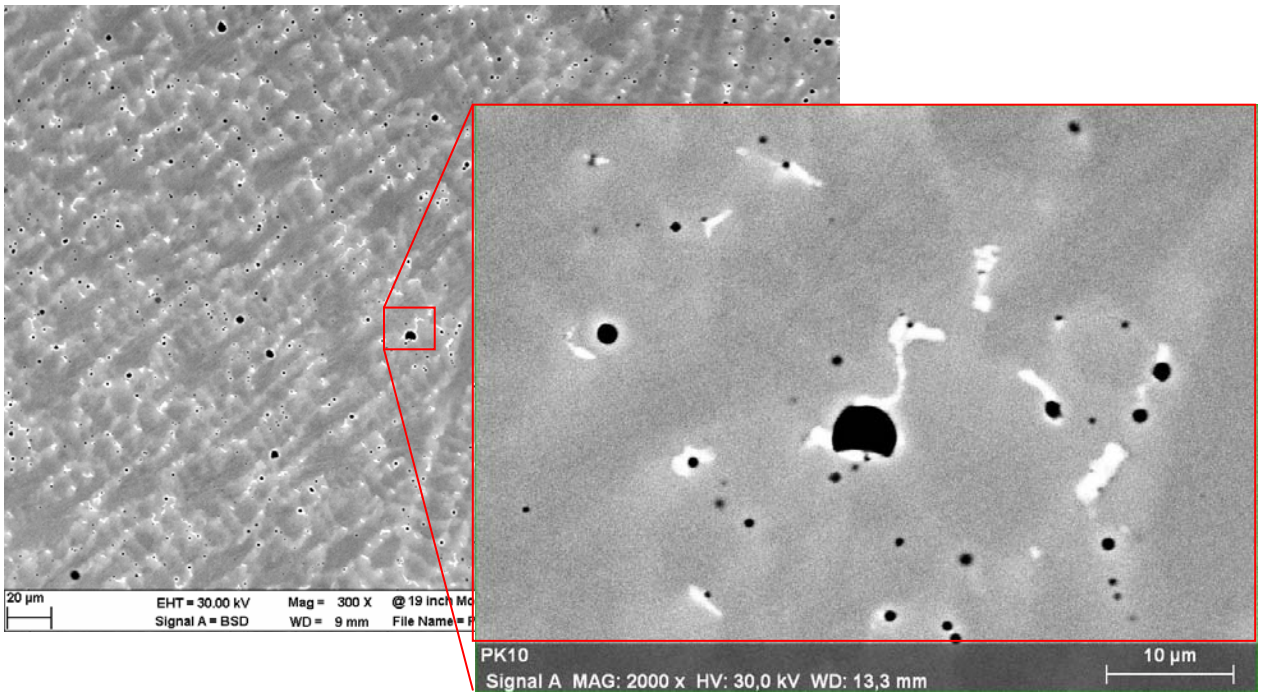

Figure 6-32: BSE images of the weld metal Masse 68

The next picture really proofs that the white areas in the picture above are areas with increased molybdenum content. It is the same picture, but in the EDX mode.

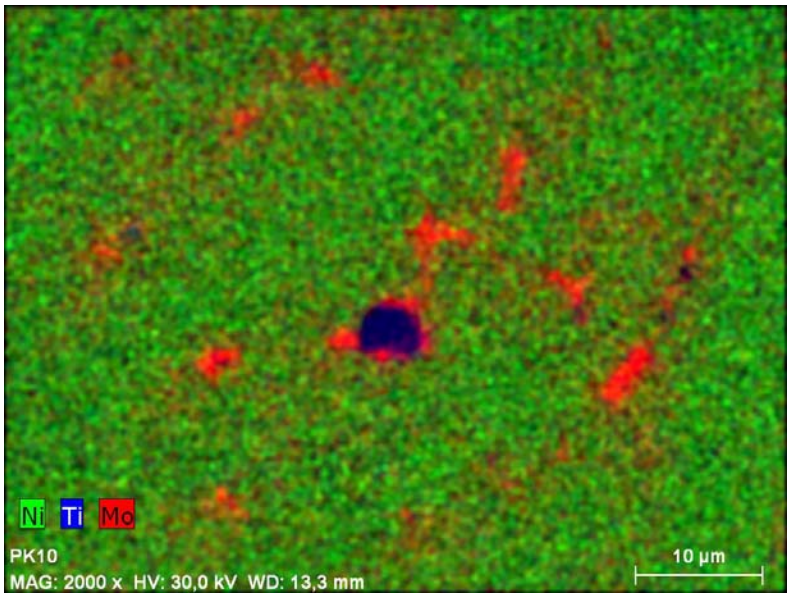

Figure 6-33: EDX image of the weld metal (Masse 68)

In Figure 6-33 nickel matrix is dyed green, molybdenum is dyed red and titanium is dyed blue. It shows the areas of intermetallic phases very well. In addition to that the slag inclusion is visible

very well. Titanium has a high chemical affinity to oxygen. Its function in the weld metal is the deoxidization as well as slag forming, resulting in TiO_2 formation, also known as rutile. The applied slags for the test wires are all rutile slag types.

7 CONCLUSION AND PERSPECTIVE

7.1 CONCLUSION

Attendant to the ongoing development of the C-276 flux cored welding wire for position welding, several supporting tasks were carried out. The main tasks were the HSC analysis of the drop transition, finding the reason and solution possibilities for the dimple problem and carrying out a Matcalc simulation to find out more about the solidification behaviour and the phase precipitation of the C-276 weld metal.

HSC analysis of the drop transition:

The most important parameter for the drop transition is the welding current, because it correlates to the power of two with the pinch force, which is the most important force for the drop release. Molten nickel is very viscous, thus the pinch force has to be high. The drop is also surrounded with slag. If the slag is very viscous too, the pinch force has to be even higher. It has to be mentioned that the current is limited, because the heat input is limited to 11kJ/cm for this alloy due to hot cracking susceptibility. Five different wires were filmed with the HSC during the welding process applying same welding parameters and the drop rate was determined by counting the drops per second. The result is a drop rate, which allows the evaluation of the viscosity of the weld metal and the welding behaviour. The results were as follows: Masse 63 83 drops/s, Masse 68 70 drops/s, Masse 73 79 drops/s, Masse 90 67 drops/s and Stoody 45 drops/s, i.e. the most viscous weld metal is the Stoody weld metal.

The dimple problem:

The reason for the dimple problem is that gas gets trapped between the weld metal surface and the slag coverage. Hence it is a degassing problem. For the solution of this problem following approaches were considered:

- Better degassing with deoxidizing elements (Al, Ti)
- Decreasing the weld metal viscosity
- Decreasing the interface tension between molten metal and slag coverage
- Varying the amount of slag coverage
- Changing the slag solidification path

The first three approaches had a negative outcome. Adding degassing elements caused an unacceptable welding behaviour. Decreasing the weld metal viscosity is only possible by raising the temperature which is limited by the maximum heat input of 11 kJ/cm. Decreasing the interface tension between slag and weld metal is possible with surface active elements like oxygen, sulphur or arsenic. Oxygen causes more dimples, sulphur lead to hot cracking and arsenic deteriorates the mechanical properties.

Varying the amount of slag coverage showed that decreasing the slag coverage improved the dimple situation, but does not solve it completely. A certain amount of slag is necessary to protect the weld and to grant the position weldability.

Changing the slag solidification behaviour is very complex. The slag solidification curve can be changed and this will lead to an improvement of the dimple problem, but some dimples will most probably always remain in the downhand position (PA), because to support the weld metal the slag always has to solidify before the weld metal. The reason for that is the position weldability must be granted, that means there is a physical limit to it. The viscosity-temperature curves of the Masse 90 slags are already at the limit for decent position welding (long solidification interval). A slower solidification would not support the weld metal properly. The optimization potential lies in the solidification path. An ideal solidification curve would show a fast solidification at the beginning and a slower solidification in the middle of the solidification interval. This approach has most probably the biggest optimization potential.

Matcalc simulation:

This simulation offers many possibilities with respect to alloy composition improvement. The simulation shows trends how the alloy composition should be concerning hot cracking susceptibility and mechanical properties as well as in matters of corrosion behaviour. It also shows the ambivalence between good corrosion resistance properties and hot cracking susceptibility.

The abstract of this simulation is that less alloying elements (Cr, Mo, Fe, W) lead to better hot cracking safety and better mechanical properties. Molybdenum has the biggest influence on the precipitation of unfavourable intermetallic phases followed by chrome.

The Matcalc simulation (Scheil) also allows the prediction of the solidification behaviour of different alloy compositions, which also can be very useful.

7.2 PERSPECTIVE:

The combination of experimental and simulation approaches can certainly be useful for the development of new welding wires. It should be a decision support for the developers.

The development of new slag systems would help to get rid of the dimple problem, even if it is complicated. The slag viscosity measurements should be carried out for each prototype welding wire to establish a slag solidification database. This will help to understand the influencing parameters on the solidification path better and it also prevents the loss of knowledge. It would be a good addition to the Böhler Welding knowledge database.

The HSC analysis should also be carried out in the future for as many prototype wires as possible, because important parameters such as the drop rate and the drop transition can be characterized very well.

The Matcalc simulations, which would be the theoretical part, are useful to find out more about the phase precipitation and the solidification of complex nickel-based or highly alloyed weld metals.

8 APPENDIX

8.1 HIGH RESOLUTION VOLTAGE AND CURRENT MEASUREMENT:

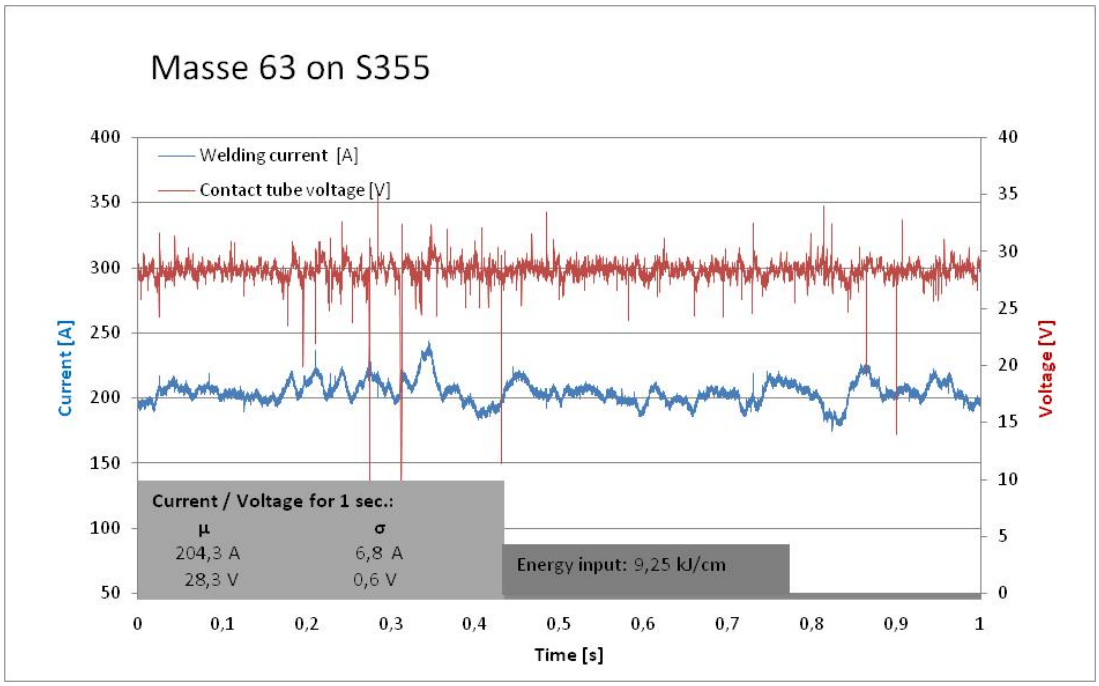

Figure 8-1: Masse 63: High resolution current-voltage measurement

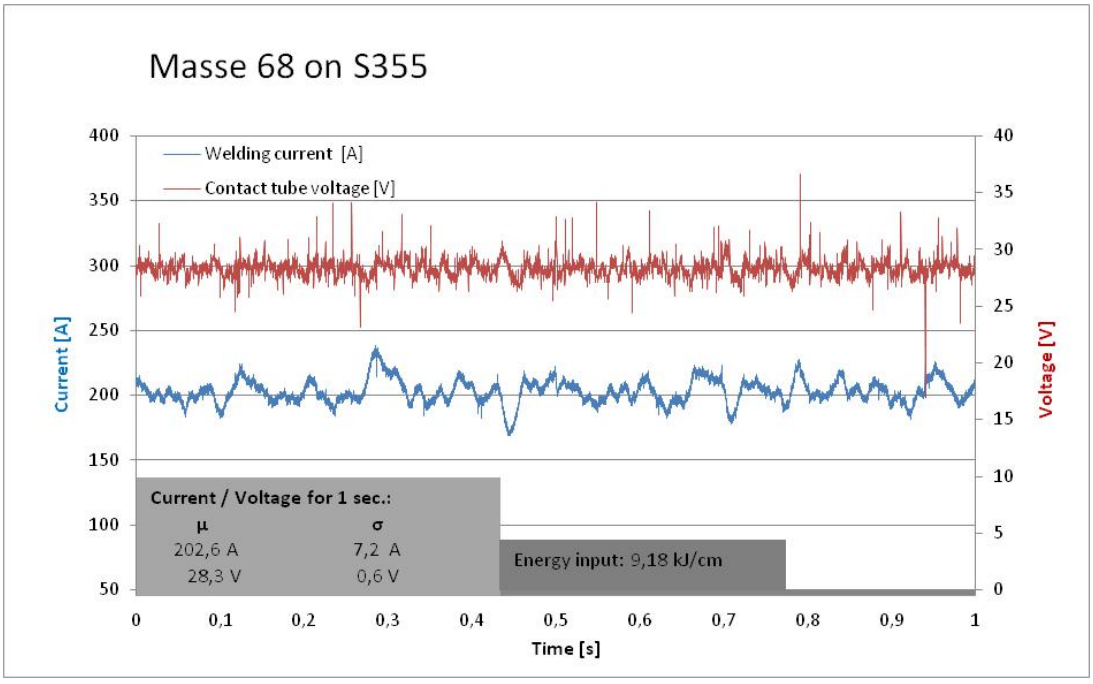

Figure 8-2: Masse 68: High resolution current-voltage measurement

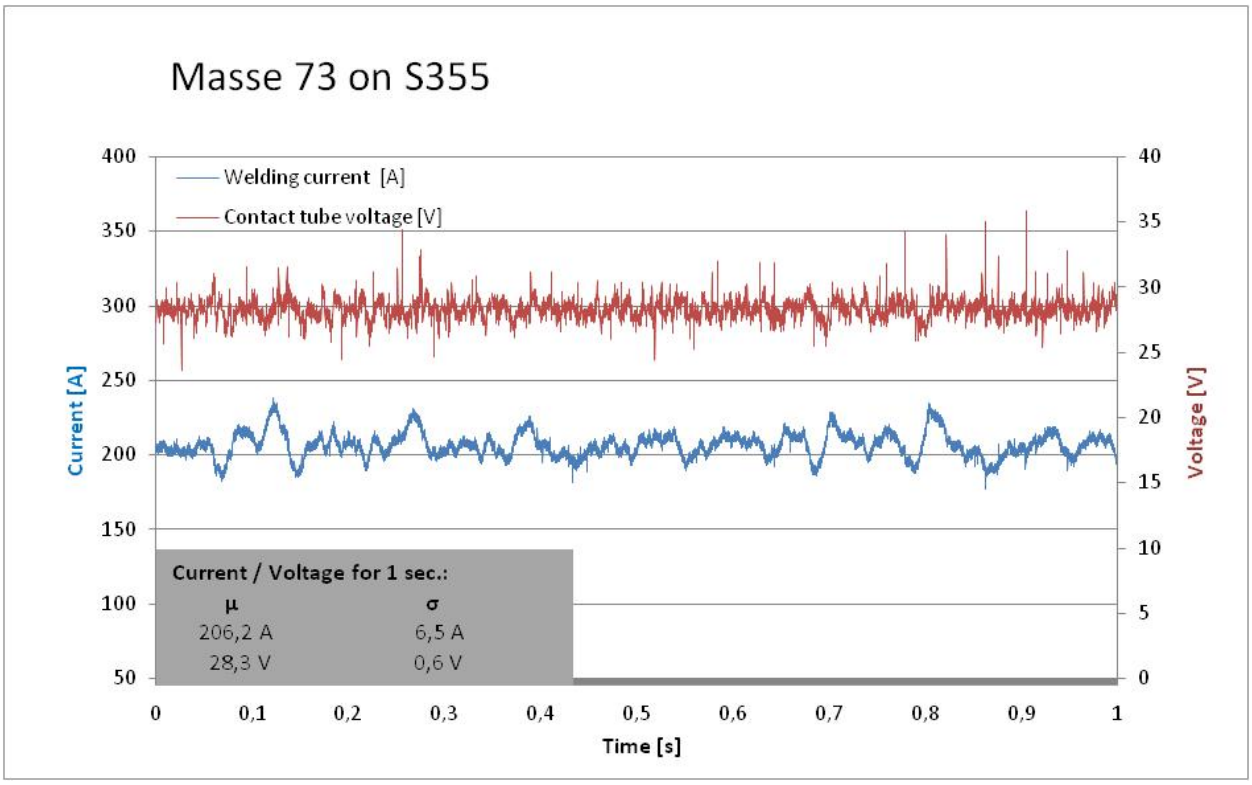

Figure 8-3: Masse 73: High resolution current-voltage measurement

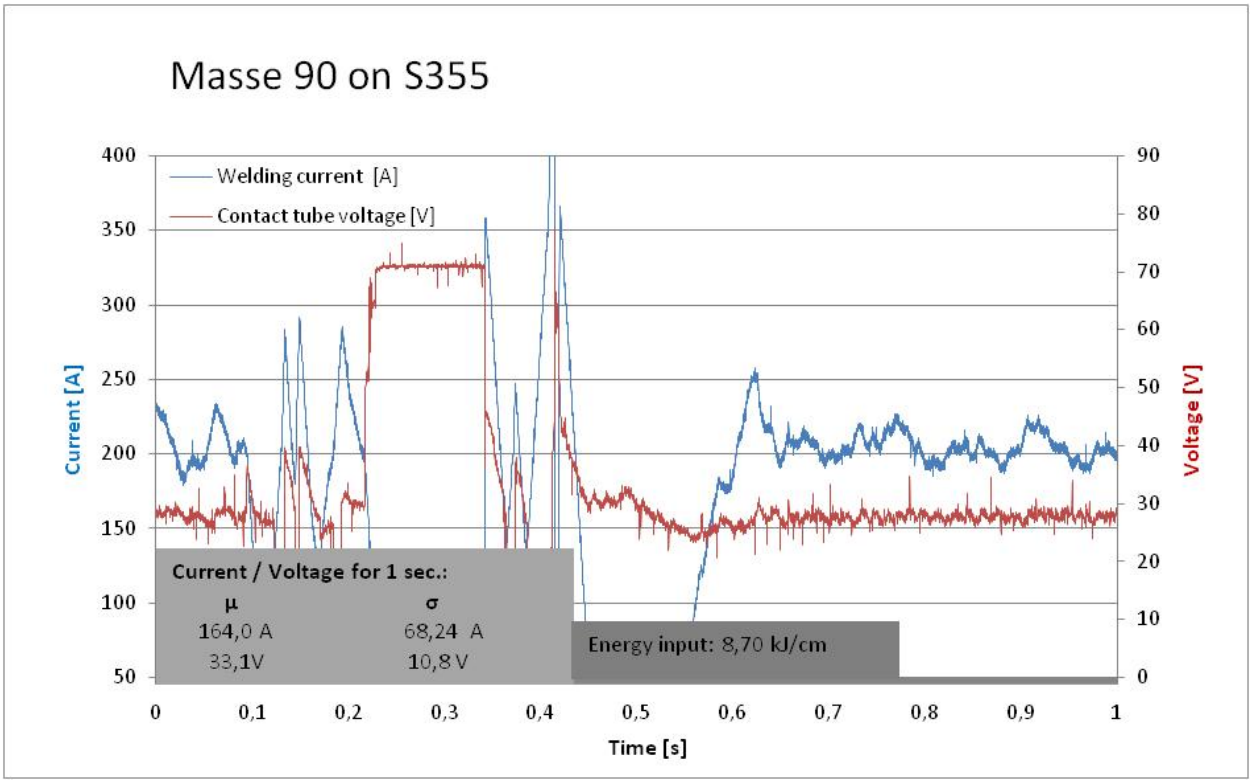

Figure 8-4: Masse 90: High resolution current-voltage measurement

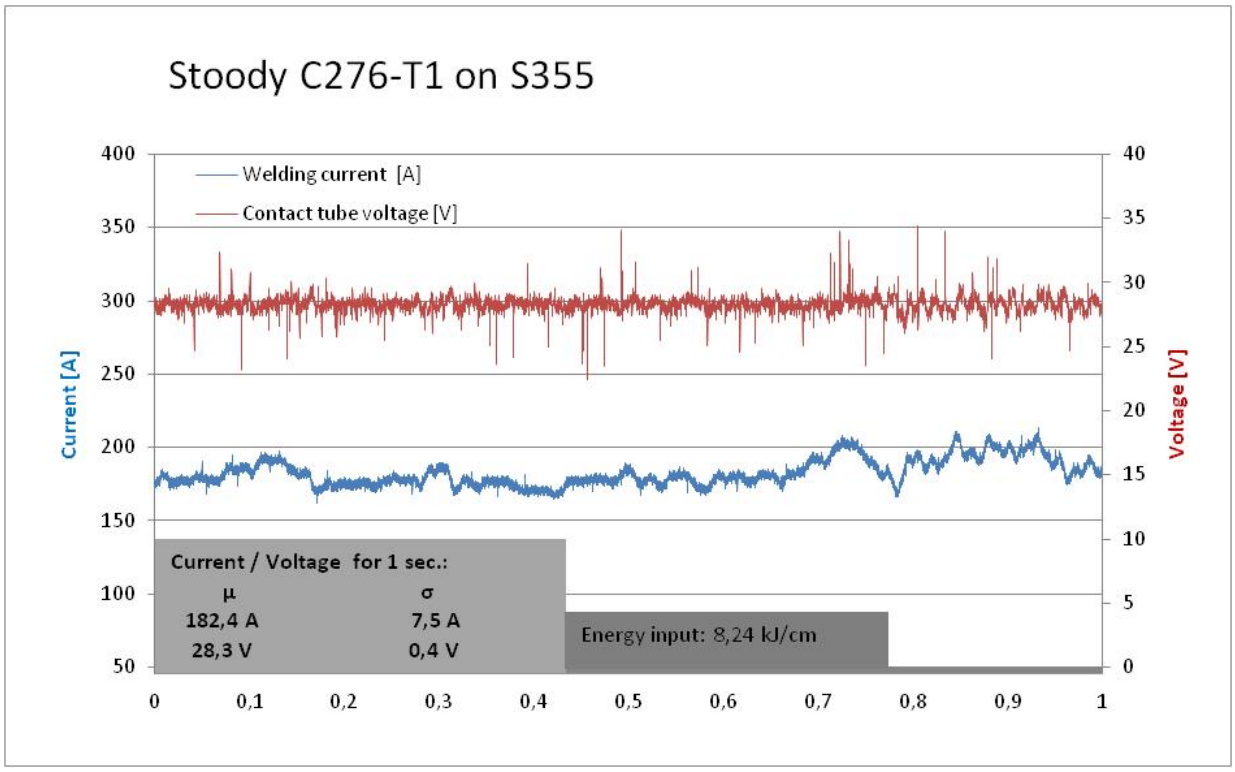

Figure 8-5: Stoody: High resolution current-voltage measurement

8.2 EXPERIMENTAL OVERVIEW OF ALL WIRES

Masse 63

Welding parameters					
Travel rate [cm/min]	Wire feed speed [m/min]	Voltage [V]	Current [A]	Shielding gas	Shielding gas [l/min]
30	11	28.2	225	Corgon 18	15

Drop rate:	**Slag deposition rate:**
83 drops/second	0.53 [g/m]

Wire X-section

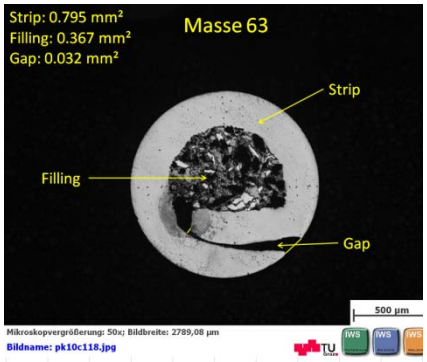

Drop transition

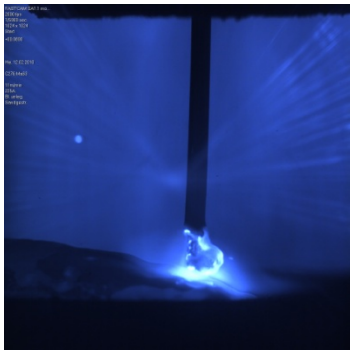

Slag solidification

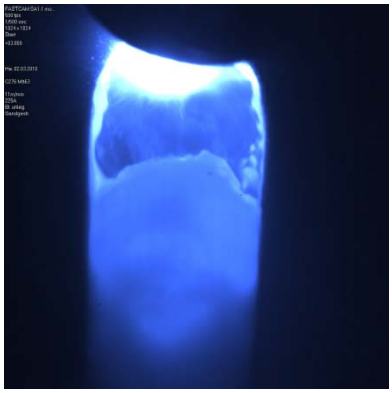

Slag coverage

Wire X-section hardness

Position	HV 0.02
1.1	522
1.2	553
1.3	576
1.4	519
2.1	658
2.2	546
2.3	547
2.4	500
3.1	577
3.2	573
3.3	525
3.4	460

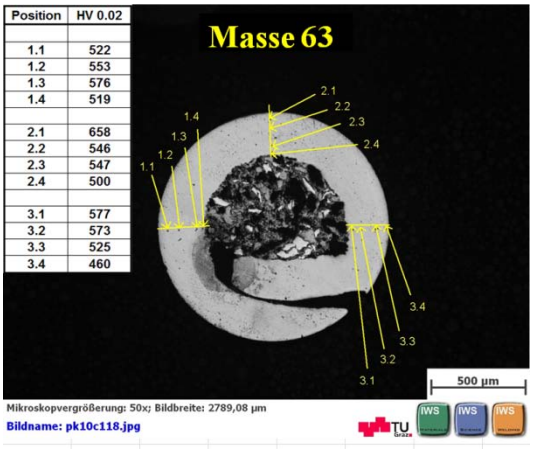

Remarks:

- Best drop rate
- Slightly convex slag solidification

Figure 8-6: Overview Masse 63

Masse 68

Welding parameters					
Travel rate [cm/min]	Wire feed speed [m/min]	Voltage [V]	Current [A]	Shielding gas	Shielding gas [l/min]
30	11	28.2	225	Corgon 18	15
Drop rate: 67 drops/second			**Slag deposition rate:** 0.56 [g/m]		

Wire X-section

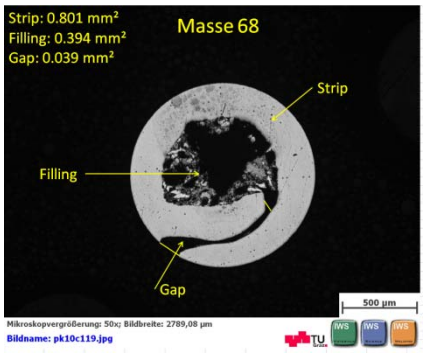

Drop transition

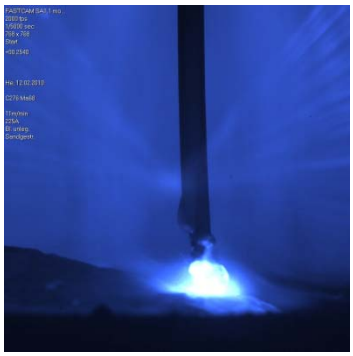

Slag solidification

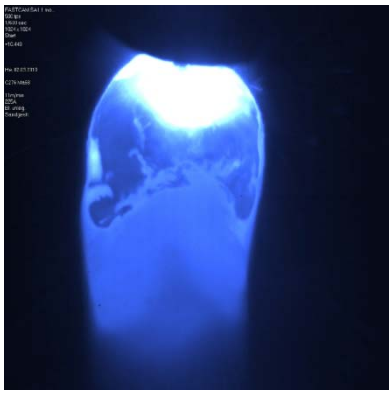

Slag coverage

Wire X-section hardness

Position	HV 0.02
1.1	522
1.2	600
1.3	569
1.4	572
2.1	650
2.2	609
2.3	516
2.4	486
3.1	577
3.2	601
3.3	593
3.4	508

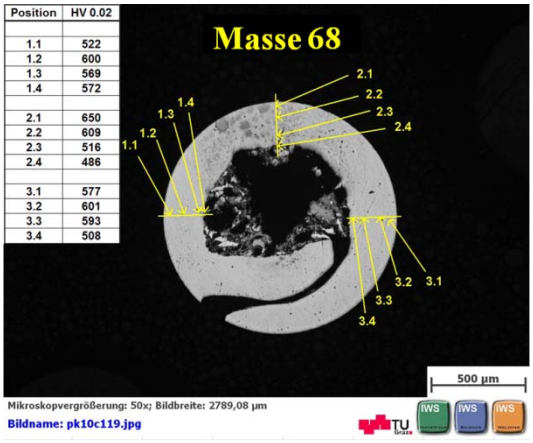

Remarks:

- Second worst drop rate
- Convex slag solidification
- Fused wire above the arc

Figure 8-7: Overview Masse 68

Masse 73

Welding parameters					
Travel rate [cm/min]	Wire feed speed [m/min]	Voltage [V]	Current [A]	Shielding gas	Shielding gas [l/min]
30	11	28.2	225	Corgon 18	15

Drop rate:	**Slag deposition rate:**
79 drops/second	0.59 [g/m]

Wire X-section

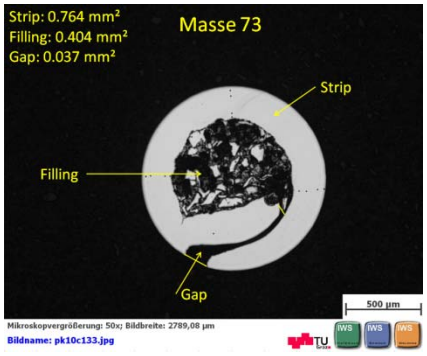

Drop transition

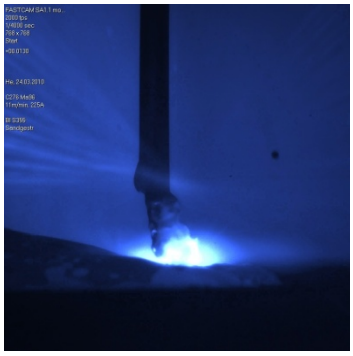

Slag solidification

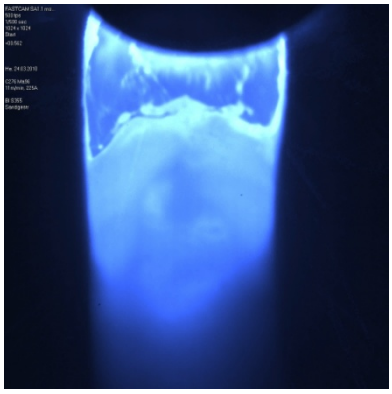

Slag coverage

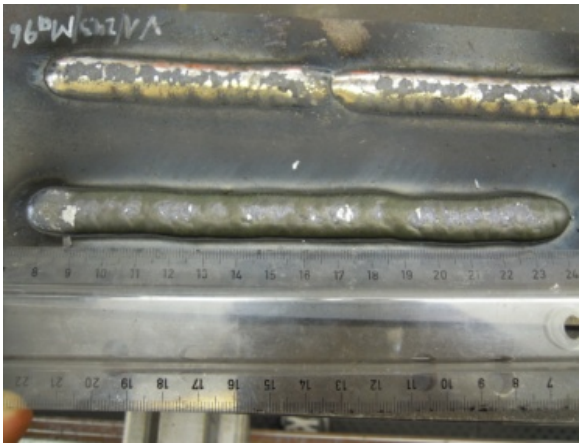

Wire X-section hardness

Position	HV 0.02
1.1	514
1.2	568
1.3	489
1.4	527
2.1	569
2.2	554
2.3	540
2.4	544
3.1	556
3.2	581
3.3	525
3.4	514

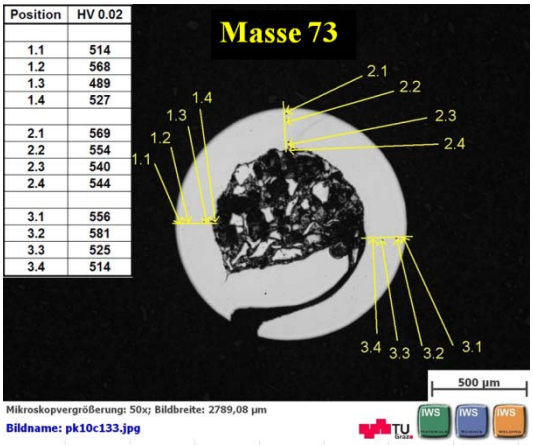

Remarks:

- Second best drop rate
- Slightly convex slag solidification
- Fused wire above the arc

Figure 8-8: Overview Masse 73

Masse 90

Welding parameters					
Travel rate [cm/min]	Wire feed speed [m/min]	Voltage [V]	Current [A]	Shielding gas	Shielding gas [l/min]
30	11	28.2	225	Corgon 18	15

Drop rate:	**Slag deposition rate:**
70 drops/second	0.63 [g/m]

Wire X-section

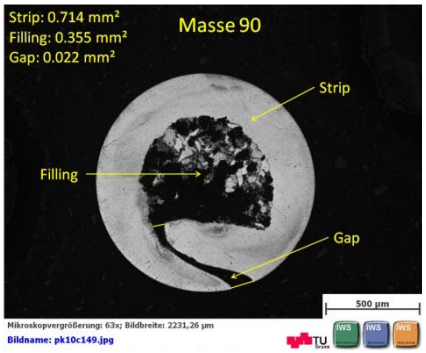

Drop transition

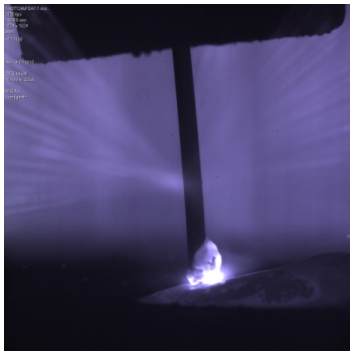

Slag solidification

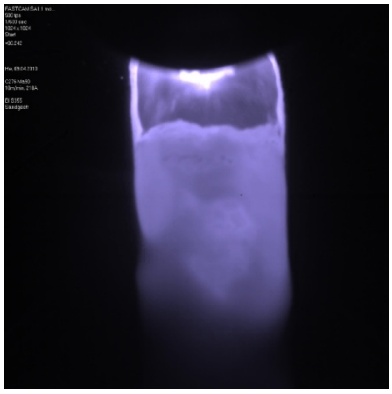

Slag coverage

Wire X-section hardness

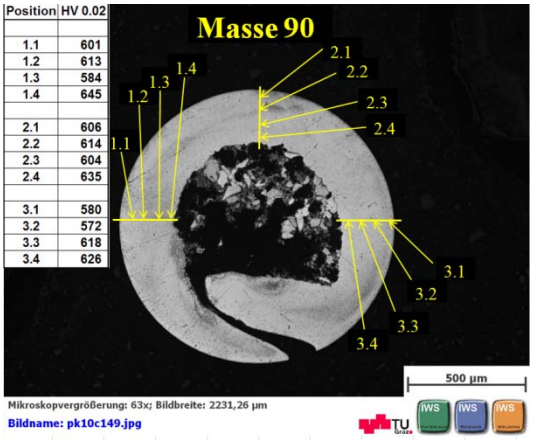

Remarks:

- Best drop rate
- Convex slag solidification
- Short circuits have been observed → wire breaks/explodes (Coated wire)

Figure 8-9: Overview Masse 90

Stoody C-276

Welding parameters					
Travel rate [cm/min]	Wire feed speed [m/min]	Voltage [V]	Current [A]	Shielding gas	Shielding gas [l/min]
30	11	28.2	225	Corgon 18	15
Drop rate: 45 drops/second			**Slag deposition rate:** 0.99 [g/m]		

Wire X-section

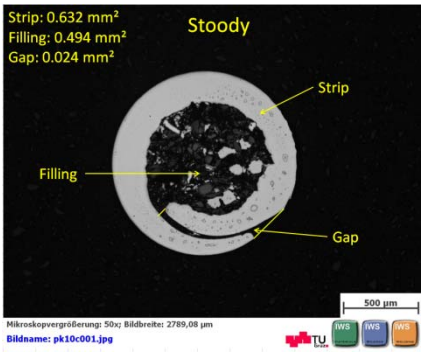

Drop transition

Slag solidification

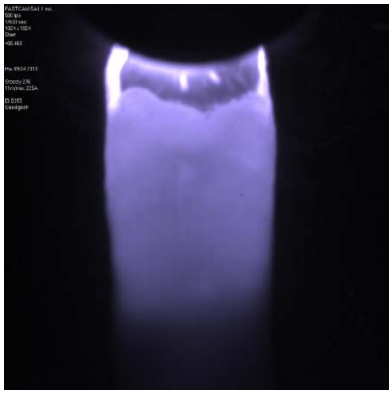

Slag coverage

Wire X-section hardness

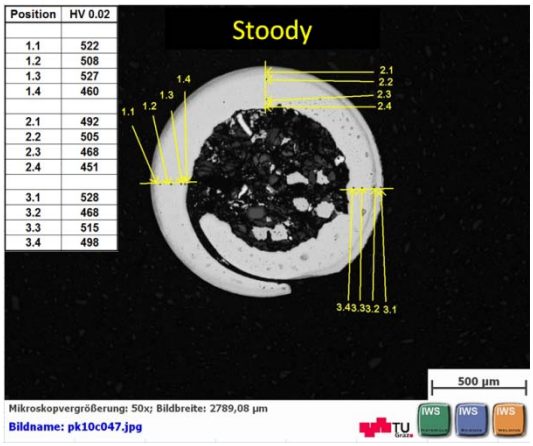

Remarks:

- Worst drop rate
- Slightly concave slag solidification
- Best slag coverage (Highest slag deposition rate)
- Short circuits have been observed → wire breaks/explodes

Figure 8-10: Overview Stoody C-276

8.3 VISCOSITY-TEMPERATURE CURVES OF DIFFERENT WELDING WIRE SLAGS

8.3.1 ALLOY 625

Alloy 625 / N16939 Japan	Basic viscosity [mPa.s]	Breakpoint [°C]	Solidification interval [°C]
	20	1435	45

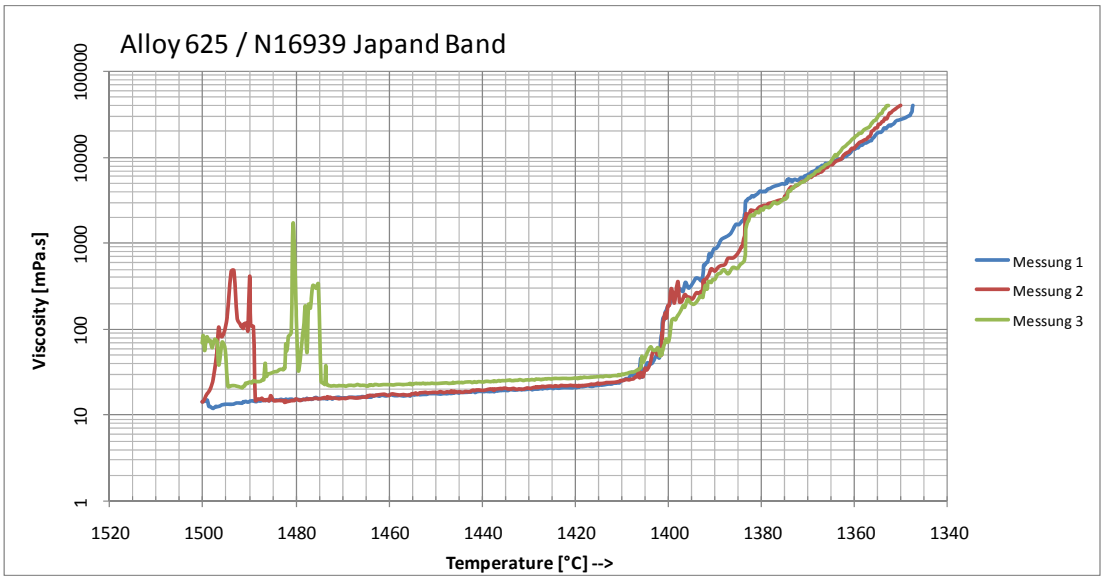

Figure 8-11: Alloy 625/N16939 Japan Band viscosity-temperature curve

Alloy 625 / 2302300	Basic viscosity [mPa.s]	Breakpoint [°C]	Solidification interval [°C]
	20	1440	50

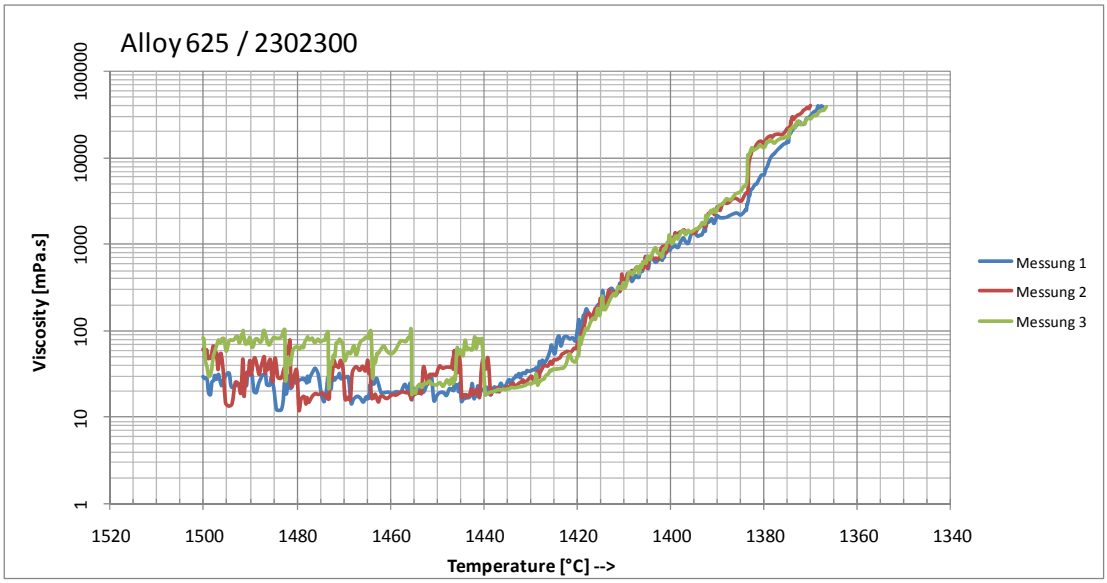

Figure 8-12: Alloy 625/2302300 viscosity-temperature curve

9 BIBLIOGRAPHY

1. **Agarawal, D. and Herda, W.** The "C" family of Ni-Cr-Mo alloys' partnership with the Chemical Process Índustry: the last 70 years. 1997, pp. 542-548.

2. **Schuster, Jochen.** Schweißen von Eisen-, Stahl- und Nickelwerkstoffen. *Schweißen von Eisen-, Stahl- und Nickelwerkstoffen.* Düsseldorf : DVS Media GmbH, 2009, pp. 136-159.

3. **Nickel Institute.** About Nickel. [Online] 18. September 2010. [Cited: 18. September 2010.] http://www.nickelinstitute.org/index.cfm?ci_id=13&la_id=1.

4. **Scheil, E. and Class, E.** *Pat.No.:3203792* USA, 1965.

5. **Special Metals.** Products. [Online] 19 May 2010. [Cited: 19 May 2010.] http://www.specialmetals.com/documents/Inconel%20alloy%20C-276.pdf.

6. **Roy, A., Pal, J. and Mukhopadhyay, C.** Dynamic strain ageing of austenitic superalloy - Temperature and strain rate effects. 2008, pp. 363-370.

7. **Kirchheiner, R, Köhler, M and Heubner, U.** Nicrofer 5923 hMo, ein neuer hochkorrosionsbeständiger Werkstoff für die chemische Industrie, die Umwelttechnik und verwandte Anwednungen. *Werkstoffe und Korrosion.* 1992, Vol. 43.

8. **Dinesh, Chand and Argawal.** Neue Anwendung der Superlegierung Alloy 59 in der Rauchgaswäsche. 2005, pp. 28-36.

9. **Hack, H.** *NACE/ASTM JOINT TASK GROUP ON TERMINOLOGY, J01.02 AND J01 COMMITTEE.* Houston : NACE International, 2009. pp. 4-5.

10. **Durand-Charre, Madeleine.** The Microstructure of Superalloys. *The Microstructure of Superalloys.* Amsterdam : Gordon and Breach Science Publishers, 1997, p. 48.

11. **Cieslak, M.J., Headley, T.J. and Romig, A.D.** The welding Metallurgy of Hastelloy Alloys C-4, C-22, and C-276. *Metallurgical Transactions.* November 1986, pp. 1986-2035.

12. **Bürgel, R.** *Handbuch Hochtemperatur - Werkstofftechnik 3. Auflage.* Braunschweig : Vieweg & Sohn Verlagsgesellschaft mbH, 2006.

13. **Cerjak, H.** Skriptum zu Werkstoffkunde. Graz, Austria : TU Graz, 2005.

14. **Shoemaker, L.E. and Crum, J.R.** Products: Special Metals. *Special Metals Web site.* [Online] [Cited: 2 February 2010.] http://www.specialmetals.com.

15. **Cline, John R, Murphy, David W and Telesz, Robert W.** *KEPCOS's first 5000 MW of Flue Gas Desulfurization.* Orlando : s.n., 1998.

16. **Kou, Sindo.** *Welding Metallurgy.* Hoboken, New Jersey : John Wiley & Sons, Inc., 2003.

17. **Rosert, R., et al.** Schweißen mit Fülldraht - Entwicklung und Perspektiven in der Anwendung. 2003, pp. 99-225.

18. **Hauck, G. and Kosfeld, G.** Entwicklungsstand von Fülldrahtelektroden zum Lichtbogenschweißen mit und ohne Schutzgas. *Der Praktiker.* 11 1973, pp. 248-250.

19. **Aichele, G. and Smith, A.A.** MAG-Schweißen. *MAG-Schweißen.* Düsseldorf : Deutscher Verlag für Schweißtechnik GmbH, 1975, pp. 171-180.

20. **Vallant, Rudolf.** *Optimierung von Schlacken beim MAG-Schweißen mit Nickelbasis-Fülldrahtelektroden der Typen NiCr 70/20 und 70/15.* Graz : s.n., 2003.

21. **Fielder, Michael.** *Potential von Nickelbasis.Fülldrahtelektroden.* Leoben : s.n., 2007.

22. **Barge, H. Jürgen and Schulze, Günter.** *Werkstoffkunde, 10.Auflage.* Berlin : Springer, 2008.

23. **ErlGmbH.** Fachwissen: Streckenenergie. *Erl-GmbH Web site.* [Online] 17 June 2010. [Cited: 17 June 2010.] http://www.erl-gmbh.de/home/fachwissen/berechnungen/streckenenergie.html.

24. **Schulze, Günther.** *Die Metallurgie des Schweißens, 3.Auflage.* Berlin : Springer, 2009.

25. **Freytag, Christoph.** *Beitrag zur Bestimmung des effektiven Lichtbogenwirkungsgrades beim MAG-Schweißen mittels eines Kalorimeters.* Graz : s.n., 2000.

26. **ThyssenKrupp VDM.** Download: Material data sheets. *Thyssen Krupp VDM.* [Online] 17 June 2010. [Cited: 17 June 2010.] http://www.thyssenkrupp-vdm-fareast.com/media/down_datasheets/ni5716e.pdf.

27. **Killing, R.** *Kompendium der Schweißtechnik: Band 1: Verfahren der schweißtechnik.* Düsseldorf : DVS-Verlag GmbH, 1997.

28. **Pomaska, Hans-Ulrich.** *MAG-Schweißen "Kein Buch mit sieben Siegeln".* Höllriegelskreuth : Linde AG, 1989.

29. **Killing.** *Handbuch der Schweißverfahren: Teil 1: Lichtbogenschweißverfahren.* Düsseldorf : DVS-Verlag GmbH, 1984.

30. **Probst, R. and Herold, H.** *Kompendium der Schweißtechnik: Band 2: Schweißmetallurgie.* Düsseldorf : DVS-Verlad GmbH, 1997.

31. **Mills, K.C.** Viscosities of molten slags. *Slag Atlas.* Düsseldorf : Verlag Stahleisen GmbH, 1995, pp. 349-402.

32. **Dilthey, Ulrich.** *Schweißtechnische Fertigungsverfahren 2: Verhalten der Werkstoffe beim Schweißen.* Aachen : Springer, 2005.

Oral references:

Weiß, Mario; developer at BSGA

Tösch, Josef; former developer at BSGA

10 LIST OF FIGURES

11 LIST OF EQUATIONS

12 LIST OF TABLES